Dissertation

submitted to the

Combined Faculties for the Natural Sciences and for Mathematics

of the Ruperto-Carola University of Heidelberg, Germany

for the degree of

Doctor of Natural Sciences

Presented by

Dipl.-Ing. Agata Pernuš

Born in Ljubljana, Slovenia

Oral examination: 27th of July

Imaging mobility and interaction of c-Fos and c-Jun transcription factors in live cells: A SPIM-FCCS study

Referees: Prof. Dr. Jörg Langowski

Prof. Dr. Victor Sourjik

This dissertation was conducted between June 2010 and June 2015 under the supervision of Prof. Dr. Jörg Langowski in the division „Biophysics of Macromolecules" at the German cancer research center (DKFZ) in Heidelberg.

Diese Dissertation wurde zwischen Juni 2010 und Juni 2015 in der Abteilung „Biophysik der Makromoleküle" am Deutschen Krebsforschungzentrum (DKFZ) in Heidelberg unter der Betreuung von Prof. Dr. Jörg Langowski erstellt.

To my parents.

Abstract

The regulation of DNA transcription into RNA and its translation into proteins is one of the most important processes determining cell behaviour. Transcription factors regulate DNA transcription into RNA, thereby controlling protein expression and cellular processes. General transcription factors like c-Fos and c-Jun participate in the regulation of processes such as proliferation, differentiation, apoptosis and oncogenesis.

Molecular dynamics inside cells can be investigated by fluorescence correlation spectroscopy (FCS). The fluorescently labeled molecules are excited by a focused laser beam and are characterized by an auto-correlation analysis to yield the information about the diffusion coefficients and concentrations. To study biomolecular interactions, a two-color fluorescence cross-correlation spectroscopy (FCCS) is used. Two molecules are labeled with different fluorophores to distinguish them spectrally. Cross-correlating the fluorescence fluctuation in the detection channels reveals their interaction. These techniques are typically implemented on a confocal microscope, which enables detection of fluorescently labeled molecules with single-molecule sensitivity using the avalanche photodiode detector. A technique that allows imaging in a thin plane and spatially resolves FCCS by analysis of fast image series is single plane illumination microscopy (SPIM). SPIM illuminates the fluorescently labeled sample by a thin light sheet formed by a laser beam focused through cylindrical optics and simultaneously images all points in the two-dimensional field of view with a fast camera. SPIM-FCCS uses two overlapping light sheets of different wavelengths and the two fluorescence channels are optically split to two half planes of the same sensor.

In this Thesis, the mobility and interaction of c-Fos and c-Jun transcription factors were studied and characterised in vivo using SPIM-FCCS. I collected mobility and interaction maps of c-Fos-eGFP and c-Jun-mRFP1 transcription factors within living cell nuclei. The c-Fos dimerizes with c-Jun to form the transcription activator protein-1 (AP-1) which binds to the specific recognition site. SPIM-FCCS monitors these processes, which provides diffusion coefficient and protein-protein interaction data in the whole image plane simultaneously, instead of just at one point on conventional confocal FCS. I find a strong correlation between diffusional mobility and interaction: regions of strong interaction show slow mobility. Controls containing an eGFP-mRFP dimer, eGFP and mRFP monomers, or c-Fos-eGFP and c-Jun-mRFP1 mutants lacking dimerization and DNA-binding domains, showed no such correlation.

Zusammenfassung

Die Regulation der DNA zu RNA Transkription und seine Translation in Proteine ist einer der bedeutendsten Prozesse die das spätere Zellverhalten festlegt. Transkriptionsfaktoren sind hierbei die Mittler der DNA-RNA Transkription. Sie kontrollieren die Proteinausprägung und haben damit Einfluß auf zellulare Prozesse. Hierbei sind die Transkriptionsfaktoren c-Fos und c-Jun die Akteure in der Regulation von Prozessen wie Proliferation, Differenzierung, Apoptose und Onkogenese.

Molekulare Zusammenhänge in einer Zelle können mittels Fluoreszenz-Korrelations-Spektoskropie (FCS) untersucht werden. Die fluoroszenzmarkierten Moleküle werden mit einem fokussierten Laserstrahl angeregt. Die resultierende und charakterisierende Fluoreszenzstrahlung können mittels Auto-Korrelations Analyse untersucht werden und geben somit Informationen über Diffusionskoeffizienten und Konzentrationen. Um die Biomolekularen Interaktionen zu studieren wird ein zwei Farben Fluoreszenzkreuzkorrelation Spektroskopie (FCCS) benutzt. Zwei Moleküle werden mit verschiedenen Fluorophoren markiert um sie in der späteren Analyse unterscheiden zu können. Diese Vorgehensweise wurde ursprünglich mit einem konfokalen Mikroskop realsiert mit Lawinenphotodioden als Detektor. Die Methode die die Untersuchung in einer Ebene mit räumliche Auflösung mit FCCS erlaubt heißt single plane illumination microscopy (SPIM). Der Versuchsaufbau ist so gewählt, dass die präparierte Probe in den Laserstrahl gebracht wird und somit das auftretenden Fluoreszenzlicht von der Kamera detektiert wird. SPIM-FCCS benutzt zwei überlappende Lichtscheiben unterschiedlicher Wellenlänge. Die beiden Kanäle werden optisch aufgetrennt und auf die zwei Halbebenen des Detektors geführt.

Im Rahmen dieser Doktorarbeit wurde die Mobilität und Interaktion von c-Fos und c-Jun *in vivo* untersucht mit SPIM-FCCS. c-Fos dimerisiert zusammen mit c-Jun und formt den Transkriptions-Aktivator Protein-1 (AP-1). SPIM-FCCS detektiert diesen Prozess und somit können Diffusionskoeffizienten und Protein-Protein Interaktionsdaten in dem gesamten Bildraum simultan gewonnen werden. Es konnte eine starke Korrelation zwischen Diffusions Mobilität und Interaktion gefunden werden: Regionen mit starker Interaktion zeigen geringe Mobilität. Kontrollversuche mit jeweils eGFP-mRFP Dimere, eGFP und mRFP Monomere, sowie c-Fos-eGFP mit c-Jun-mRFP1 Deletionsmutanten ohne Dimerisierungs und DNA Bindungsdomäne zeigten keine derartige Korrelation.

List of Figures

1 INTRODUCTION

2 MATERIAL AND METHODS

3 RESULTS

APPENDIX

List of Tables

Abbreviations

ACF	Auto-correlation function
AP-1	Activator protein 1
APD	Avalanche photodiode
ATP	Adenosine triphosphate
ATF	Activating transcription factor
bp	Base pair
bZip	Basic zipper
c-Jun	Cellular Jun
CCF	Cross-correlation function
CRE	cyclic AMP-response element
DMEM	Dulbecco's modified eagle medium
DNA	Deoxyribonucleic acid
DoF	Degree of freedom
eGFP	Enhanced green fluorescent protein
EDTA	Ethylendiamintetra acetat
EM-CCD	Electron-multiplying charge-coupled device
FCS	Fluorescence correlation spectroscopy
FCCS	Fluorescence cross-correlation spectroscopy
FFM	Fluorescence fluctuation microscopy
FRET	Fluorescence resonance energy transfer
FOV	Field of view
HeLa	Human cervical carcinoma cell line
Hz	Hertz
IRES	Internal ribosomal entry site
JNK	Jun N-terminale kinase
LB	Luria-Bertani
LED	Light emitting diode

LSFM	Light sheet fluorescence microscopy
MAF	Musculoaponeurotic fibrosarcoma
MAPK	Mitogen-activated protein kinase
MCF-7	Human breast cancer cell line
MDS	Molecular dynamics simulations
mRFP1	Monomeric red fluorescent protein 1
MSD	Mean squared displacement
NA	Numerical aperture
NLS	Nuclear localization site
NPC	Nuclear pore complex
PSF	Point spread function
RNA	Ribonucleic acid
ROI	Region of interest
SPIM	Single plane illumination microscopy
TIFF	Tagged image file format
TF	Transcription factor
TRE	TPA (12-*O*-tetradecanoyl-phorbol-13-acetate) response element
QF	QuickFit 3 data evaluation software
v-Jun	Viral Jun
wtGFP	Wildtype green fluorescent protein

Table of contents

I. INTRODUCTION

1. EUKARYOTIC CELLS

Cells are the basic structural and functional unit of all living organisms. They are composed of numerous structures, each of which has an accurately defined specific function, but all working together in harmony which is essential for cell functioning. Although a great variety of cells exist, their main functions are chemical reactions including energy conversion, transport (of molecules), and reproduction [1].

Eukaryotic cells are cells in which genetic material is surrounded by a nuclear envelope. They are found in multi-cellular organisms, such as mammals and plants, and in uni-cellular microorganisms like yeast. Eukaryotic cells are separated from the rest of their environment by a phospholipid bilayer based membrane. The membrane is responsible for the control of transport of substances in and out of the cell. An illustration of a eukaryotic cell is shown in *Figure 1.1*.

As the average size of a cell is 10-20 μm, cells can only be visualized under the microscope. The microscopy thus helps us to look inside the cell with the aim to study its interior structure and function. With a light microscope we can observe a cell as a bag surrounded with a cell membrane, a nucleus, and filled with cytoplasm, containing several organelles. We can examine the structure of cell organelles in more detail with the help of electron microscope [2].

The inside of the cell is full of organelles. Different organelles play different roles in the cell. To understand how the eukaryotic cell functions, we need to know how each individual organelle functions, how the organelles are cooperating, and how molecules move between them.

The most critical of all eukaryotic organelles is the nucleus which functions as the information and administrative center of the cell. A visible structure within the nucleus is the nucleolus, which produces the protein production essential ribosomes. The nuclear envelope separates the nucleus from the cytoplasm. It provides suspension to the organelles and keeps the shape of the cell. The cytoplasm consists of cytosol and cytoplasmic organelles. All organelles have their own membrane, based on lipid bilayers, that separates them from the rest of the cellular space. This permits them to maintain different biochemical reactions. For

example, mitochondria generate energy by releasing it in the form of ATP (adenosine triphosphate), endoplasmic reticulum assemble proteins and lipids, the Golgi apparatus modifies, sorts and packages proteins, and lysosomes contain enzymes that break down and recycle proteins, lipids and carbohydrates [1].

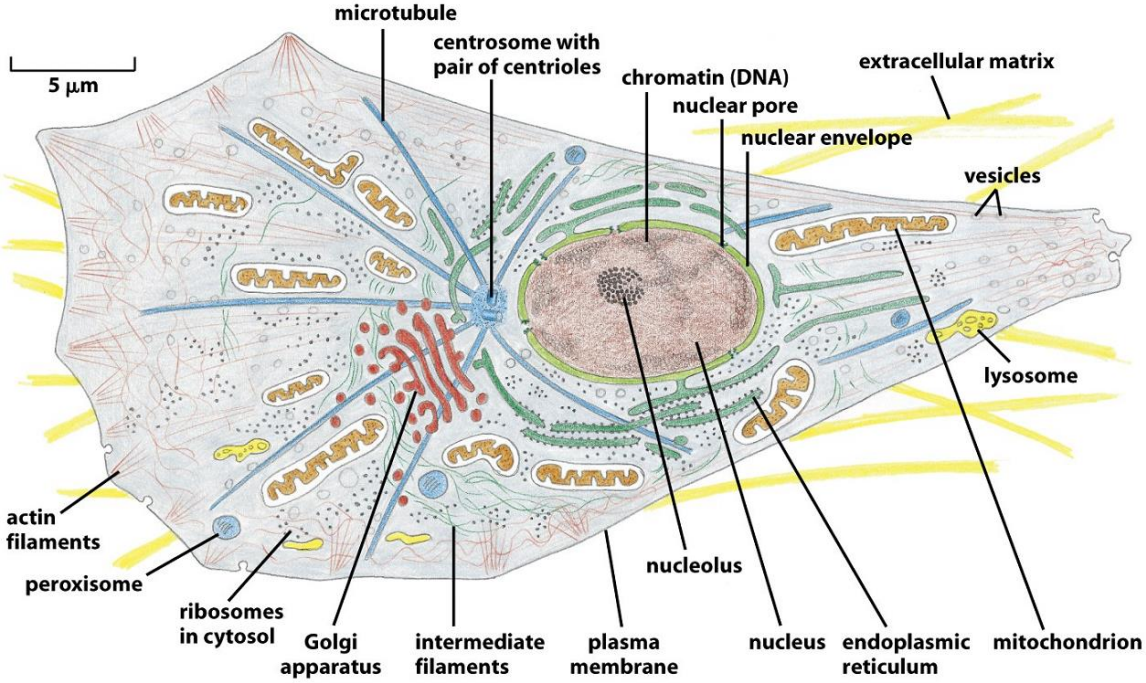

Figure 1.1: A eukaryotic cell and its organelles. The image is obtained from [1, 3].

The nucleus contains Deoxyribonucleic Acids (DNA), the hereditary information present in all living organisms. DNA is a double-stranded molecule formed from long unbranched paired polymer chains. The smallest unit of DNA is the nucleotide, consisting of a sugar called deoxyribose with a phosphate group and a base. A base can be adenine, guanine, cytosine or thymine. The nucleotides are structured in a chain through a covalent bond composed of a sugar and a phosphate group. Each base in a DNA-strand is linked to the complementary base in another strand by a hydrogen bond: adenine with thymine, and guanine with cytosine. This double-stranded structure is twisted to form a double helix [1].

The DNA copies its information during the replication process. The process is synthesized by an enzyme DNA Polymerase that synthesizes a DNA molecule for the reproduction of two identical DNA molecules. The information on the DNA is synthesized by a RNA polymerase, an enzyme which breaks up the double-stranded DNA and produces an almost identical copy

of the molecule, the Ribonucleic Acid (RNA). This process is called transcription and is initiated and regulated by transcription factors (described below). Proteins, amino acids arranged in a linear chain, are synthesized by ribosomes during translation (*Figure 1.2*).

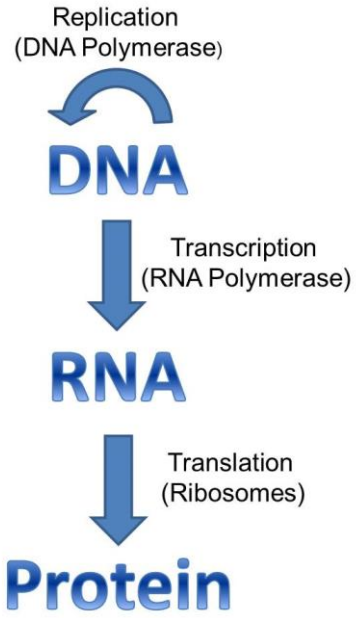

Figure 1.2: The central dogma of molecular biology [4]: Replication is a process where a copy of a DNA molecule is made using the enzyme DNA Polymerase. During transcription, DNA information is copied to RNA by the enzyme RNA Polymerase. Translation is a process where RNA dictates the production of the proteins and occurs on a ribosome.

2. CELL CYCLE

During the cell cycle a cell splits into two daughter cells. The newly created cells must retain all genetic information during the cell division. The genetic material from the mother cell needs to duplicate first before it can be split between two daughter cells. Each of the daughter cells will continue to divide through the same process. This cycle of duplication and division is important for production of a functional organism [1].

In eukaryotic cells the cell cycle consists of four distinct phases: the mitosis (M), the growth phase (G1 and G2) and the synthesis phase (S). The G1, S and G2 phases together form the interphase. The cell cycle is shown in *Figure 1.3*. During interphase, the cell grows and prepares for cell division. This process takes longer than mitosis. In the mitosis phase of cell division, the cell divides into two daughter cells with identical genetic material. The process involves

nuclear division (mitosis) and cytoplasmic division (cytokinesis). After cell division, the daughter cells enter the interphase. Cell division can stop or the cell continues with a new division.

Each of these phases has different functions and responsibilities. During the interphase a cell doubles its cytoplasm and synthesizes DNA. The two gap phases G1 and G2 give the cell time to grow. The biggest part of interphase takes the G1 phase. Here the cell increases in mass and ensures the conditions are suitable for the cell to enter the S phase. This is a period during which the DNA is synthesized. The chromosome and the centrosome (organelle as the main microtubule-organizing center) duplicate. During G2 phase, the cell continues to grow and synthesizes additional proteins. It prepares itself for the mitosis phase.

The mitosis is divided into additional five phases: prophase, prometaphase, metaphase, anaphase and telophase, which are characterized based on the chromosome behavior. First, the chromosomes condense and migrate to the center of the cell. The nuclear envelope breaks and the centrosomes migrate to the opposite poles. Then, the chromosomes align between the centrosome poles. The chromosomes separate and form two daughter chromosomes, which are moved to the opposite poles of the cell. The division is completed after cytokinesis, where the cytoplasm is divided and two daughter cells are formed, each with its own nucleus.

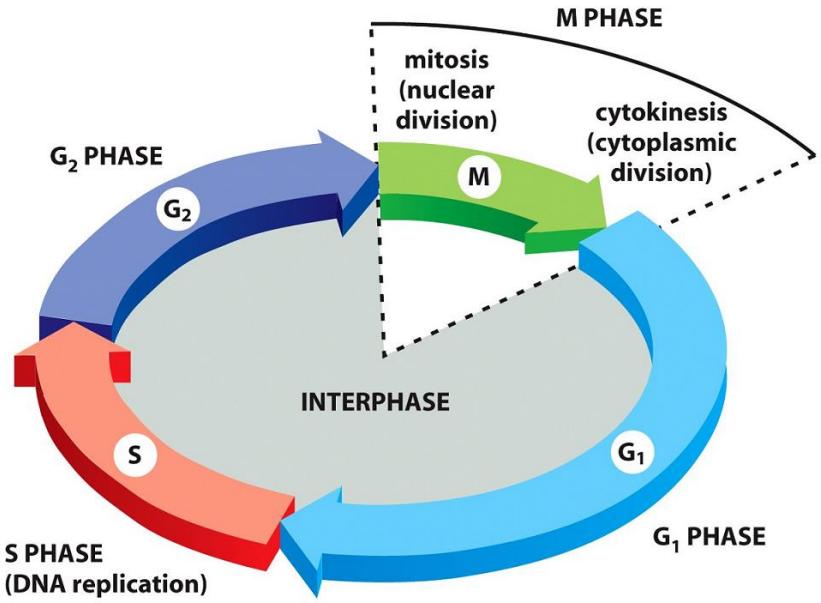

Figure 1.3: The cell cycle: in G1 and G2 phases the cell grows, the organelles duplicate and the cell prepares for DNA replication or cell division, in S phase the DNA and the centrosome duplicate, in M phase (mitosis) the cell divides into two daughter cells. The image is obtained from [1, 3].

3. TRANSCRIPTION FACTORS

Transcription is the first step of gene expression, where an RNA copy is created by using one strand of the DNA as a template (*Figure 1.4*). DNA and RNA are nucleic acids, using nucleic bases to transfer genetic information from DNA into RNA. The bases found in RNA are adenine, guanine, cytosine and the base uracil instead of the thymine present in DNA. The whole process of transcription is catalyzed by the RNA Polymerase enzyme [1].

Transcription begins by splitting the double helix DNA into two strands and exposing the bases on each DNA strand. This happens by breaking the hydrogen bonds between the base pairs. One strand of the opened DNA helix serves as a template for creating a RNA molecule. RNA Polymerase binds to the promoter, a regulatory region on the DNA indicating the starting point for RNA synthesis. It synthesizes the RNA chain always in the direction from 5' to 3' end. Transcription continues until an entire gene in RNA is rewritten and the new RNA strand dissociates from the DNA.

When a new RNA segment is made, the DNA zips back and re-forms the double helix. The RNA is released and migrates through the nuclear pore complex from nucleus to cytoplasm and to the ribosomes. It is then used to create a protein in a process called translation.

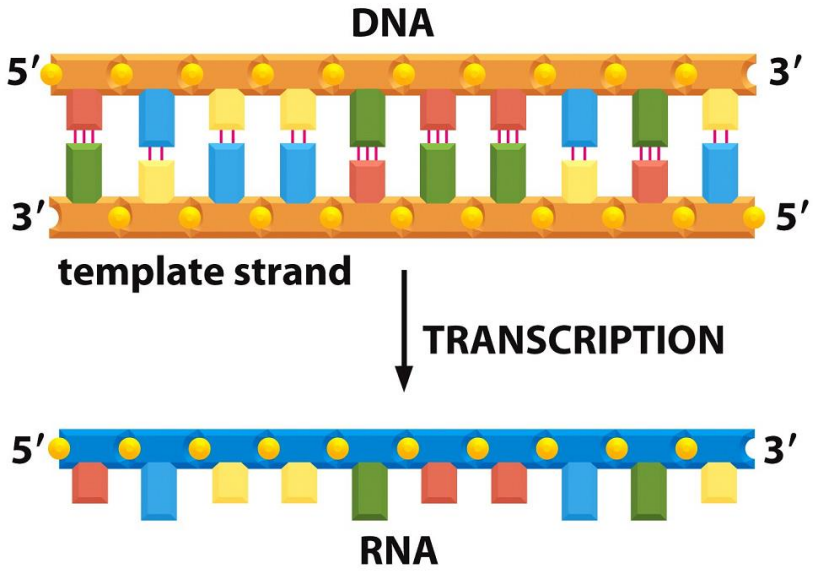

Figure 1.4: Transcription: DNA transcription produces a single-stranded RNA molecule that is complementary to one strand of DNA. The image is obtained from [1, 3].

The regulation of DNA transcription into RNA and its translation into proteins is one of the most important steps determining cell behavior. Transcription factors, DNA binding proteins which promote or repress the action of RNA polymerase, control this process. Transcription factors bind to DNA, typically upstream from and close to the transcription start site of the gene, and activate or repress the promoter. They can perform its function alone or with other proteins in a complex. There are also transcription factors that do not bind directly to the DNA, but to other DNA-binding proteins. We distinguish general and gene-specific transcription factors. General transcription factors take on different tasks and bind either directly to the DNA (for example on promoter element such as TATA box), the RNA Polymerase or other proteins of the preinitiation complex. Specific transcription factors mediate the Polymerase, which gene they need to activate. They bind to specific DNA sequence to stimulate or repress the transcription [5, 6].

The main functional regions of c-Fos and c-Jun from Activator Protein 1 transcription factor family are the transactivation domain, the dimerization domain and the DNA-binding domain (*Figure 1.5*). The transactivation domain is a region that can activate transcription by contacting the transcription machinery (RNA Polymerase or other transcription factors). The dimerization domain is a region that allows transcription factors that work as dimers to interact with another subunit. The DNA-binding domain contains a motif that recognizes the DNA. It includes different parts, such as helix-turn-helix motif, zinc finger domain and the leucine zipper motif. The latter mediates both DNA binding and protein dimerization [5, 6].

Transcription factors are diverse in their structure, have different tasks and are found in all living organisms. They play an important role in cell cycle and development. Mutations in transcription factors can lead to different diseases like diabetes, autoimmune diseases and cancer. The transcription factor that controls many important cellular processes, such as cell proliferation, differentiation and apoptosis, is the Activator Protein 1 complex [7, 8]. Its structure and function are described in detail in the next chapter.

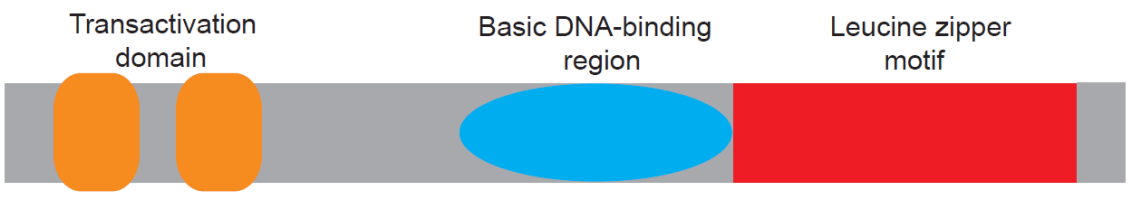

Figure 1.5: The domain structure of Activator Protein 1 transcription factors, composed of the transactivation domain, DNA-binding region and a leucine zipper motif.

4. ACTIVATOR PROTEIN-1

The Activator Protein 1 (AP-1) transcription factor is a dimer complex, composed of JUN, FOS, ATF (activating transcription factor) and MAF (musculoaponeurotic fibrosarcoma) protein families. These include c-Jun, JunB, JunD, c-Fos, FosB, Fra1 and Fra2. Each of these proteins has different functions, which play a crucial role in variety of cellular events, let it be in normal cell development or in cancer [8]. The AP-1 can form hetero- and homodimers by recognizing different DNA sequences and in this way they regulate different sets of genes [9, 10].

All the AP-1 proteins share the same structural domains. They possess a leucine zipper at the carboxy (C) terminal end [11] and contain additional two domains, a DNA-binding and a transactivation domain at the amino (N) terminal end (*Figure 1.6*). The proteins dimerize through their leucine zipper by twisting and forming a so-called coiled coil and then bind to DNA [12, 13]. Next to the leucine zipper is a basic region that serves as a contact to DNA (*Figure 1.6*). Together they form a basic zipper (bZip) domain, which is found in many DNA-binding proteins. To date, over 40 such bZip proteins were discovered in a human genome [14, 15].

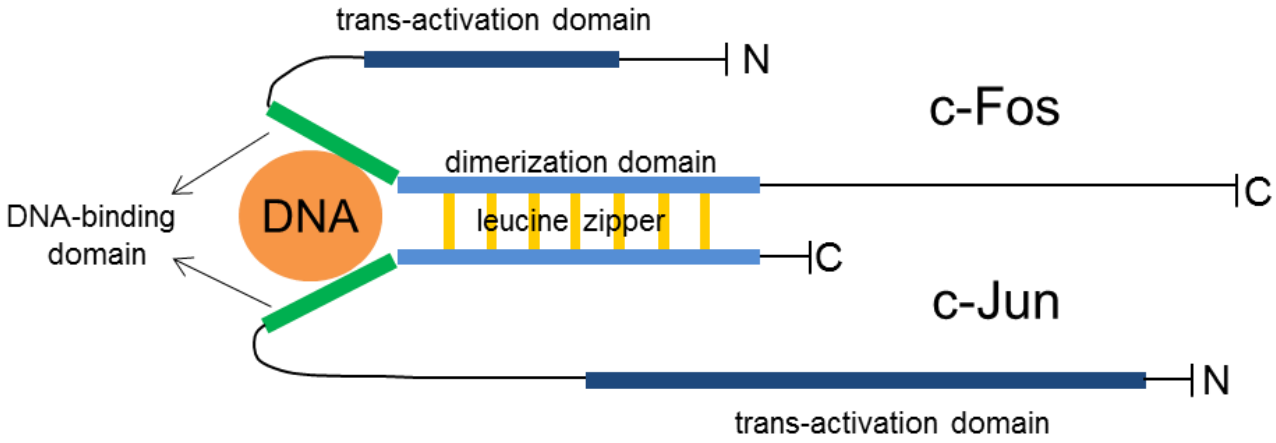

Figure 1.6: The dimeric AP-1 transcription factor is composed of c-Fos and c-Jun proteins. They dimerize through their leucine zipper domain and bind to DNA with their DNA binding domains. The image is adapted from [16, 17].

The activity of the AP-1 transcription factors is induced by a broad range of physiological and pathological stimuli, such as growth factors, stress, cytokines and tumour formation [18]. As AP-1 plays an important role in cell proliferation, signal transduction, oncogenesis and apoptosis, it regulates many aspects of cell physiology in response to the environmental changes. The regulation of AP-1 is complex. It includes different factors like the expression level of each monomer, the composition of dimers and posttranscriptional modification of the protein. The most common posttranscriptional modification that further modulates the activity of the AP-1 transcription factors is phosphorylation [19]. Phosphorylation is involved in the activity of the AP-1 transcription factor by having an influence on the stability, dimerization of the proteins and DNA binding.

The AP-1 binds primarily to the palindromic DNA sequence TGACTCA, which is referred to as the TPA (12-*O*-tetradecanoyl-phorbol-13-acetate) response element (TRE). TRE has been found in the promoter or intron region of many TPA responsive genes [20, 21]. The binding of the AP-1 complex to the TRE sequence is induced by cytokines, growth factors and oncoproteins, which are involved in the proliferation, transformation and differentiation of cells [22]. When c-Jun dimerizes with c-Fos, they bind with high affinity to the TRE element, whereas the c-Jun and ATF2 dimer prefers to bind to the cyclic AMP response element (CRE) [15].

The AP-1 transcription factors are present only in the cell nucleus due to their nuclear localization site (NLS). NLS is an amino acid sequence (positively charged lysine and arginine) that is present in proteins to direct them from cytoplasm, through the nuclear pore complex (NPC) into the nucleus. NLS usually consists of two basic amino acids on the N terminus, followed by a 10 amino acid spacer and a 3 to 4 amino acids on the C terminus [1].

The c-Jun and c-Fos are the main components of the AP-1. c-Jun proteins form homodimers or heterodimers with Fos proteins through their leucine-zipper domains [23, 24]. The crystal structure of c-Fos and c-Jun bZip regions bound to the DNA was determined by x-ray in 1995 [25]. The c-Jun can form dimers with all Jun and Fos related proteins [26 – 33]. *In vitro* studies showed that c-Jun and c-Fos heterodimers are more stable than c-Jun homodimers and have a stronger DNA binding. They bind 25 times more efficiently to the DNA site as a heterodimer as does the c-Jun homodimer [34]. A model of c-Jun and c-Fos dimerization and DNA binding is presented in *Figure 1.7*.

Different studies of AP-1 transcription factors showed that dimerization is necessary for DNA-binding [34, 35]. Later, the kinetic studies, where the association of Jun and Fos was detected by stopped-flow fluorescence resonance energy transfer (FRET) in the absence and

presence of DNA, suggested that the protein monomers prefer to bind to DNA separately and then dimerize [36]. Other studies showed that bZip domain is not required for binding of c-Fos to other cellular components and transcription factors, for example the interaction of Fos to four and a half LIM domain protein 2 (FHL2) [37] and GATA transcription factors [38].

Most recent studies examined the interaction of c-Fos and c-Jun *in vivo* by fluorescence correlation spectroscopy (FCS) [16]. This single-point measurements on a confocal setup indicated that dimerization is a prerequisite to DNA binding. Furthermore, the FRET was used to study the relative position of the C terminus of c-Jun and c-Fos, plus the truncated form of c-Fos [17]. They also performed molecular dynamics simulations (MDS), which were in good agreement to the FRET measurements.

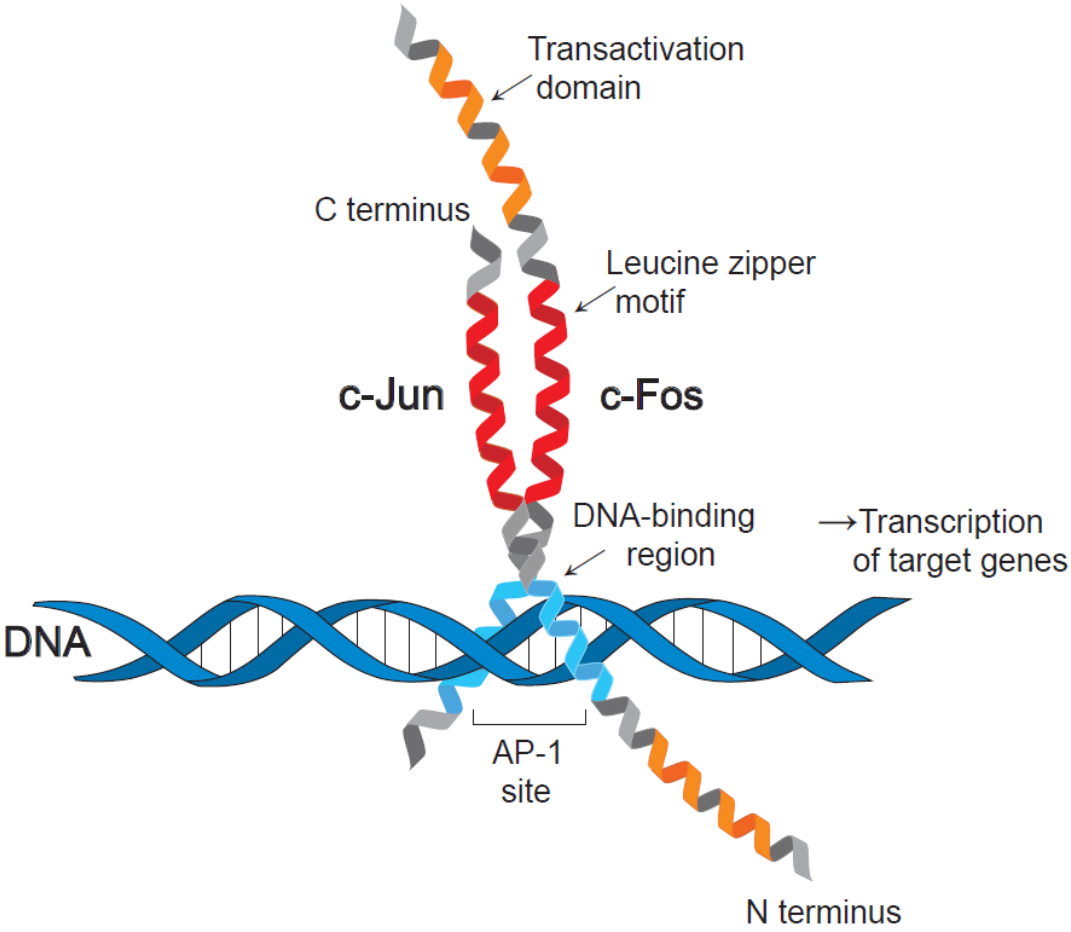

Figure 1.7: A model of c-Fos and c-Jun dimers bound to the AP-1 site on the DNA. The c-Jun and c-Fos transcription factors contain a basic domain for DNA-binding, NLS and leucinne zipper motif at the C terminus.

4.1 c-Jun

The transcription factor c-Jun is probably the best characterized, but also the most critical member of the AP-1 family [10, 14]. Jun was first identified as an oncoprotein encoded by a cellular insert in the genome of avian sarcoma virus 17 in 1987 [39]. It shared the same sequence homology with the Gcn4, which was identified as a protein that has the same DNA binding motif as the AP-1 [40, 41]. This identified Jun as a component of AP-1.

The c-Jun protein is composed of 334 amino acids. At the C terminus there are three main domains, the bZip domain, the DNA binding domain and the transactivation domain, that are present also in other members of AP-1. The bZip motif serves for the dimerization with other partner proteins. The c-Jun can form homodimers with itself or can dimerize with c-Fos to form the AP-1 complex. It can also interact with the ATF transcription factor members by binding to the CRE DNA sequence [15].

All Jun proteins contain a docking site for JNK (Jun N terminal kinase) at the N terminus. The JNK phosphorylates c-Jun and enhances Jun-dependent transcriptional activation. The JNK also distinguishes the c-Jun (cellular Jun) from the v-Jun (viral Jun) [42]. The v-Jun oncoprotein cannot be regulated by JNK, which might be a possible reason for the high oncogenic potential. The binding of c-Jun to the AP-1 binding site in the c-Jun promoter region activates the c-Jun transcription. At the same time, the DNA binding activity of the AP-1 is increased by the phosphorylation at the C terminus and causes an enhanced binding of AP-1 target genes [43, 44].

All AP-1 transcription factors also have an important role in proliferation and cell cycle progression. The cell cycle progression can be regulated by Jun proteins. For example, the c-Jun transcription factor activates the transcription of cyclin D1, a cell cycle promoting gene, and it represses the tumor suppressor gene p53, a cell cycle inhibiting gene [45, 46].

4.2 c-Fos

The transcription factor c-Fos was discovered in rat fibroblasts. An important step in identification of c-Fos was the discovery that c-Fos binds to the same DNA recognition sequence as c-Jun [28, 30]. The c-Fos is, like c-Jun, involved in many cellular processes like proliferation, differentiation, transformation and apoptotic cell death [19]. The expression of c-Fos is rapidly increased upon a variety of stimuli, including growth factors, cytokines, physical and environmental stress. Both c-Jun and c-Fos are involved in the tumorigenesis [22, 47]. The

c-Fos and c-Jun co-operatively repress the Fos promoter. These modifications can take place in the nucleus or in cytoplasm, but occur more frequently in the cell nucleus [48].

The structure of c-Fos is similar to Jun proteins. The c-Fos contains a DNA binding domain and a bZip domain that mediates interactions with other proteins. The leucine zipper is also required for the dimerization with c-Jun [34, 35, and 49]. The c-Fos contains multiple transactivation modules in the N and C terminus. The phosphorylation of c-Fos is responsible for the increased supression of transcription, also when this phosphorylation doesn't harm the ability of c-Fos to dimerize or bind to DNA *in vitro* [50, 51]. Additionally, the activity of c-Fos is regulated by posttranslational modifications caused by phosphorylation of PKA, PKC, cdc2 and MAPK (mitogen-activated protein kinase). These different kinases influence the DNA binding activity, the stability and the transactivating potential of the c-Fos protein [50].

5. MOBILITY IN LIVING CELLS

A cell is a complex structure and its interior can be seen as a space filled with liquid (cytoplasm) and containing molecules (e.g. proteins, DNA, RNA), single ions (e.g. sodium) and also bigger cellular organelles (e.g. the nucleus). The cytoplasm can be thus considered as a molecularly crowded environment, as the macromolecules inside occupy around 30% of the volume. Different structures, like cytoskeletal filaments, mitochondria and endoplasmic reticulum can severely restrict the movement of macromolecules in such an environment. Similar motion restrictions can be observed in the cell nucleus, where the mobility of macromolecules is influenced by the nucleosol and a solid matter, such as chromatin [1].

The barrier between the cell and the outer environment is the cell membrane. It regulates which materials can be exported from the cell and also which substances the cell can receive from outside. Cells have evolved different ways of transporting specific molecules and ions across their membranes to absorb the essential nutrients, eliminate metabolic waste products and balance the intracellular ion concentrations.

The cell function depends on chemical reactions of the molecules inside the cell. These reactions are generally catalyzed by proteins and are located close to cellular structures. Transport allows cells to absorb and release compounds in accordance with its biological function. Particular type of cellular transport depends on the size of the substance and the direction of its concentration gradient, which means that the cell needs to pump from areas of low to high concentrations. As reactions and cell transport are essential and vital functions of cells, there understanding is of utmost importance.

There are two main modes of transport in cells. First, cell transport can be an active process that requires energy. Cell needs to use energy to maintain a proper balance of molecules and ions. Often proteins have to work against a concentration gradient. Active transport involves movement of molecules from regions of low to regions of high concentration, and needs energy for this type of transport (usually energy in the form of ATP). This kind of transport mostly happens when individual molecules are moving across the cell membrane [2].

Second, transport can be a passive process that does not require energy. The dominant transport process is diffusion. Diffusion is a tendency of molecules to spread from regions of high to low concentrations. One example is osmosis, a particular type of diffusion that involves the transport of water across a selectively permeable membrane, going from areas of high water concentration to areas of low water concentrations. More about diffusion and its properties is given in the next chapter.

5.1 DIFFUSION

Diffusion is the random motion of molecules caused by Brownian motion. Molecules will move from the more concentrated region to where it is less concentrated. The simplest mathematical description of diffusive processes can be defined by the diffusion coefficient. The diffusion coefficient unit $\mu m^2/s$ describes how far a particle may reach due to its diffusive motion. The diffusion coefficient characterizes the speed of a particle and it contains information about the size of the moving particle. The diffusive processes can take place in different and very complex environments. Basically, we can distinguish two different types of diffusion: a normal diffusion and an anomalous diffusion that may occur due to molecular crowding in a cell.

5.1.1 NORMAL DIFFUSION

In cells, the particles move around in constant random motion and through the gel-like environment of the cytoplasm. In most transport processes in living cells the particles move in solution with a random Brownian motion. Collisions with neighboring molecules cause constant motions of the particles. In a simple solution like water, the particles collide with water molecules and will thus be moved in random directions. Each collision slightly changes the direction and velocity of the particle. Such behavior leads to a random trajectory $\vec{r}(t)$ that may

be characterized by the mean squared displacement (MSD) $\langle r^2 \rangle$ of a particle and will increase linearly with time t:

$$\langle r^2 \rangle \propto t \tag{5.1.1}$$

Here r is the distance from the starting point at t=0 and $\langle\ \rangle$ indicates the average. This MSD is a linear function of time and describes the amount of space the particle may cover in a given time t. For example, in the same time t, a fast and a slow particle will cover different amounts of space. The faster the particle moves, the larger is its MSD. The random walk can then be characterized by a linear MSD (normal diffusion, *Figure 1.8*) in terms of diffusion coefficient D and described by the time t as:

$$\langle r^2 \rangle = 2d \cdot D \cdot t \tag{5.1.2}$$

where D is the diffusion coefficient of the particle that moves in a d-dimensional space. This equation determines the distance a particle makes within a given time, and the relation of MSD to diffusion coefficient implies that the faster the particle moves the larger will be the diffusion coefficient. Typically, intermediate sized proteins inside cells have a diffusion coefficient between 10 – 100 μm²/s.

The diffusion coefficient is associated with the characteristics of the particles and the medium they move in. The diffusion coefficient of spherical particles with hydrodynamic radius R_h can be described by the Stokes-Einstein equation:

$$D = \frac{k_B \cdot T}{6\pi \cdot \eta_{visc} \cdot R_h} \tag{5.1.3}$$

Where k_B is Boltzmann's constant, T is the absolute temperature and η_{visc} is the viscosity of solution in which the particles move. R_h is the hydrodynamic radius of the particles, which is the radius of a comparable sphere with the same diffusion coefficient as the given molecule [52, 53]. The Stokes-Einstein relation (*Equation 5.1.3*) allows us to quickly and accurately estimate the diffusion coefficients of a typical molecule inside a cell [2].

Diffusion gives information about the dynamical properties of particles. Diffusion plays an important role and in many cellular reactions the diffusion controlled. The restriction of space inside a cell greatly influences the movement of particles. Each of different protein species

exists in a small number, but the small cell volume helps to preserve a high molecule concentration. Due to this small cell volume large molecules and objects may be greatly restricted in movement. Their diffusion can differ from the diffusion of smaller particles [52].

5.1.2 ANOMALOUS DIFFUSION

The normal diffusion may be hindered in case of a restricted and densely crowded environment. The restricted and complex space in cells prevents the particles to move like in in a simple liquid where normal diffusion can be observed. The diffusion may no longer be described as particles colliding with small water molecules, but can be presented as an assortment of small and big sized particles colliding with each other, or as particles binding to different structures within the cell. Hindered, anomalous diffusion affects the biochemical reactions. The MSD of a random walk in d-dimensions has then a non- linear relationship to time in contrast to the normal diffusion process demonstrated in *Equation 5.1.2*. The MSD for the anomalous diffusion can be described as:

$$\langle r^2 \rangle = 2d \cdot \Gamma \cdot t^{\alpha}, \qquad 0 < \alpha < 1 \tag{5.1.4}$$

Here, α is an "anomaly parameter" and Γ proportionality constant. A more densely crowded cellular space does not only reduce the diffusion coefficient, but also influences the behavior of the particles. When α is greater than 1 it leads to super-diffusion, which can be a result of an active cellular transport process and when it is smaller than 1 it leads to sub-diffusion. Sub-diffusion could serve as a measure of macromolecular crowding in the cytoplasm [54 – 56]. When α is 1, *Equation 5.1.4* describes a typical normal diffusion process. *Figure 1.8* shows a comparison of MSD in case of a normal and an anomalous diffusion.

Eukaryotic cells possess internal membranes that encase their organelles and control the exchange of essential cell components. These internal membranes and the space in between enriched with macromolecules greatly affect the diffusion of particles. For example, the nucleus contains chromatin and many proteins involved in the DNA transcription, which can hinder the diffusion [52]. Crowding can also just slow down the diffusion without leading to anomalous diffusion [57, 58].

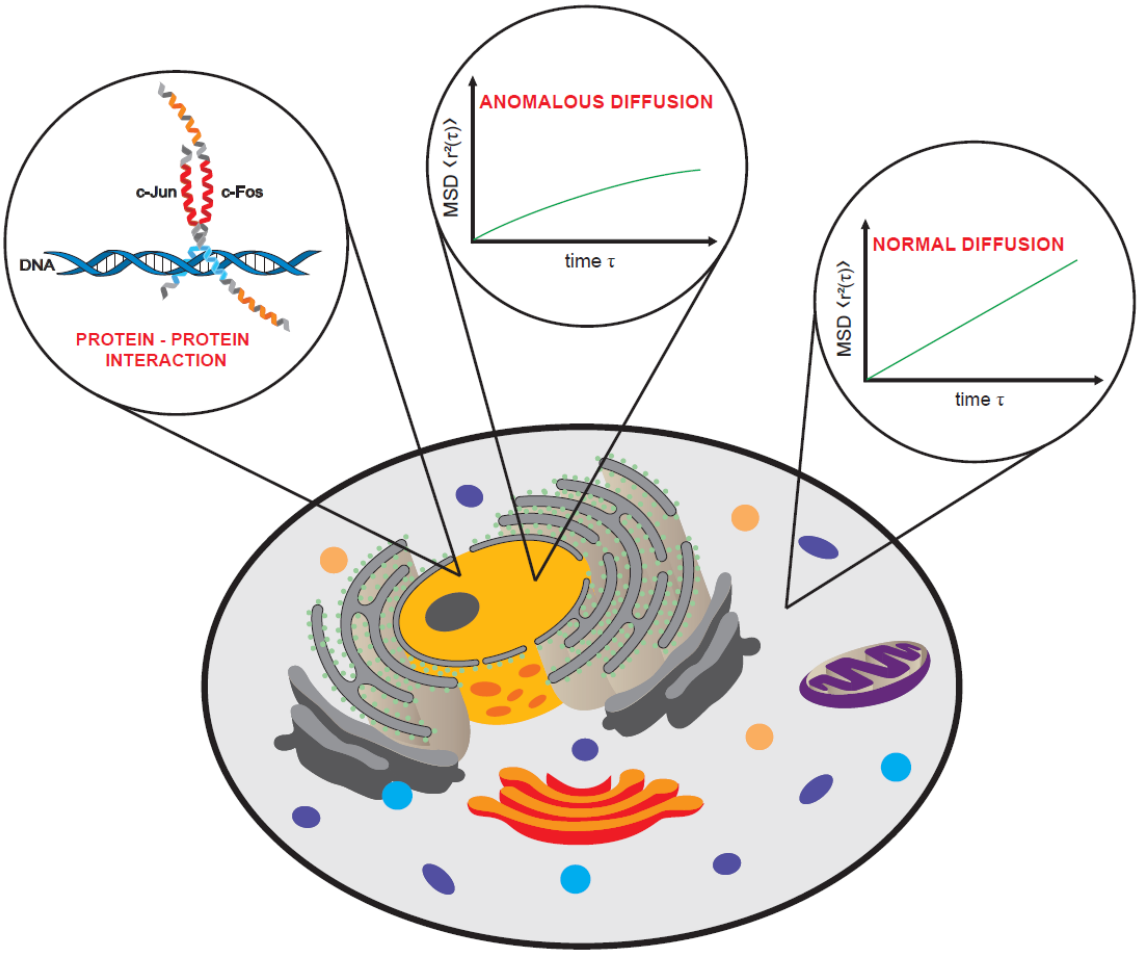

Figure 1.8: A cell indicating interaction of c-Fos and c-Jun transcription factors in the cell nucleus and different types of transport with mean squared displacements. The anomalous diffusion is presented as sub-diffusion with α smaller than 1. The normal diffusion is characterized by a linear MSD dependence to time.

6. MEASURING MOBILITY AND INTERACTIONS IN LIVING CELLS

To get physiologically relevant answers and gather enough information about the diffusion processes, studies need to be performed in live cells. There are several experimental techniques that can be used to measure cellular transport processes and biomolecular interactions *in vivo*. To be able to detect such processes and distinguish the molecules from their surroundings, the molecules of interest need to be labeled. There is a wide range of available dyes with different excitation and emission spectra, but most techniques use fluorescence molecules as labeling tags.

A widely used measurement method is fluorescence correlation spectroscopy (FCS), which is based on analysis of the fluorescence intensity caused by diffusion of fluorescence particles. Fluorescence correlation spectroscopy enables measurements in individual cells without any interference with neighboring cells. It is mainly used to study the mobility and dynamics of fluorescent proteins in living cells. The technique allows detection of diffusion and interactions between biomolecules through their correlated motion with single-molecule sensitivity. The method is very applicable and has been used to characterize most parts of the cells from organelles, nucleus, cytoplasm and membrane.

6.1 FLUORESCENCE (CROSS-) CORRELATION SPECTROSCOPY

Fluorescence correlation spectroscopy is a method that monitors fluorescence intensity fluctuations of single molecules moving in and out of the observation volume (*Figure 1.9 A*). The fluorescence intensity fluctuates around its mean value due to random motion of the particles. The fluorescence fluctuations are characterized by their auto-correlation function, which gives information about the average number of fluorescence particles and average diffusion time in the observation volume. The method and its theoretical foundations have been first introduced by Magde et al. in 1970s [59, 60]. The theory was established to characterize translational diffusion coefficients and chemical rate constants of fluorescently labeled particles fluctuating through a focused laser beam. Nowadays, systems which are composed of a confocal microscope with a high numerical aperture objective and avalanche photodiodes (APDs) as detectors allow single-molecule detection [61]. In confocal optics, the fluorescently labeled molecules are excited in a small volume by a focused laser beam. The emitted fluorescence is then detected through the same optics and a pinhole to eliminate the out-of-focus signal. Due to the small observation volume created by a laser beam, it is possible to perform measurements inside single living cells.

Typically, there are several molecules present at the same time in the observation focus. The overall particle number $N(t)$ at time t is split into the average number of particles $\langle N \rangle$ and the fluctuations $\partial N(t)$ around the average value: $N(t) = \langle N \rangle + \partial N(t)$. At a concentration *c*, the overall particle number $N(t)$ in the small observation volume of the sample V_{obs} is $N(t) = c(t) \cdot V_{obs}$.

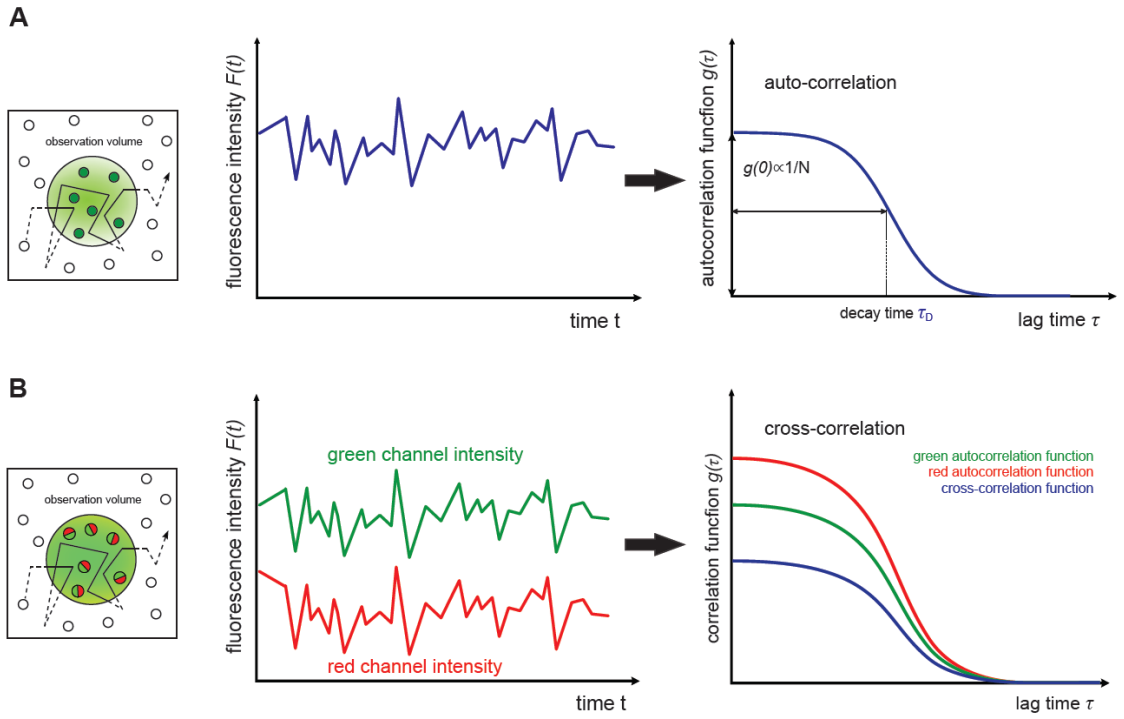

Figure 1.9: The principle of (A) fluorescence correlation spectroscopy (FCS) and (B) fluorescence cross-correlation spectroscopy (FCCS).

The diffusion of fluorescently labeled particles in an out of the detection volume causes random fluorescence intensity fluctuations. Their fluorescence emission causes signal fluctuations that are recognized by a detector. Therefore, the primary data that is obtained in FCS measurements is the time-dependent fluorescence intensity fluctuation $F(t)$ which is proportional to the particle number $N(t)$. The $F(t)$ can therefore also be split into the average $\langle F \rangle$ and the fluctuations $\partial F(t)$. From the detected signal it is now possible to extract the information on how fast the molecules fluctuate in the sample. These fluorescence fluctuations are characterized by a mathematical tool, the autocorrelation analysis. The autocorrelation function $g(\tau)$, which describes the random motion of the fluorophores in V_{obs}, is defined as:

$$g(\tau) = \frac{\langle F(t) \cdot F(t+\tau) \rangle}{\langle F(t) \rangle^2} \qquad (6.1.1)$$

This auto-correlation analysis extracts the characteristic timescale of the fluctuations, which is directly related to the diffusion coefficient of the particle. The quicker are the fluctuations,

the larger is the diffusion coefficient. Observing the concentration fluctuations in a very small volume of known size, it is thus possible to determine its concentration and diffusion coefficient. The diffusion time τ_D of the particle depends on the characteristic size of the observation volume V_{obs} and can be directly measured from the auto-correlation function:

$$g(\tau) = \frac{1}{N} \cdot \left(1 + \frac{\tau}{\tau_D}\right)^{-1} \cdot \left(1 + \frac{\tau}{(\frac{z_0}{w_{xy}})^2 \cdot \tau_D}\right)^{-1/2} \tag{6.1.2}$$

The size of the observation volume is shaped like an ellipsoid and defined by its half-width w_{xy} in the xy-plane and the half-length z_0 in the z-plane. *Figure 1.10* illustrates fluorescence intensity fluctuations and the corresponding autocorrelation functions for fast and slow moving particle. FCS can be used to measure the mobility of fluorescent molecules inside biological structures and living cells to determine their diffusion coefficient and concentration. These can be determined from the correlation curves. The amplitude $g(0)$ corresponds to the inverted number of particles $N(t)$ in the observation volume. From the half amplitude it is then possible to determine the diffusion time τ_D, which differs depending on the size, environment of the particles and their association with other molecules. The next chapter presents some important FCS applications.

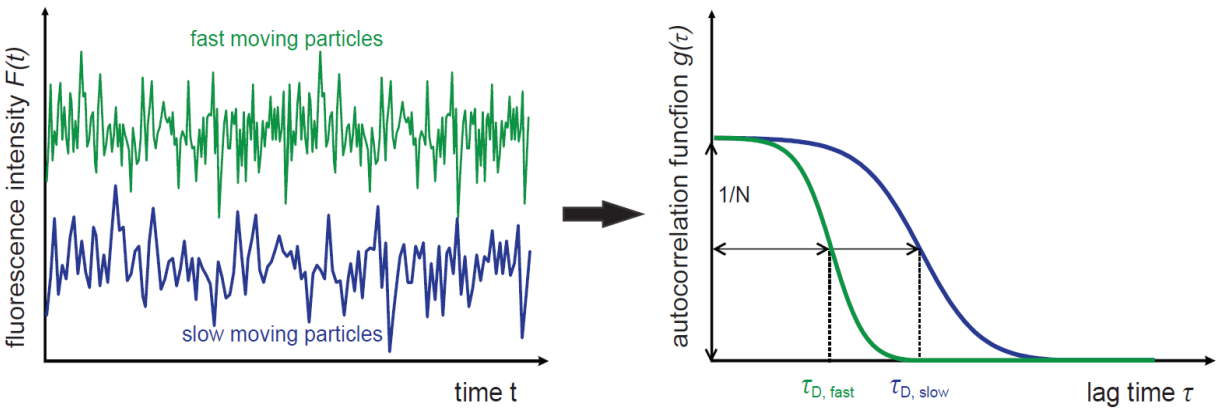

Figure 1.10: Illustration of fluorescence correlation spectroscopy showing the difference in fluorescence intensity fluctuations and thus autocorrelation curves for fast and slow moving particles.

The extension of FCS to fluorescence cross-correlation spectroscopy (FCCS) allows to measure molecular interactions between molecules. FCCS detects the fluorescence from two particles labeled with different fluorophores in the same observation volume. Each fluorescence intensity trace is auto-correlated and the cross-correlation analysis is performed between two fluorescence intensities. When the two molecules interact, the fluorescence intensity traces show correlated fluctuations and result in high cross-correlation amplitude. The method is illustrated in *Figure 1.9 B.*

6.2 TECHNIQUES AND APPLICATIONS

Fluorescence correlation spectroscopy (FCS) is routinely used in live cell measurements to obtain quantitative data on molecular level [62, 63]. The technique (*Figure 1.9 A*) provides information on the diffusion properties and concentrations of the observed molecule. It has been for example used to assess the anomalous diffusion of proteins [57], relevant to reveal hindered motion versus the free random diffusion and to map eGFP oligomer mobility in living cell nuclei, depending on the chromatin compaction level [64, 65].

Its extension to dual-color fluorescence cross-correlation spectroscopy (FCCS) allows measurements and analysis of biomolecular interactions within living cells. Schwille et al. were the first to show the feasibility of two-color FCCS [66]. The method simultaneously detects fluorescence of two molecules labeled with different fluorophores to distinguish them spectrally in the same detection volume (*Figure 1.9 B*). The cross-correlation in the two detection channels reveals the interaction between the two fluorescent molecules. Some of the applications of FCS and FCCS *in-vivo* measurements have been described before [67]. FCCS is particularly well adapted for time-resolved studies of protein-protein interactions. First protein-protein interactions, using two autofluorescent protein-labeled interaction partners, were performed with c-Fos and c-Jun transcription factors in HeLa cells [16]. The results showed their interaction in the cell nuclei and indicated that dimerization is a prerequisite to DNA binding. Other FCCS studies have looked at the interaction and localization of membrane-bound proteins [68, 69].

One of the main problems of confocal FCS is that only single point measurements can be performed at a time within a cell. However, to determine the characteristic spatial or temporal patterns, the measurements must be performed across the whole cell. The earlier solution to this was repeated measurement at different observation points within a cell. However, longer

acquisition times may cause photobleaching and cell damage, which limits the number of measurements that can be reliably taken. In 2010 Wohland et al. proposed a better solution - FCS based on light sheet microscopy (SPIM-FCS) [70].

Light sheet fluorescence microscopy (LSFM) [71, 72] uses a cylindrical lens to form a thin sheet of light to illuminate the sample. The detection is performed perpendicular to the illumination with a second microscope objective, allowing simultaneous imaging of all points in the two-dimensional field of view with a fast camera (*Figure 1.11*). Wohland et al. applied a camera based SPIM-FCS, i.e. imaging FCS, to characterize fluorescent beads moving in the bloodstream of living zebrafish embryos [70]. Imaging FCS allows two-dimensional imaging and thus spatially resolved FCS. SPIM-FCS allows live cell measurements of mobility at many positions simultaneously. First SPIM-FCS live cell measurements were performed on the heterochromatin protein HP1α mobility in the cell nucleus by Capoulade et al. [73], providing high-resolution diffusion maps showing euchromatin areas with heterochromatin-like HP1α-chromatin interactions. Brazda et al. [74] used SPIM-FCS to continue their studies on the nuclear receptors. They measured the interaction of the nuclear retinoid x receptor (RXR) with chromatin and showed that the interaction seems to be homogeneously distributed over the whole cell nucleus.

The extension of SPIM-FCS to dual color SPIM-FCCS and its feasibility was first presented in Krieger et al. [75]. SPIM-FCCS raised the potential to simultaneously observe interactions and mobility throughout the whole image plane and can therefore provide interaction and mobility maps in living cells. They demonstrated the light sheet based FCCS measurements of protein dynamics in the cytosol, membrane and the nucleoplasm in live cells. Recent applications of imaging fluorescence correlation spectroscopy have been summarized by Singh et al. [76].

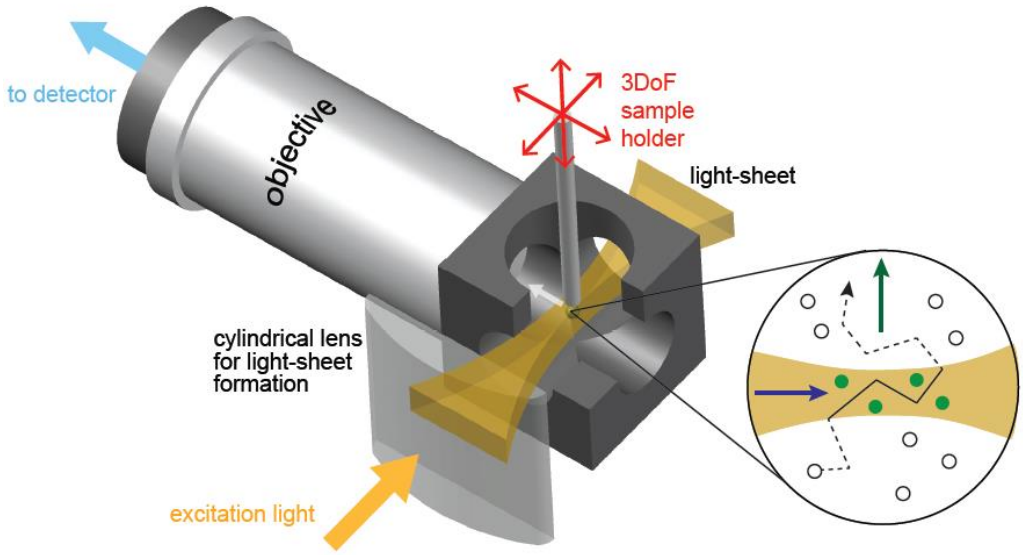

Figure 1.11: The principle of light sheet fluorescence microscope (LSFM). A thin light sheet is formed with a cylindrical lens to illuminate the sample. The fluorescence is collected perpendicular to the illumination with a fast camera.

7. PROBLEM FORMULATION

The regulation of DNA transcription into RNA and its translation into proteins is one of the most important steps determining cell behavior. Transcription factors (TFs), DNA binding proteins, which promote or repress the action of RNA polymerase, control this process. They must enter the cell nucleus and find their specific target site. There is not much known about the molecular events that take place when TFs alone or together with other cellular components exert their function.

To understand the function of TFs, detailed knowledge about their localization, dynamics of binding/dissociation, and translocation to their sites of action in the cell nucleus is required. Due to availability of the autofluorescent proteins like eGFP and mRFP1, and of detection methods with single molecule sensitivity, such as fluorescence correlation and cross-correlation spectroscopy (FCS and FCCS), the dynamics of this cellular processes can be measured. I used these techniques to study the Transcription Activator Protein (AP-1) complex.

AP-1 is a transcription factor and it consists of dimers composed of members of the Fos, Jun and the activating transcription factor (ATF) protein families. Jun proteins form

homodimers or heterodimers with Fos proteins through their leucine-zipper domains. The AP-1 controls many important cellular processes, such as cell proliferation, differentiation, apoptosis and oncogenesis.

The c-Fos and c-Jun were studied before using a confocal FCCS microscope [16] and molecular modelling [17]. The study of the dimerization of c-Fos and c-Jun and their interaction by FCCS showed that the proteins Fos-eGFP and Jun-mRFP1 interact in vivo in the nucleus while they are bound to the DNA. They are located only in the cell nuclei, due to the nuclear localisation sites (NLS) that are present in all full length AP-1 proteins. The results showed two diffusive, decaying components, a fast and a slow component, corresponding to the unbound and bound proteins. The AP-1 deletions mutants, where dimerization and DNA binding domain are deleted showed no interaction. The combination of data with molecular modeling gave a structure model for the fluorescently labeled Fos-Jun dimer and their deletion mutants.

The aim of this thesis is to further characterize the behavior of c-Fos and c-Jun transcription factors in live cells. Using a light sheet microscope in combination with a fast electron multiplying charge coupled device (EM-CCD) camera, I could detect the dynamics of both proteins respectively and spatially resolve the protein-protein interactions throughout the whole cell nucleus. I show SPIM-FCCS maps of live cells expressing the c-Fos and c-Jun transcription factors. This method allows diffusion coefficient and protein-protein interactions measurements simultaneously in the whole image plane, instead of single point measurements in conventional confocal FCS. Now, one can localize the regions where the TFs bind to DNA and learn about the interaction mechanism: do TFs associate first before binding to DNA or do TFs bind directly to DNA, what are the differences in interactions within the nucleus and do these interactions change if one uses TF mutants. To do this, I examined the correlation between their diffusional mobility and interaction. I show the first 2D mobility and interaction maps of c-Fos-eGFP and c-Jun-mRFP1 transcription factors in live HeLa cell nuclei and find a strong correlation between diffusional mobility and interaction.

For control measurements, cells producing the two-color fusion protein eGFP-mRFP1, and eGFP and mRFP1 that are expressing eGFP and mRFP1 simultaneously but separately. Another control measurement was performed with c-Fos and c-Jun mutants lacking dimerization and DNA-binding domains. All results are given as diffusion and interaction maps, as well as correlation controls between the diffusion coefficient and interaction.

II. MATERIAL AND METHODS

1. THEORY

1.1 FLUORESCENCE

Fluorophores play the central role in biological imaging and fluorescence spectroscopy. A fluorophore causes a molecule to absorb energy of a specific wavelength and emits energy at a different, but identically specific wavelength. The wavelength and amount of the emitted energy depend on the fluorophore, as well as its environment [77]. Fluorescence is then a property where a molecule or a part of a molecule emits light at a specific wavelength when it is irradiated by light. Fluorescence has been used to create images in microscopy since the 1940's, but the arrival of the laser scanning confocal microscope in the late 1980's raised a greater interest in using fluorescent molecules in microscopy [78].

The different energy levels involved in the fluorescence process can be illustrated with the Jablonski diagram (*Figure 2.1*). The diagram shows the different energy levels of the electrons and the jumps between these states in fluorescence. The energy spectrum is divided into electronic states: the ground state S_0 and the exited states S_1, S_2, etc. Within each electronic state there are multiple vibrational states and each of these states can be further divided into rotational energy levels. The Jablonski diagram presented in *Figure 2.1* omits such detailed demonstration of the energy spectrum and shows only the electronic and vibrational states.

When a fluorophore absorbs a photon of wavelength λ_{ex}, it takes up its total energy. The energy required for this electronic transition can be given by a photon of the appropriate frequency. This is described by the Planck relation, where the energy is proportional to its frequency ν_{ex} and inversely proportional to its wavelength λ_{ex}:

$$E_{photon} = h\nu_{ex} = \frac{h \cdot c_0}{\lambda_{ex}} \tag{2.1}$$

where h is the Planck's constant and c_0 is the speed of light in vacuum [79, 80].

When the electron is excited with light of suitable wavelength, the fluorophore typically resides in one of the vibrational levels of an excited singlet state [77]. When excited by the right wavelength of light, some of the molecules will absorb a photon of sufficient energy to lift an electron from the ground state energy level (S_0) to the excited state energy level (S_1) as shown in *Figure 2.1*. There are a number of vibrational levels within the excited state. The electronic transition from one vibrational energy level to another will most likely occur if the two vibrational wave functions overlap [77]. The excited electron quickly drops to the lowest vibrational level within the same excited state and down to the ground state resulting in the emission of a photon of light. The fluorescence is a direct route to get from the excited state back to the ground. The light that excites the electron has a shorter wavelength and therefore higher energy than the emitted light. This is due to energy loss of the electron when it drops through vibrational levels when it is in the excited state [77, 79 and 81].

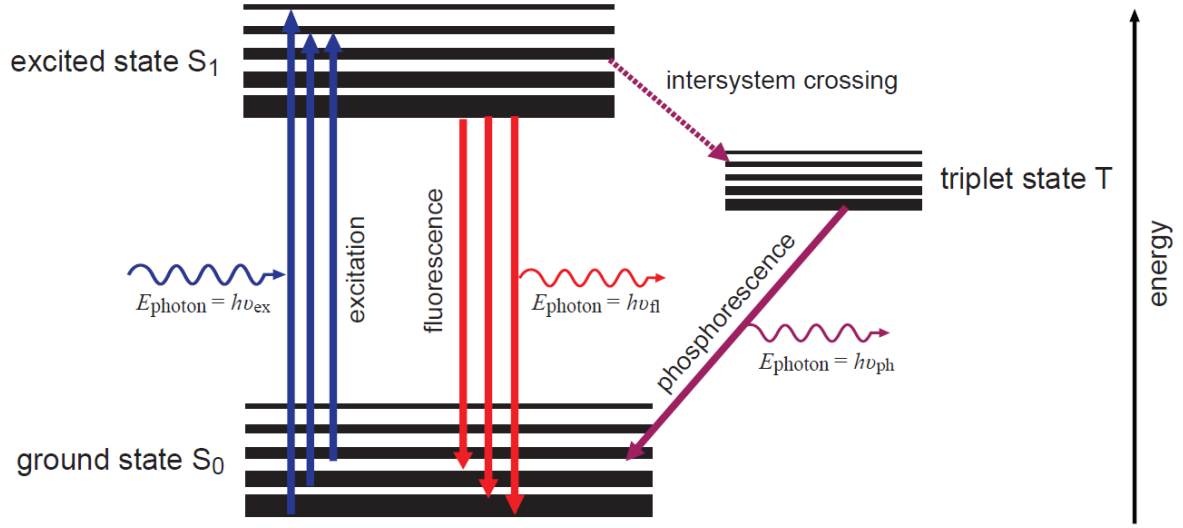

Figure 2.1: Jablonski diagram: An electron (fluorescent molecule) is promoted from the ground state S_0 to a higher energy state (S_1) by the absorption of a photon of energy $h\nu_{ex}$ (excitation). The released energy is converted into vibrations. There are two ways for the electron to return to its ground state S_0. The direct route to the ground state is by emission of a photon of energy $h\nu_{fl}$ and has the greatest statistical probability (fluorescence). The other possibility is the decay in the triplet state T which the electron can reach without emission of radiation (intersystem crossing). The return to the ground state is accompanied by the emission of a longer wavelength light as fluorescence and is called phosphorescence [77].

The described pathway is not the only possibility for the energy release. An excited electron can also decay from the singlet to the triplet state T, which the electron can reach without emission of radiation (intersystem crossing). The decay of the photon back to a singlet ground state is known as phosphorescence. The transition of the electron through the triplet state is a slower process than the direct route from the exited to the ground state. Due to the long lifetime of the triplet state, triplet states are, compared to singlet states, more often involved in photo-chemical reactions [77]. This process is called photo-bleaching. The fluorophore can permanently lose the ability to fluoresce due to an irreversible reaction that dramatically changes its absorption and emission capabilities. In microscopy, photo-bleaching can damage the fluorophores and therefore disturb the observation of fluorescent molecules.

The absorption process can be described by the Lambert-Beer law, which is expressing how light is absorbed by matter (liquid, gas or solid). This relation can be used for determining the sample concentration. The law states that the amount of light passing through the sample is diminished by the probability of how strong the sample absorbs light at a given wavelength, the sample concentration and the distance the light makes through the sample, and can be written in terms of the absorption *A*:

$$A = \log\left(\frac{I_0}{I}\right) = \varepsilon \cdot c \cdot L \tag{2.2}$$

Here, I_0 and I are the incident and transmitted intensities, respectively ε is the molar absorptivity coefficient given in units $M^{-1}cm^{-1}$, c the sample concentration and L the optical path length, given in molarity M and cm, respectively [77].

1.2 FLUORESCENCE CORRELATION SPECTROSCOPY (FCS)

Basics of Fluorescence correlation spectroscopy (FCS) have been already described in the Introduction, section 6.1 [59, 60]. FCS measures the fluorescence intensity of the fluorescent molecule fluctuations through a small, sub-femtoliter observation volume. The focal measurement volume is produced by a laser that illuminates the sample containing fluorescently tagged target molecules. The molecules move in and out of the focus and create bursts of fluorescence photons that can be detected with sensitive detectors. *Figure 2.2* illustrates the principle of FCS.

FCS is a statistical method and is based on analyzing the fluorescence fluctuations. The primary data obtained is the time-dependent fluorescence intensity $F(t)$, which is proportional

to the particle number $N(t)$ in the observation volume at time t. $N(\mathrm{t})$ is constantly fluctuating around the mean value $\langle N \rangle$ due to the diffusive particle motion. It can be therefore described as:

$$N(t) = \langle N \rangle + \delta N(t) \rightarrow F(t) = \langle F \rangle + \delta F(t) \tag{2.3}$$

Here $\delta N(t)$ and $\delta F(t)$ are the fluctuations of the number of particles and the fluorescence intensity, respectively, and the brackets $\langle\ \rangle$ symbolize the average. The particle motion can be slower or faster, depending on the size of the particle. If a small molecule binds to a larger one, it hinders the speed of motion and emits photons for a longer time during its diffusion through the observation volume. The relative fluctuations increase with decreasing number of particles. Therefore, for higher concentrations, an observation volume as small as possible has to be created [82, 83].

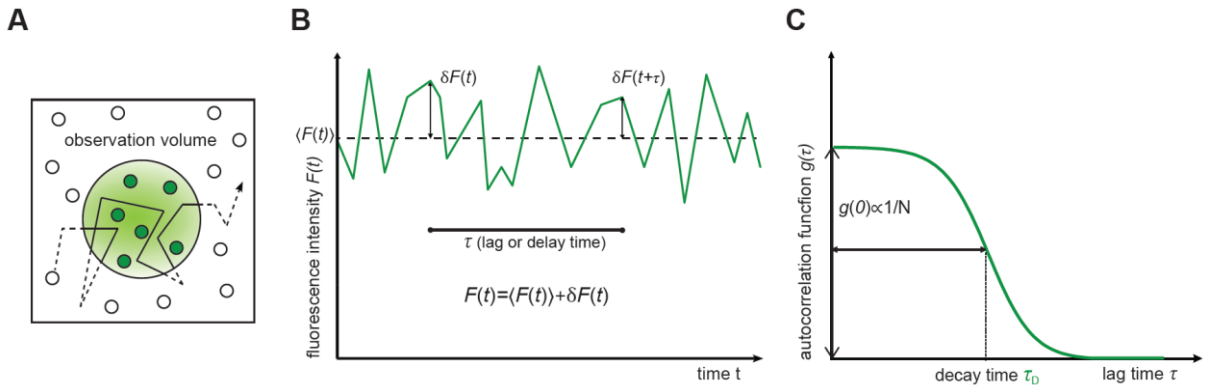

Figure 2.2: The principle of fluorescence correlation spectroscopy (FCS). (A) An illustration of fluctuating particles and a trace of a molecule traveling through the observation volume. (B) A representative fluctuation trace with the definitions of parameters applied in *Equation 2.4*. The intensity is fluctuating around the mean intensity $\langle F(t) \rangle$. (C) Autocorrelation function $g(\tau)$ calculated from the intensity trace in (B). The decay time of the autocorrelation function is defined by $g(\tau_D) = g(0)/2$ and the zero-lag amplitude $g(0)$ is inversely proportional to the number of particles in the observation volume.

Fluorescence fluctuations are characterized by their auto-correlation function $g(\tau)$ that describes the random motion of the fluorophores. The auto-correlation function transforms the data from the measured time domain to the correlated time domain, which tells us how fast the fluctuations are. The auto-correlation analysis provides a measure of the self-similarity of a

time serial signal $F(t)$ if compared to its variant $F(t+\tau)$ after a delay time τ. The normalized FCS auto-correlation function of a fluctuating signal $F(t)$ is defined as [62]:

$$g(\tau) = \frac{\langle \delta F(t) \cdot \delta F(t+\tau) \rangle}{\langle F \rangle^2} = \frac{\langle F(t) \cdot F(t+\tau) \rangle}{\langle F \rangle^2} - 1 \tag{2.4}$$

The mean value $\langle\ \rangle$ is defined as a time average:

$$\langle F(t) \rangle = \frac{1}{T} \cdot \int_0^T F(t) dt \tag{2.5}$$

Here $\delta F(t)$ and $\delta F(t+\tau)$ are the amplitudes of fluctuations from the mean at time t and $t+\tau$, respectively, and $\langle F \rangle$ is the mean value of the signal (*Figure 2.2*). The time τ is the delay time (or lag time), presenting the time over which the fluctuations are compared. If we observe the fluctuations at $\delta F(t)$ and $\delta F(t+\tau)$ with a small delay time τ, the signal does not significantly change and the auto-correlation function is high. If the delay time is longer, there is no correlation between the signal at $t+\tau$ and the auto-correlation function approaches 0.

The auto-correlation function is the Fourier transform of the power spectrum. To extract conclusions and gain quantitative information, the measured auto-correlation function $g(\tau)$ has to be fitted to a mathematical model. When the appropriate mathematical model is known, the information about the photo-physics that cause the characteristic fluorescence intensity fluctuations can be extracted from the auto-correlation function. There are two important pieces of information that can be obtained rather precisely from the auto-correlation function: the diffusion time and the number of particles in the observation volume. To obtain these quantities, the theoretical model has to contain these quantities as free parameters.

The diffusion time τ_D is the average time the molecule travels through the observation volume. The half-life of the auto-correlation function corresponds to the average time of the particle in the focus and is defined as $g(\tau_D) = g(0)/2$. It tells us how long did the fluctuating molecule stay in the observation volume. The diffusion coefficient *D* can be easily derived from the characteristic diffusion time of the auto-correlation function. The diffusion time τ_D is given by the size of the focus and the diffusion coefficient of the molecule [62]:

$$\tau_D = \frac{w_{xy}^2}{4D} \tag{2.6}$$

where τ_D is the diffusion time, D is the diffusion coefficient and w_{xy} is the lateral radius of the detection volume determined by calibration of the system using a dye with a known diffusion coefficient. The average time that molecules stay within the observation volume depends on their size. The diffusion coefficient is related through the Stokes-Einstein equation (*Equation 5.1.3* in Introduction) with the particle size, the absolute temperature and the viscosity of solution in which the particles move. By a FCS measurement, the diffusion coefficient can be determined and therefore the size of fluorescently labeled molecules.

The average number of particles $\langle N \rangle$ in the observation volume is determined from the zero-lag amplitude $g(0)$ of the auto-correlation function (*Equation 2.4*). *Figure 2.2* illustrates that the auto-correlation amplitude is inversely proportional to the average number of particles $\langle N \rangle$ detected in the observation volume [62]:

$$g(0) = \frac{1}{\langle N \rangle} \tag{2.7}$$

If the size of the focus is known, its effective volume V_{eff} can be estimated and the concentration c of the fluorescing molecules can be determined [62]:

$$c = \frac{N}{V_{eff}} \tag{2.8}$$

The fluorescence intensity fluctuations will be longer for lower concentrations of the molecules. Depending on the average particle number, the shape of the auto-correlation function $g(\tau)$ changes. Different example curves are illustrated in *Figure 2.3*. The amplitude of the auto-correlation function decreases for increasing particle number N. Fast diffusing particles will have a shorter diffusion time than the slow diffusing particles. The diffusion time τ_D increases and the decay of the auto-correlation curve shifts to the right. By visual inspection of the FCS curve, it is possible to read off the approximate particle number and the decay time of the molecule [82, 83].

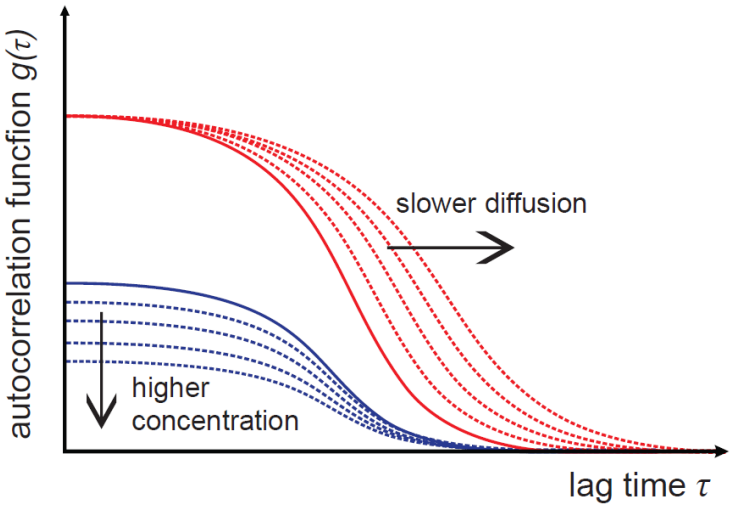

Figure 2.3: The auto-correlation function $g(\tau)$ is calculated from the intensity traces produced by the diffusion of labeled particles through the observation volume. The characteristic decay time of $g(\tau)$ shows the mobility of the particles (red curves) and the inverse amplitude $g(0)$ is proportional to the particle concentration (blue curves) in the observation volume.

1.3 FLUORESCENCE CROSS-CORRELATION SPECTROSCOPY (FCCS)

Dual-color fluorescence cross-correlation spectroscopy (FCCS) detects the fluorescence at two distinct wavelengths in the same observation volume (*Figure 2.4*) [66, 84]. Two spectrally different dyes are excited using two overlapping laser beams and separate detection pathways. Here, the cross-correlation function is calculated as:

$$g_{gr}(\tau) = \frac{\langle \delta F_r(t) \cdot \delta F_g(t+\tau) \rangle}{\langle F_r(t) \rangle \cdot \langle F_g(t) \rangle} \tag{2.9}$$

Typical experiments use green and red fluorescent dyes, therefore the subscripts *g* and *r* are used to denote the two channels. The difference between the auto-correlation function and the cross-correlation function is that with the cross-correlation we relate the fluorescence of the molecule $\langle F_r(t) \rangle$ at time t to the fluorescence of molecule $\langle F_g(t) \rangle$ at various times τ later. The cross-correlation function is measured along with the green and red auto-correlation functions.

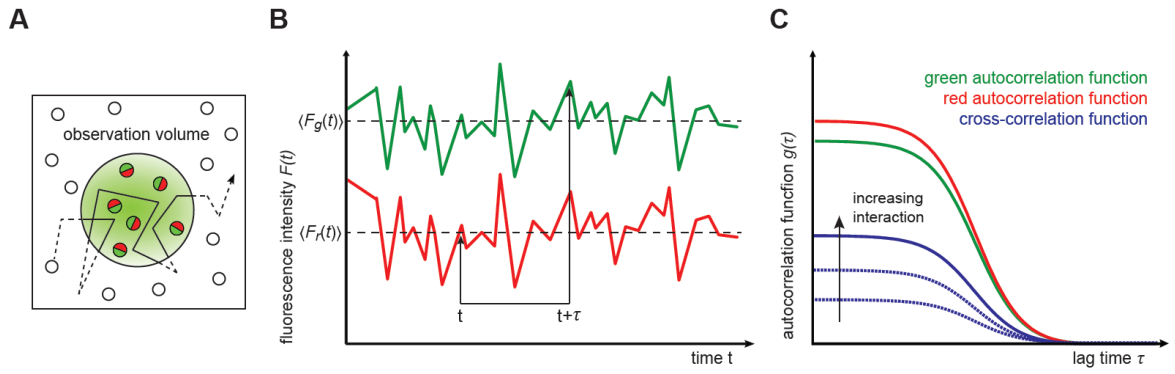

Figure 2.4: The principle of two-color fluorescence cross-correlation spectroscopy (FCCS). Two spectrally distinct fluorophores produce fluctuating intensity traces in the respective color channels. Each intensity trace is auto-correlated (green and red curves) and their cross-correlation function (blue curve) is computed. The cross-correlation amplitude determines the degree of binding between the two fluorophores.

Dual-color cross-correlation is a powerful tool to investigate interactions between different molecules. The cross-correlation function of intensity fluctuations in two different channels (the green and the red channels) shows the amount of binding between the two fluorescently labeled molecules. Typically, the green-labeled and red-labeled particles diffuse at approximately the same rate. When the particles diffuse simultaneously, there is interaction between the fluorescence signals $F_r(t)$ and $F_g(t)$, which results in a high cross-correlation amplitude $g_{gr}(0)$ (*Figure 2.5 A*). If the particles diffuse independently, there is no interaction between the particles, the fluorescence signals $F_r(t)$ and $F_g(t)$ are non-correlated and the cross-correlation amplitude is close to 0 (*Figure 2.5 B*) [66, 84].

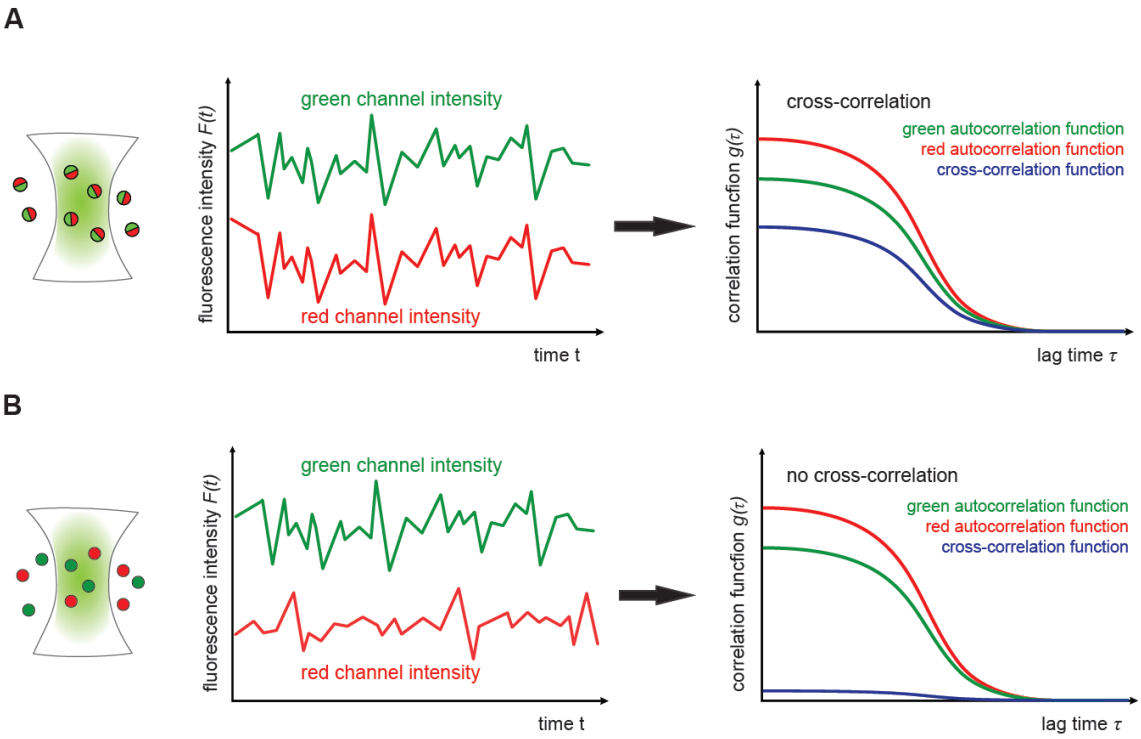

Figure 2.5: Two-color fluorescence cross-correlation spectroscopy (FCCS). (A) Double-labeled molecules: The fluorescence intensity traces correlation results in high cross-correlation amplitude. (B) Single-labeled molecules: The fluorescence non-correlated intensity traces result in cross-correlation amplitude close to 0.

In FCCS, the amount of binding between two fluorescently labeled molecules can be obtained by measuring the cross-correlation amplitude $g_{gr}(0)$. This amplitude is proportional to the concentrations c_A, c_B and c_{AB}, which represent the green, red and double-labeled species, respectively. From these concentrations, the amount of binding presented as relative concentration p_{AB} of species AB can be calculated:

$$p_{AB} = \frac{c_{AB}}{c_A + c_B + c_{AB}} \tag{2.10}$$

The amount of binding can also be defined as the relative cross-correlation (CCF) amplitude q and can be calculated by dividing the cross-correlation function by the smaller of the two auto-correlation functions:

$$q = \frac{g_{gr}(\tau)}{min[g_{gg}(\tau), g_{rr}(\tau)]} \tag{2.11}$$

where τ is the minimum delay time. In this Thesis, the latter was used to measure interaction for the confocal FCCS measurements. For the SPIM-FCCS measurements, the relative concentration p_{AB} was used as a measure of binding, because the amplitudes could not be precisely determined due to temporal resolution of the camera.

Fluorescence correlation and dual-color cross-correlation spectroscopy are ideal analytical tools to study concentrations, transport and mobility properties and interactions of molecules in living cells [67, 85 – 90]. They are typically confocal microscope-based methods, where it is possible to measure at a single position [83]. The recently re-discovered single plane illumination microscopy (SPIM) technique has emerged as a great tool for FCS and FCCS measurements [70]. SPIM is an imaging method that allows simultaneous measurements in the whole image plane. In order to determine the mobility and interaction properties of the molecules, the measured data needs to be fitted to a theoretical model. The models used in this Thesis are described in the next chapter. The details about the confocal and SPIM microscopy are described in Chapters 3.1 and 3.2, respectively.

1.4 THEORETICAL MODELS AND FITTING ALGORITHMS

For the FCS and FCCS analysis, a theoretical function has to be fitted to the auto- and cross-correlation functions to yield the information about diffusion, concentration and interaction of the fluorescent molecules. The goal is to use mathematical models that on one side are simple enough to fit the data with sufficient reliability, and on the other side complex enough to yield all the parameters that are necessary to understand the system. The fitting model typically includes one or two diffusion components. Auto- and cross-correlation functions obtained by confocal and SPIM microscope measurements have been fitted to a model function using the Marquardt-Levenberg algorithm implemented in the in-house developed software *QuickFit 3.0* [91].

1.4.1 CONFOCAL FCS

To analyze the auto-correlation function $g(\tau)$, a theoretical model needs to be fit to the measured auto-correlation function. For single component three-dimensional Brownian motion, a single component model equation of the auto-correlation function $g(\tau)$ is used to fit the curve:

$$g(\tau) = \frac{1}{N}\left(1 + \frac{4D\tau}{w_{xy}^2}\right)^{-1} \cdot \left(1 + \frac{4D\tau}{z_0^2}\right)^{-1/2} \tag{2.12}$$

where w_{xy} is the half-width in the xy-plane and z_0 is the half-length in the z-plane of the focal volume shaped like an ellipsoid as illustrated in *Figure 2.6* [78]. To exactly determine the diffusion coefficient D, the size of the focal volume needs to be known. Knowing the size of the focus, the effective volume V_{eff} is determined as:

$$V_{eff,confocal} = \pi^{3/2} \cdot w_{xy}^2 \cdot z_0 = \pi^{3/2} \cdot \gamma \cdot w_{xy}^3 \tag{2.13}$$

The size of the focus w_{xy} is determined by a calibration measurement of a solution with a known diffusion coefficient. The γ is a structure factor defined as $\gamma = z_0/w_{xy}$. It has been determined for our setup from an image stack of immobile particles and fixed to 6 during data evaluation. A careful calibration procedure of the microscope needs to be performed before and after the measurements to ensure the focal volume has not changed.

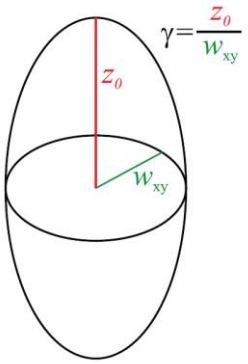

Figure 2.6: An illustration of the laser focus of a confocal microscope. The ratio between the lateral radii w_{xy} and the axial radii z_0 gives the structure factor γ.

Knowing the structure factor γ , the auto-correlation function for normal diffusion FCS can be re-written as:

$$g(\tau) = \frac{1}{N} \cdot \left(1 + \frac{\tau}{\tau_D}\right)^{-1} \cdot \left(1 + \frac{\tau}{\gamma^2\tau_D}\right)^{-1/2} \tag{2.14}$$

When we measure a mixture of molecules with different diffusion coefficients, the auto-correlation function $g(\tau)$ is a sum of contributions of individual species. The measured data was fitted using a 2-component normal diffusion model, meaning that two distinct populations of molecules, a slow and a fast component, could be detected based on their diffusion properties.

The fraction of the diffusion component ρ represents how much of each component is present in the system. The $g(\tau)$ can then be defined as:

$$g(\tau) = \frac{1}{N} \cdot \begin{pmatrix} \rho_1 \cdot \left(1 + \frac{\tau}{\tau_{D1}}\right)^{-1} \cdot \left(1 + \frac{\tau}{\gamma^2 \tau_{D1}}\right)^{-\frac{1}{2}} + \\ \rho_2 \cdot \left(1 + \frac{\tau}{\tau_{D2}}\right)^{-1} \cdot \left(1 + \frac{\tau}{\gamma^2 \tau_{D2}}\right)^{-\frac{1}{2}} \end{pmatrix} \tag{2.15}$$

Most of the FCS studies are focused on measuring the mobility and concentration of the molecules, but beside molecular motion, there are other fluctuations to contend with. The most frequently observed is the triplet behavior, which was mentioned before in the chapter about fluorescence. The transition of the excited molecule into the triplet state (intersystem crossing) appears as a series of dark intervals that can continuous interrupt fluorescence emission of the particles as they move through the detection volume. The FCS autocorrelation function then changes and is extended by a triplet component [92, 93]:

$$G(\tau) \rightarrow G(\tau) \cdot T(\tau) \tag{2.16}$$

$G(\tau)$ is the previously defined autocorrelation function and $T(\tau)$ is a triplet component defined as:

$$T(\tau) = \frac{1 - \Theta_{trip} + \Theta_{trip} \cdot exp^{\frac{\tau}{\tau_{trip}}}}{1 - \Theta_{trip}} \tag{2.17}$$

The τ_{trip} is the decay time of the triplet component and Θ_{trip} is the fraction of the particles in the triplet state. *Figure 2.7* illustrates the effect of the triplet on the FCS autocorrelation function. The decay time τ_{trip} is typically much faster than the diffusion time of the molecules τ_D. This gives rise to a bump at short time scales in the FCS curve. The change between the diffusive component and the triplet component can therefore be easily distinguished, especially if there is a significant difference between the triplet and diffusive time scales. It is important that the triplet dynamics is incorporated in the fit of the FCS analysis software. Regardless of the attempt to avoid the triplet behavior, some molecules have a strong triplet behavior, which is impossible to exclude.

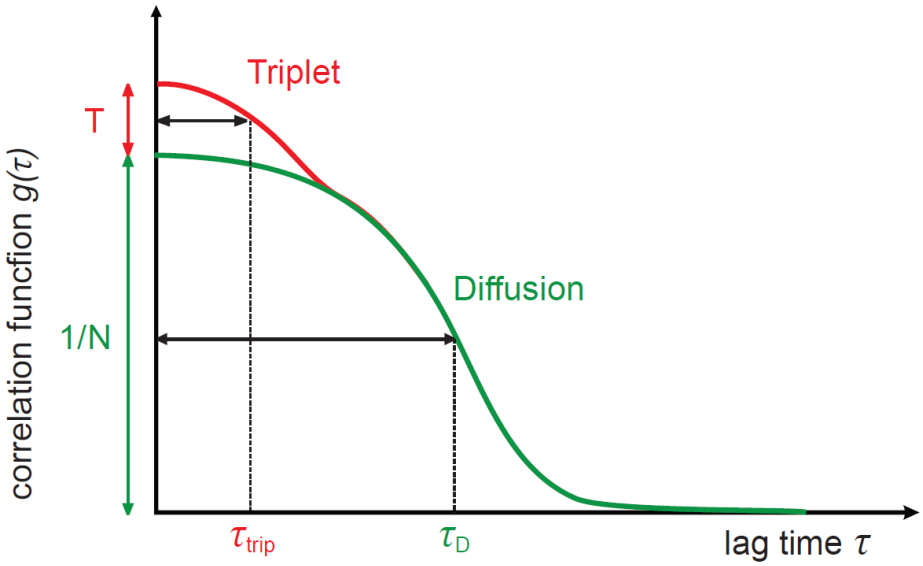

Figure 2.7: Autocorrelation function $g(\tau)$ containing a diffusing component with decay time τ_D and a triplet component with decay time τ_{trip}. The triplet decay lifetime gives the rate of triplet crossing and its amplitude gives the proportion of time spent in the triplet state.

1.4.2 SPIM FCS

Single plane illumination fluorescence cross-correlation spectroscopy allows measurements in all points of the image plane simultaneously and not just in one point like on conventional confocal FCS [70]. Two auto- and a cross-correlation curves are obtained for each pixel of the image detector. For the evaluation of the auto- and cross-correlation data from each pixel, a global fit has been chosen, fitting each pixel separately. By a global fitting approach, the optimum set of parameters is found, minimizing the least-squares deviations of the fit functions from the measurements. The measured data was, like the confocal FCS measurements, fitted using a 2-component normal diffusion model.

To determine the diffusion coefficients and concentrations for SPIM-FCS measurements I used theoretical models in the case of a binding reaction $A + B \rightleftharpoons AB$. In this thesis, the A and B represent the green and red labeled monomers, respectively, and AB is a double-labeled dimer consisting of A and B. The c_A, c_B and c_{AB} are the particle concentrations, which were linked over all three curves during the fit to reduce the complexity of the model. The diffusion coefficients were specific to each detection channel and not to the species. The normalized FCCS auto- and cross-correlation functions can be therefore written as [53, 75]:

$$g_{gg}(\tau) = \frac{1}{\langle c_A \rangle + \langle c_{AB} \rangle} \cdot G_{gg}(\tau) \tag{2.18}$$

$$g_{rr}(\tau) = \frac{\eta_r^2 \cdot [\langle c_B \rangle + \langle c_{AB} \rangle] + \kappa_{gr}^2 \eta_g^2 \cdot [\langle c_A \rangle + \langle c_{AB} \rangle] + 2\kappa_{gr}\eta_r\eta_g\langle c_{AB} \rangle}{\left(\kappa_{gr}\eta_g\langle c_A \rangle + (\eta_r + \kappa_{gr}\eta_g) \cdot \langle c_{AB} \rangle + \eta_r \langle c_B \rangle\right)^2} \cdot G_{rr}(\tau) \tag{2.19}$$

$$g_{gr}(\tau) = \frac{\eta_g\eta_r\langle c_{AB} \rangle + \kappa_{gr}\eta_g\eta_r\langle c_A \rangle + \kappa_{gr}\eta_g^2 \cdot \langle c_{AB} \rangle}{(\eta_g\langle c_A \rangle + \eta_g\langle c_{AB} \rangle) \cdot (\kappa_{gr}\eta_g\langle c_A \rangle + (\eta_r + \kappa_{gr}\eta_g)\langle c_{AB} \rangle + \eta_r\langle c_B \rangle)} \cdot G_{gr}(\tau) \tag{2.20}$$

where κ_{gr} is the cross-talk of the green into the red channel and is measured with a sample containing only the green dye. It is assumed there is no cross-talk of the red into the green channel. The η_g and η_r are molecular brightnesses of fluorophore A in the green channel and fluorophore B in the red channel and can be estimated from the measured and background corrected average fluorescence intensities $\langle F_g \rangle$ and $\langle F_r \rangle$:

$$\eta_g = \frac{\langle F_g \rangle}{\langle c_A \rangle + \langle c_{AB} \rangle} \qquad \text{and} \qquad \eta_r = \frac{\langle F_r \rangle}{\langle c_B \rangle + \langle c_{AB} \rangle} \tag{2.21}$$

In *Equations* (*2.18 – 2.20*), $G_{gg}(\tau)$, $G_{rr}(\tau)$ and $G_{gr}(\tau)$ are the factors describing the non-normalized (cross-) correlation functions of species A, B or AB between the green and the red channels, respectively. If γ and ρ denote channel one and channel two (gg, rr or gr) and χ denotes to the species (A, B or AB), then $G_{\gamma\rho}^{\chi}(\tau)$ can be defined as a product of three directional factors: $G_{\gamma\rho}^{\chi}(\tau) = \langle c_\chi \rangle \cdot G_{\gamma\rho,x}^{\chi}(\tau) \cdot G_{\gamma\rho,y}^{\chi}(\tau) \cdot G_{\gamma\rho,z}^{\chi}(\tau)$. Each of the factors can be calculated as [53, 75]:

$$G_{\gamma\rho,x}^{\chi}(\tau) = G_{\gamma\rho,y}^{\chi}(\tau) = \frac{1}{a} \cdot \left(erf\left(\frac{\sqrt{2} \cdot a}{\sqrt{8D_x\tau + w_\gamma^2 + w_\rho^2}} \right) + \frac{\sqrt{8D_x\tau + w_\gamma^2 + w_\rho^2}}{a \cdot \sqrt{2\pi}} \cdot \left(e^{-\frac{2 \cdot a^2}{8D_x\tau + w_\gamma^2 + w_\rho^2}} - 1 \right) \right) \tag{2.22}$$

$$G_{\gamma\rho,z}^{\chi}(\tau) = \frac{\sqrt{2/\pi}}{\sqrt{8D_x\tau + z_\gamma^2 + z_\rho^2}} \tag{2.23}$$

If we measure the diffusion only in two dimensions, the factor $G_{\gamma\rho,y}^{\chi}(\tau)$ or $G_{\gamma\rho,z}^{\chi}(\tau)$ is excluded, depending on the orientation of the two-dimensional motion.

In the model functions described above (*Eqs. 2.22*, *2.23*) it is assumed that the setup has been aligned correctly, therefore, the shift δ between the green and the red focus has been neglected. Misalignment in the optics may lead to an offset between the green and the red channels. The value a is the distance between pixels and is known accurately for the EMCCD camera that I used ($a = 400nm$). The value $w_{\gamma\rho}$ is the lateral point spread function (PSF) determined from the diffusion time of 100 nm TetraSpec beads in water measured by the SPIM-FCS, and $z_{\gamma\rho}$ is the longitudinal PSF determined from the z-scan of 100 nm TetraSpec beads in gel. A detailed protocol of the calibration procedure has been described in detail in Chapter 3.2.5.

Fitting the data with the 2-component normal diffusion model, the correlation curves for the green and the red channels are described by a fast and a slow component. Their relative contributions are defined by the fraction of the slow diffusion component. The correlation function (an example for the green channel) can then be defined as [53, 75]:

$$G_{gg}(\tau) := (1 - \rho_{slow}) \cdot \frac{G_{gg,fast}(\tau)}{\langle c_{gg,fast} \rangle} + \rho_{slow} \cdot \frac{G_{gg,slow}(\tau)}{\langle c_{gg,slow} \rangle} \tag{2.24}$$

The functions $G_{gg,fast}(\tau)$ and $G_{gg,slow}(\tau)$ are defined by *Equations* (*2.22*, *2.23*) with D_{fast} and D_{slow} diffusion coefficients.

2. MATERIAL

2.1 USED MATERIAL AND DEVICES

The material and devices were used for the preparation of the plasmid, for cell culture, cell preparation and transfection, for confocal and SPIM measurements, and are listed below.

PRODUCT	MANUFACTURER
CHEMICALS	
DMEM growth medium	Invitrogen Life Technologies
Fetal calf serum	Invitrogen Life Technologies
Hanks' balanced salts solution	PAN-Biotech
Trypsin	Biochrom
FuGENE transfection reagent	Promega GmbH
Aphidicolin	Sigma-Aldrich
PLASMID DNA PURIFICATION	
XL10-GOLD E.coli cells	Stratagene
Luria-Bertani (LB) medium: LB-Agar, Miller, LB-Broth, Miller	Becton Dickinson
Miniprep® NucleoSpin plasmid kit	Macherey-Nagel
Maxiprep® NucleoBond plasmid kit	Macherey-Nagel
FLUORESCENT PROBES	
Alexa 488	Molecular Probes
Alexa 594	Molecular Probes

Yellow-green fluorescent microspheres 100nm, carboxylate modified: FluoSpheres YG	Invitrogen
Red fluorescent microspheres 100nm, carboxylate modified: FluoSpheres RT	Invitrogen
Multi-colored microspheres 100nm: TetraSpec	Invitrogen
SPIM sample mounting	
Phytagel gel for SPIM bead scans	Sigma-Aldrich
LumoxFolie 25M foil for sample bags	Sarstedt AG&Co
No.3 cover slips for cell culture	Neolab

Table 1: List of used material.

PRODUCT	**MANUFACTURER**
CELL CULTURE	
Olympus CK-40 (culture microscope)	Olympus
Infinity 2-1R CCD camera	Lumenera
CONFOCAL MICROSCOPY	
Fluorescence Fluctuation Microscope (FFM)	Development of the department*
Olympus IX-70 microscope	Olympus
Argon-Krypton laser	Melles Griot
Avalanche Photodiode (SPCM-AQR-13)	Perkin-Elmer
ALV-5000 multi-tau correlator card	ALV Laser GmbH

CHAMO: sample chamber for 32mm glass microscope slide	Development of the department*
SINGLE PLANE ILLUMINATION MICROSCOPY	
Single Plane Illumination Microscope (SPIM)	Development of the department*
Blue DPSS laser (491nm): Calypso	Cobolt
Green DPSS laser (561nm): Jive	Cobolt
LED (W42182/U2)	Seoul Semiconductor
EMCCD camera, iXon X3 860	Andor
DualView DV2	Photometrics
Objective lens 10x/NA 0.3: Plan Flour	Nikon
Objective lens 60x/NA 1.0: CFI Apo-W NIR	Nikon
Neutral density filter OD=3: NE30A-A	Thorlabs
Neutral density filter OD=4: NE40A-A	Thorlabs
Green longpass: Edge Basic 488 LP	Semrock
Green bandpass: BrightLine HC525/50	Semrock
Red longpass: EdgeBasic 561LP	Semrock
Red bandpass: BrightLine 641/75-25	Semrock
SOFTWARE	
QuickFit 3.0: data evaluation and SPIM instrument control software	Development of the department*
Adobe Illustrator: graphic design software	

*Biophysics of Macromolecules, DKFZ, Heidelberg

Table 2: List of used devices and software.

2.2 FLUORESCENT DYES

Fluorophores are fluorescent chemical compounds that emit a photon within nanoseconds after they absorb another photon, typically with a shorter wavelength [77, 79]. In fluorescence microscopy, fluorophores are used to make structures visible for the measurement. Fluorophores can be used alone or as a dye for staining certain tissues or cellular structures. They are used to label the molecules of interest in order to sensitively detect and track only a specific species of particles and measure mobility processes. When more than one fluorophore simultaneously labels different proteins, the interaction in living cells can be measured. Typically, they are introduced into cells from outside using transfection so they can specifically associate with selected proteins. Transfection is the introduction of a nucleic acid molecule into cultured eukaryotic cells. A process, when the introduced nucleic acid is not integrated into the genome and exists in the cell only for a limited time, is called transient transfection. This kind of transfection has been used for labeling the proteins of interest for the measurements presented in this Thesis.

Fluorescent dyes are not only used to label the molecules, but also to calibrate the system, such as the confocal microscope, before the measurements. For the calibration procedures and measurements in this Thesis, two types of fluorescent dyes have been used: Alexa fluor dyes, which are chemical fluorophores, and fluorescent proteins, described in the next two chapters.

2.2.1 ALEXA FLUOR DYES

Alexa Fluor dyes are a family of fluorescent dyes and have been produced by Invitrogen (Life Technologies Corporation). They have been designed to be maximally excited by the commonly available laser lines that are used in confocal microscopy. Alexa Fluor dyes have significantly higher quantum yield than spectrally similar probes, like for example FITC and green rhodamine derived fluorophores. This results in more intense fluorescence for the same concentration of dye. They have several improved features, including pH insensitivity and a high degree of water solubility. When used with normal laser intensities, Alexa Fluor dyes are almost unaffected by photobleaching.

Alexa 488 was specifically designed for the excitation by the blue 488 nm Argon and Argon-Krypton laser line used in confocal microscopy. The usual excitation light source for Alexa 594 is the 647 nm Argon-Krypton laser line. Alexa 488 absorbs blue and emits green light while Alexa 594 absorbs orange and emits red light. The absorption and fluorescence

spectra of Alexa 488 and Alexa 594 are shown in *Figure 2.8 A* and *B*, and the spectroscopic properties are summarized in *Table 3* [77, 79].

Alexa 488 and Alexa 594 have been used to calibrate the confocal microscope before *in-vivo* measurements on cells. Knowing the diffusion coefficients of these two dyes diluted in water at room temperature, the size of the focus and therefore its volume can be determined [77, 79]. For the FCSS *in-vitro* control measurements on confocal and light-sheet microscopes, a 170bp DNA, labeled with Alexa 488 and Alexa 594 on each end, has been used.

2.2.2 FLUORESCENT PROTEINS

A large family of autofluorescent proteins derived from wildtype green fluorescent protein (wtGFP), extracted from the jellyfish *Aequorea victoria* in 1962 [94]. It was found to exhibit a high degree of fluorescence without the aid of additional substrates. The discovery and development of fluorescent proteins and mutated derivatives made fluorescent proteins widely used as fluorescent markers. This provided the ability to visualize, monitor and track individual molecules, and allowed the investigation of intracellular processes in living organisms.

The protein is composed of a tightly constructed barrel of β-sheets and is about 4nm long and 3nm in diameter. The barrel is threaded up the center by α-helix. Buried deep within the α-helix are the residues that become the chromophore, responsible for the fluorescence, when exposed to oxygen. This protects the fluorophore from photobleaching.

During this Thesis the enhanced green fluorescent protein (eGFP) [94] and the monomeric red fluorescent protein (mRFP1) proteins have been used for the measurements. The enhanced green fluorescent protein is one of the first variants of wtGFP [95] and the monomeric red fluorescent protein (mRFP1) is a form of the red fluorescent protein DsRed, extracted from the coral *Discosoma* [96].

In confocal microscopy, the usual excitation light source for eGFP fluorescent protein is from Argon and Argon-Kryption lasers with the 488 nm spectral line. The excitation light source for mRFP1 is the 647 nm Argon-Krypton. In light-sheet microscopy, the excitation light sources are the Blue 491 nm DPSS and the Green 561 nm DPSS lasers. The absorption and fluorescence spectra of eGFP and mRFP1 are shown in *Figure 2.8 C* and *D*, and the spectroscopic properties are summarized in *Table 3* [79].

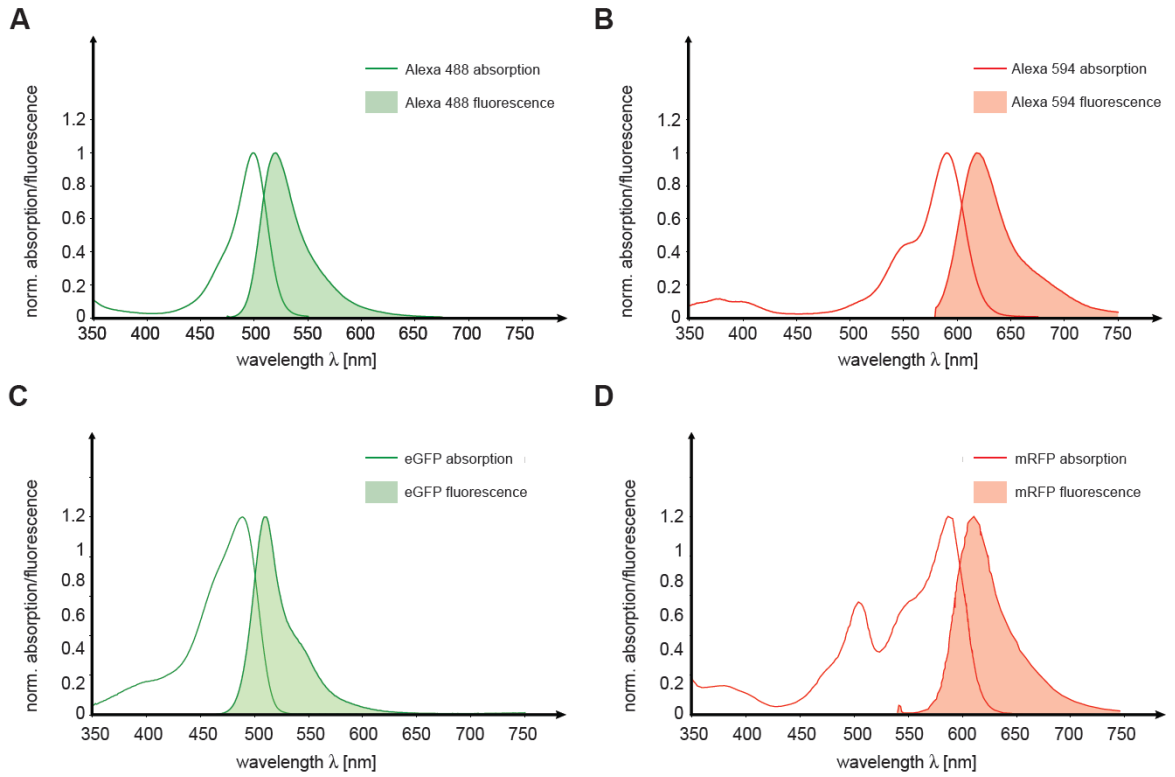

Figure 2.8: Absorption and fluorescence spectra of (A) Alexa 488 and (B) Alexa 594 dyes, and (C) eGFP and (D) mRFP1 fluorescent proteins. The spectra were constructed using the Fluorescence SpectraViewer from Invitrogen Life Technologies.

Fluorescent dye	**Molecular weight [Da]**	**λ_{abs} [nm]**	**λ_{fl} [nm]**	**$\Delta\lambda_{Stokes}$ [nm]**
Alexa 488	643	495	519	24
Alexa 594	820	591	618	27
eGFP	27k	488	507	19
mRFP1	30k	584	607	23

Table 3: Spectroscopic properties of Alexa fluor dyes Alexa 488 and Alexa 594, and Fluorescent proteins eGFP and mRFP1, where λ_{abs} is the maximum absorption, λ_{fl} is the maximum fluorescence wavelength and $\Delta\lambda_{Stokes}$ is the Stokes shift [79].

2.3 CELL LINES

2.3.3 HeLa CELLS

HeLa cells are human epithelial cells from a fatal cervical carcinoma [97]. The cell line was derived from cervical cancer cells taken from Henrietta Lacks in 1951. The genome of HeLa cells was created by a horizontal gene transfer from a human papillomavirus 18 (HPV18) to the human cervical cells. It is different from other parent genomes, also in its number of chromosomes. HeLa cells have a modal chromosome number of 82 with four copies of chromosome 12 and three of the chromosomes 6, 8 and 17. Its number of modal chromosome can reach from 70 to 164. HeLa cells are adherent cells (they stick to the surfaces) and have a typical shape. A microscopic image and a SPIM image of HeLa cell line is shown in *Figure 2.9*.

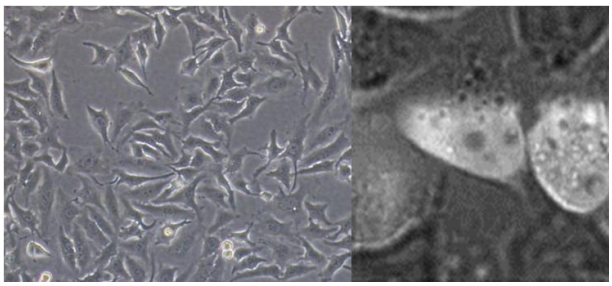

Figure 2.9: A microscopic image and SPIM image of HeLa cell line.

2.3.4 MCF-7 CELLS

MCF-7 cells are human breast cancer cells that were first isolated in 1970 from the adenocarcinoma breast tissue of a 69 year old woman [98]. The MCF-7 is the acronym of the Michigan Cancer Foundation 7, the institute in Detroit, where the cell line was established. A microscopic image of MCF-7 cell line is shown in *Figure 2.10*.

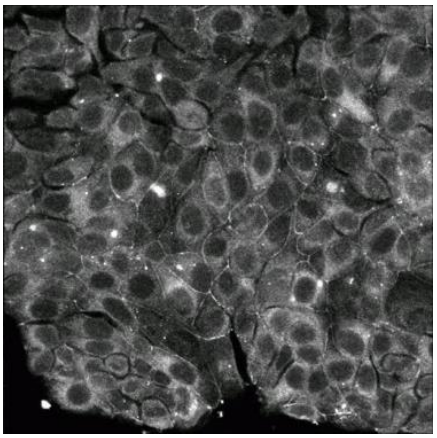

Figure 2.10: A microscopic image of MCF-7 cell line.

2.4 PLASMID CONSTRUCTION

The vectors pSV-c-Fos-EGFP and pSV-c-Jun-mRFP1, their mutants pSV-c-FosΔΔ-eGFP and pSV-c-JunΔΔ-mRFP1, and the vectors pSV-eGFP-mRFP1 and pIRES2-eGFP-mRFP1 were constructed by Nina Baudendistel and are described in detail in [7, 16].

The expression vectors **pSV-c-Fos-eGFP** and **pSV-c-Jun-mRFP1** were constructed using a multi-step cloning strategy. Briefly, a pSV-EYFP vector originating from pECFP-1 (BD Biosciences) was used as a starting vector to construct the expression vectors. The SV40 promoter region was inserted in the HindIII restriction site of the multiple cloning site (MCS) to drive overexpression of the protein constructs. The vector pSV-c-Fos-eGFP consists of full-length human Fos fused to eGFP with a linker sequence RDPPVAT and the vector pSV-c-Jun-mRFP1 consist of full-length human Jun fused to mRFP1 with the linker sequence RDPPV cloned to create the protein Jun-mRFP1.

The vectors **pSV-c-FosΔdimΔDNA-eGFP** and **pSV-c-Jun-ΔdimΔDNAmRFP1** are mutants that are lacking the dimerization and DNA-binding domains. First, the DNA (417-480 bp) and dimerization (495-579 bp) of c-Fos were removed by PCR amplification of c-Fos. The amplified fragment was digested with EcoRI and BamHI and inserted in the MCS of pSV-eGFP. For the construction of the deletion mutant c-Jun, the c-Jun fragment from the vector RSV-c-JunΔ146-220 (P. Angel, DKFZ) was digested with HindIII and BgIII and inserted into the HindIII and BamHI sites of the pSV-eYFP. The SV 40 promoter region was inserted in the HindIII restriction site and the mRFP1 was integrated in the vector as for the vector pSV-c-Jun-mRFP1. The co-expression of these two mutants served as a negative control in the study of dimerization and DNA binding.

The vector **pSV-eGFP-mRFP1** is a fusion protein of the two dyes separated by a seven amino acids linker. The amplified fragment and the plasmid pSV-mRFP1 (constructed by G. Müller and N. Baudendistel) were digested using SaiI and BamHI restriction enzymes. The amplified fragment was then ligated with the pSV-mRFP1 vector to construct the fusion protein pSV-eGFP-mRFP1. The vector was used as a positive control for the FCCS measurements.

As a negative control for the FCCS measurements, a vector expressing separately, but simultaneously both, red and green, fluorescent proteins was required. **pIRES2-eGFP-mRFP1** is a vector expressing the eGFP and mRFP1 dyes separately. It has an Internal Ribosomal Entry Site (IRES) before the coding sequence of eGFP, which allows simultaneous expression of two individual genes by only one mRNA. Briefly, the amplified fragment and the plasmid vector

pIRES2-eGFP (Clontech) were digested using SalI and BamHI and the ligated to generate the vector pIRES2-eGFP-mRFP1.

Throughout the Thesis, the resulting fusion proteins pSV-c-Fos-eGFP and pSV-c-Jun-mRFP1 are termed as c-Fos and c-Jun, pSV-c-FosΔΔ-eGFP and pSV-c-Jun-ΔΔmRFP1 as c-Fos and c-Jun mutants, pSV-eGFP-mRFP1 as fusion protein and pIRES2-eGFP-mRFP1 as monomers.

2.5 QUICKFIT

QuickFit 3.0 (QF) [91] is a software package used for data evaluation and control of the light sheet microscope (SPIM). The program itself is actually a project manager and all the data and evaluation items are defined by plug-ins. The data obtained from the confocal FCS and imaging FCS measurements can be analyzed with QF program. QF includes model fits with predefined models to the measured data in order to determine the information about the diffusion time of the fluorescent particles and the number of fluorescent particles in the laser focus. A couple of screenshots of QF are shown in *Figure 2.11*.

The QF software has installed hardware control plug-ins to control the SPIM setup. It can communicate with different hardware components of the microscope, like the camera, lasers and 3DoF stage. QF allows live view from the camera. Among other functions, QF is used for the acquisition of fast image series (saved as tagged file format – TIFF), the correlation and evaluation of image series, acquisition of image stacks, and for plotting images, graphs and histograms [53].

A

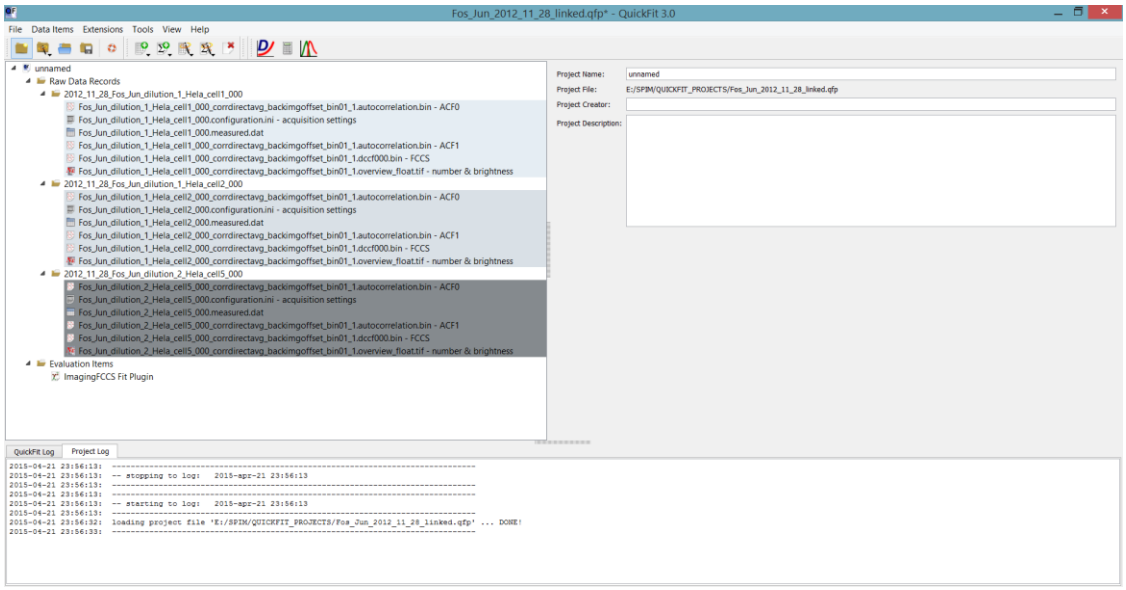

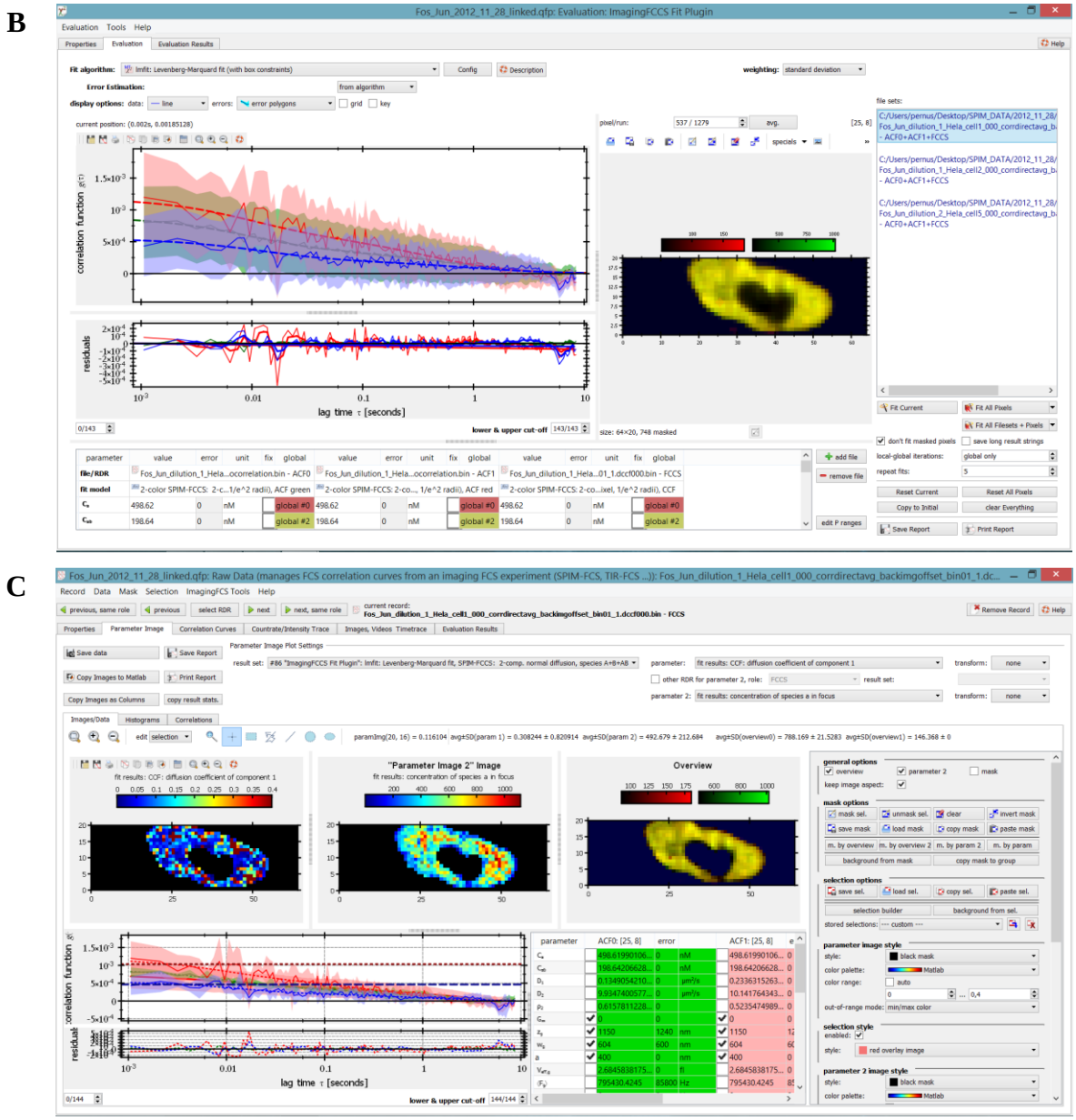

Figure 2.11: Screenshots of *QuickFit 3.0*. (A) Project manager, (B) imaging FCCS evaluation fit plug-in and (C) imaging FCCS results display [91].

3. METHODS

3.1 CONFOCAL MICROSCOPY

Most of FCS setups are based on confocal microscopy [83]. The confocal microscopy offers several advantages in comparison to conventional light microscopy. These include the controlled narrow focus depth and the elimination of out-of-focus light, which reduces the contrast and damages the image quality. Confocal microscopy overcomes this by the use of a pinhole. The fluorescence light that is not focused exactly on the plane and is exceeding the size of the pinhole will be eliminated and only a small fraction of it will pass through. A disadvantage of a confocal microscope is that only a single point can be observed and therefore only a single point FCS measurement performed at a time.

The light from a laser is expanded and projected on the water immersion objective that focuses the laser beam inside the sample. The fluorophore gets excited and the emitted fluorescence light is collected by the same objective. The light passes through the pinhole to filter the out-of focus light to the detector. In confocal microscopy the fluorescence signal is usually detected by the single-photon avalanche diode. If two different fluorophores are used, a dichroic mirror located behind the pinhole splits the signal in two detection channels. A typical confocal microscope is illustrated in *Figure 2.12*.

3.1.1 CONFOCAL MICROSCOPE SETUP

The confocal microscope used in this Thesis (*Figure 2.13*) is an in-house constructed setup built around an inverted Olympus IX-70 microscope with a 60x / NA=1.2 water immersion objective [99, 100]. The sample is excited with an Argon-Krypton laser with 488 nm (green channel) and 568 nm (red channel) wavelengths at intensities of ~2 kW/cm^2. The laser power above the objective was 2 kW. The fluorescence is separated from the excitation light by a dichroic mirror, then filtered with a band-pass filter in the green and a long-pass filter in the red channel and detected in two color channels with single photon counting avalanche photodiodes (APD). Two APDs enable to collect signals in both green and the red channel, respectively. The integrated galvanometer scanner allows fluorescence imaging of the cell and positioning of the focus point within the cell where we want to perform the FCS measurement. Real-time computation of photon correlation functions is performed on an ALV-5000 multi-tau correlator card. The card allows computation of cross-correlation as well as auto-correlation functions.

The cell measurements are typically performed at a room temperature, but can also be performed at 37°C and 5% CO_2 due to the integrated incubator chamber.

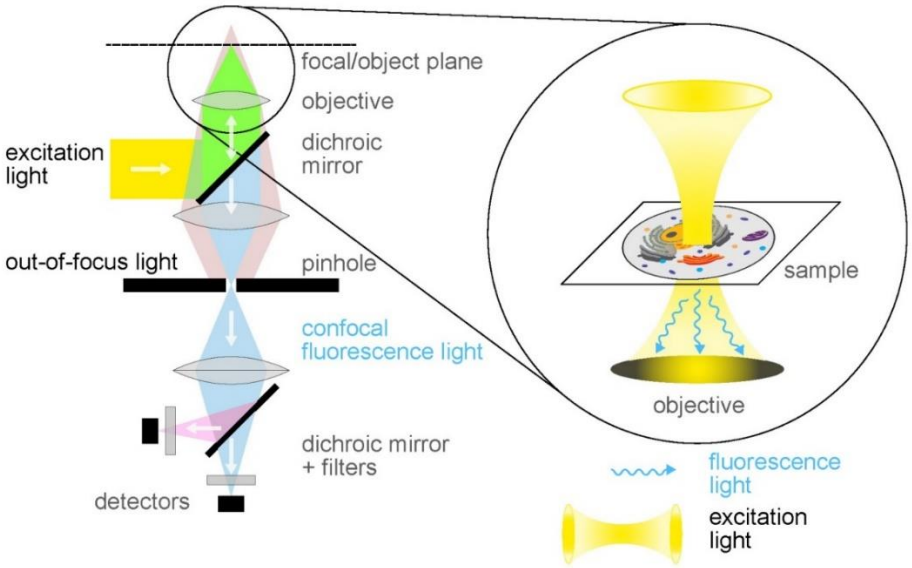

Figure 2.12: Schematic setup of a dual-color confocal microscope. The light from a laser is focused on the sample by a high NA objective. The emitted light is collected by the same objective and passes through the pinhole to filter the out-of-focus light. A dichroic mirror splits the emitted light in two detection channels to distinguish between different dyes. The emitted fluorescence is detected by a fast detector (typically an avalanche photodiode). The figure is adapted from [53].

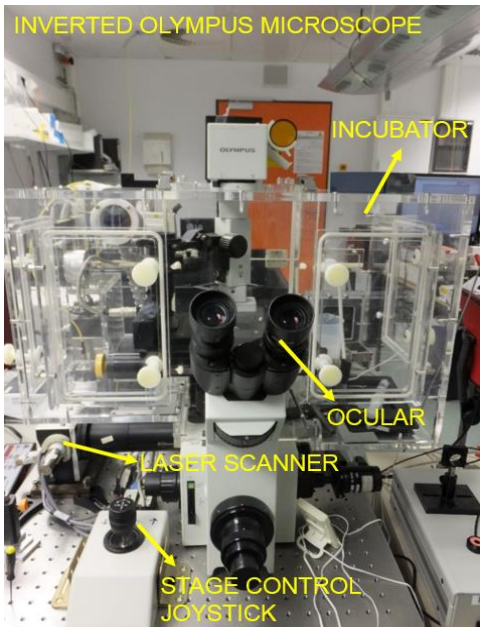

Figure 2.13: An image of the in-house constructed confocal microscope setup built around an inverted Olympus IX-70 microscope [99, 100].

3.1.2 SAMPLE PREPARATION

The cells are grown on 32 mm glass cover slides in a 60 mm petri dish. For the FCS measurement, the glass cover slide is put into a CHAMO measuring chamber (*Figure 2.14*). The measuring chamber (developed by Nicolas Dross [101, 65] consists of an aluminium plate with integrated handles, a silicon seal and a steel clamp ring (*Figure 2.14*). It has been designed especially for the FCS measurements in living cells using the confocal microscope. The advantage of this chamber is that its size is very large in comparison to commercially available chambered cover slides (491 mm^2 at a diameter of 25 mm). The chamber can be filled with up to 3 ml of medium, which allows longer observation and measurement times. Cell measurements can thus last for several hours without changing the medium.

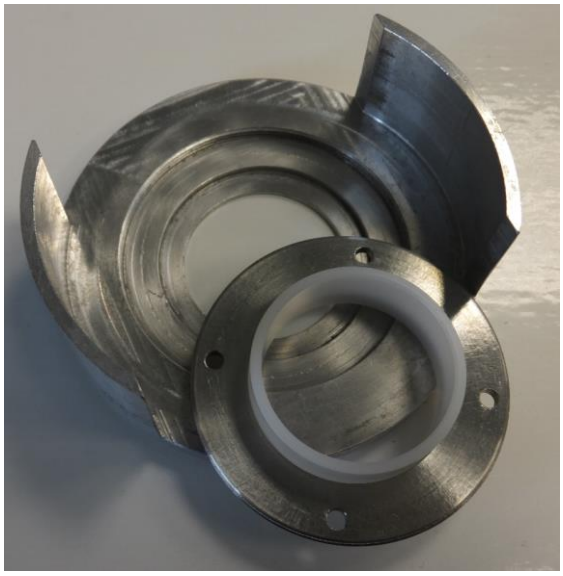

Figure 2.14: CHAMO sample chamber for 32 mm glass microscope slide used for confocal FCS cell measurements [64, 65].

3.1.3 DETECTION

There are different types of detectors available to measure fluorescence fluctuations *in-vitro* and *in-vivo* [102]. In this Thesis, the FCS based confocal microscope uses avalanche photodiode detectors (APD) with single-molecule sensitivity [103]. APD records single photons emitted by dye molecules. It includes two basic structural elements, an absorption and a multiplication region. The fluorescence photons induce an electrical pulse at the detector, which creates an electron-hole pair in the crystal of the semiconductor. One electron-hole pair is created for each single photon. The multiplication region exhibits a high-electric field and the field accelerates

the electrons to such high speed that it creates more electron-hole pairs through collisions. This process is called impact ionization and creates a whole avalanche of secondary electrons. The electrical pulses are counted, processed by the computer and a hardware correlator attached behind the detector calculates the auto- and cross-correlation functions.

3.1.4 MEASUREMENT AND EVALUATION PIPELINE

Switch on procedure:

- Turn on the lasers and cooling 1h before the measurement.
- Turn on the epi and the UV light.
- Turn on the APD power supply. The APDs stay turned off until the measurement.
- Turn on computer. Start ALV software and FFM software.

Calibration:

- Measure the laser power above the microscope objective (~2 kW/cm^2).
- Measure the temperature (usually room temperature at 22.5°C).
- Put water on the objective lens before inserting the sample chamber.
- The calibration is performed with 20 nM Alexa 488 solution for the green and the 20 nM Alexa 594 solution for the red channel. The calibration for maximum cross-correlation is performed with 170bp DNA labeled with Alexa 488 and Alexa 594. It is important that calibration measurements are performed in the same type of sample chamber as the cells (CHAMO sample chamber).
- Choose the laser line (#1 is 488 nm and #3 is 568 nm).
- Find the laser focus and move in the z direction until the second focus appears sharp. Move 20 µm into the solution (z direction).
- Check the count rate in the ALV program. To maximize the count rate, the cover slide correction ring is adjusted.
- In the ALV program set the data acquisition time to 10 runs of 30 s.
- Measure FCS.
- Calculate the focal volume w_{xy}.

Live cell FCS measurements:

- Find a transfected cell that is not too bright, but still visible.
- Move 4 μm into the solution (z direction).
- Acquire a confocal image of the cell.
- Choose and set 4 – 5 FCS measuring points.
- In the ALV program set the data acquisition time to 6 runs of 10 s.
- Measure FCS.
- Acquire additional confocal image of the cell to see if the cell moved.

Data evaluation:

- Data evaluation is performed by *QuickFit 3.0* software program.
- The measurements need to be sorted to exclude any errors or artifacts. This could happen due to water evaporation between the objective and sample holder, by diffusion of aggregates through the focus or by the cell movement. Such measurements are excluded from further data analysis. An example of an auto-correlation curve obtained by a moving cell in shown in *Figure 2.15*.
- Auto- and cross-correlation functions are fitted to a model function assuming one or two diffusing fluorescence components and a triplet correction using the Marquardt-Levenberg algorithm as described in Chapter 1.4.1. A model is fit to the average and their standard deviation is used for weighting.
- Cut off the first three to five data points.
- Set the calculated focal volume w_{xy} according to the calibration with Alexa 488 and Alexa 594, and fix G_∞ to 0 and the structure factor γ to 6.
- When all the values are set, fit all runs.
- The amount of binding is defined as the relative cross-correlation amplitude (*Equation 2.11*).

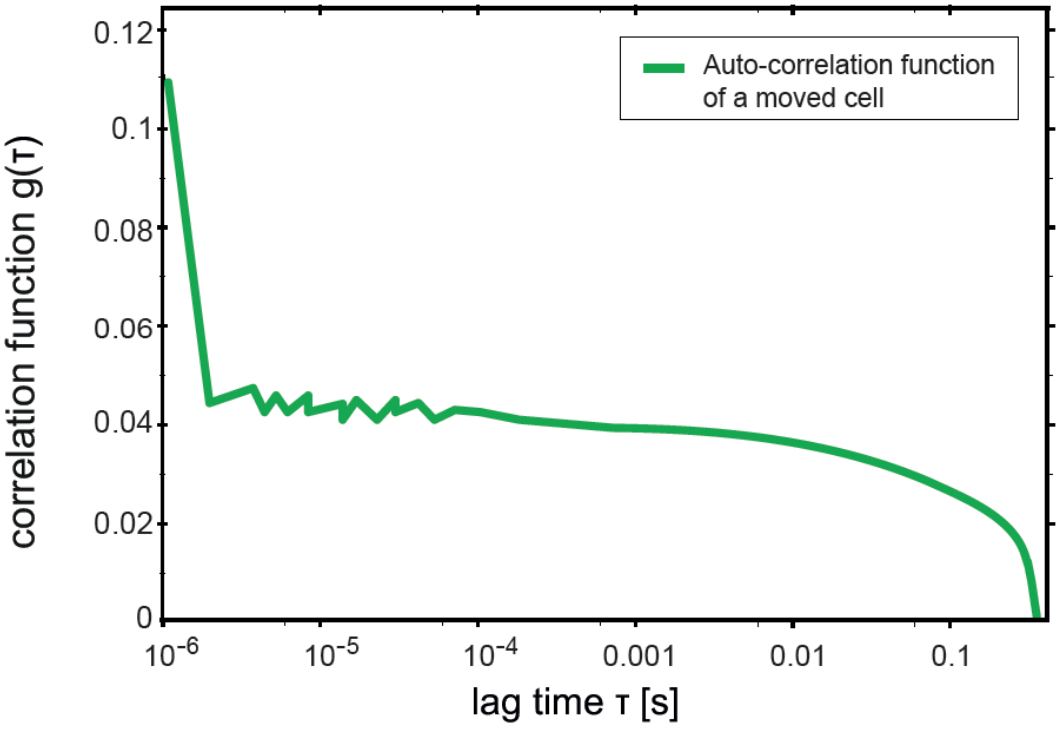

Figure 2.15: An example of a FCS auto-correlation function obtained from a cell that moved during the measurement. Such data was eliminated and not considered for further evaluation.

3.1.5 ALIGNMENT PROCEDURE

Before performing FCS cell measurements it is important to calibrate the microscope. The system is calibrated with 20 nm Alexa 488 for the green and 20 nm Alexa 594 for the red channel, respectively. The dyes need to be measured in conditions that are as close as possible to the cellular environment. The diffusion coefficients of Alexa 488 [104] and Alexa 594 [105] are known and change with temperature: $D_{488}(22.5°C) = 435\mu m^2/s$ and $D_{594}(22.5°C) = 346\mu m^2/s$. The acquisition time consisted of 10 runs of 30 s. Fitting an appropriate model function to the measured auto-correlation function yields information about the diffusion coefficient and the concentration. By knowing the diffusion coefficients, the size of the observation volume can be calculated. The size of the observation volume stays the same throughout the measurements and is used for fitting the cell FCS data. Alexa 488 and Alexa 594 auto-correlation functions are shown in *Figure 2.16*.

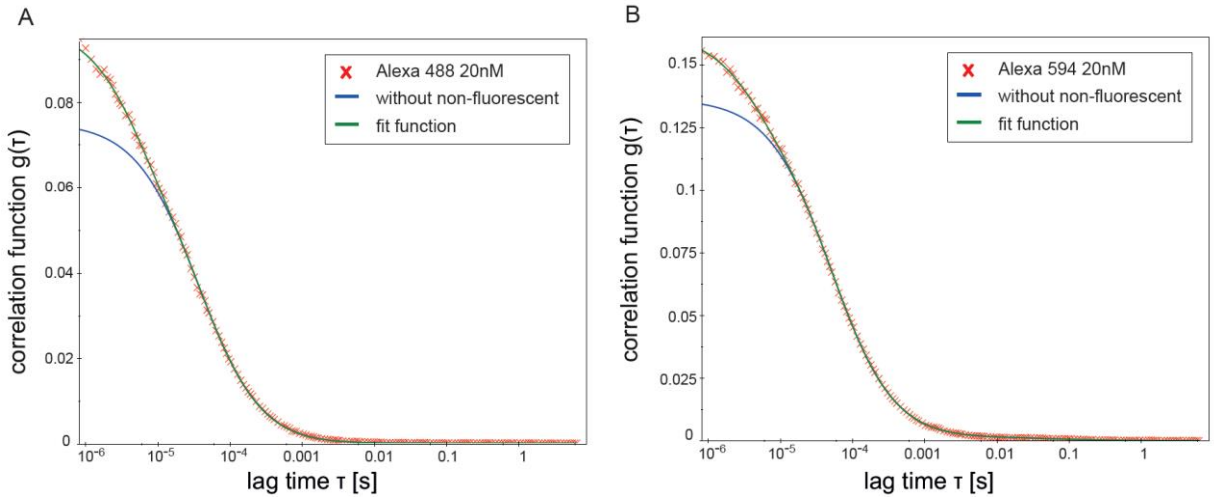

Figure 2.16: Auto-correlation functions obtained by confocal *in-vitro* FCS measurements on (A) Alexa 488 20 nM and (B) Alexa 594 20 nM solutions. The red crosses represent the average, the green line is the fit function and the blue line is the fit function without the non-fluorescent component (triplet). The acquisition consisted of 10 runs of 30 s.

As a calibration standard for maximum cross-correlation a 170bp double-stranded DNA, labeled with Alexa 488 at one and Alexa 594 at the other end was used. The DNA was diluted in TE buffer to reach a concentration of around 30 – 50 nM. The acquisition consisted of 10 runs of 30 s. FCCS measurement with this sample resulted in a maximum cross-correlation of about 55%. The auto- and cross-correlation curves are shown in *Figure 2.17*.

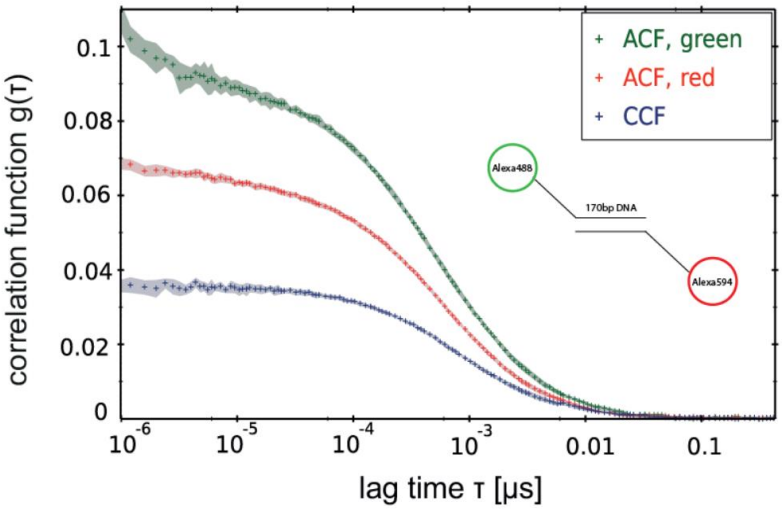

Figure 2.17: Auto- and cross-correlation functions obtained by confocal *in-vitro* FCCS measurement on a 170bp double-stranded DNA labeled with Alexa 488 and Alexa 594 at the two ends. The pluses represent the average and the transparent ranges are the standard deviations consisting of 10 runs of 30 s.

3.2 SINGLE PLANE ILLUMINATION MICROSCOPY (SPIM)

Confocal microscopy allows routine FCCS measurements of mobility and biomolecular interactions in living cells. However, its drawback is that measurements can be performed only at one or at most few spots at a time. Although FCCS provides information on the mobility of proteins ant their interaction at selected spots, data collection is tedious and slow, and motion of cells hampers data collection.

A technique that allows FCCS measurements at different positions in the cell in parallel is selective plane illumination microscopy (SPIM) [70]. The basic principle of SPIM is to illuminate the sample from the side by a micrometer-thin light sheet. The fluorescence from the sample is collected perpendicular to the illumination and projected onto the image sensor. High-speed electron-multiplying charge coupled device (EMCCD) cameras are currently the best choice in the sense of acquisition speed and photosensitivity. The camera images simultaneously all points in the two-dimensional field of view (FOV). This reduces the exposure of the cells to light, meaning that much longer observation times are possible. *Figure 2.18* shows the comparison of the illumination and detection schemes of confocal and SPIM microscopy.

The combination of SPIM and FCS provides diffusion coefficient and interaction data in the whole image plane simultaneously and allows us to create spatially resolved mobility and interaction maps.

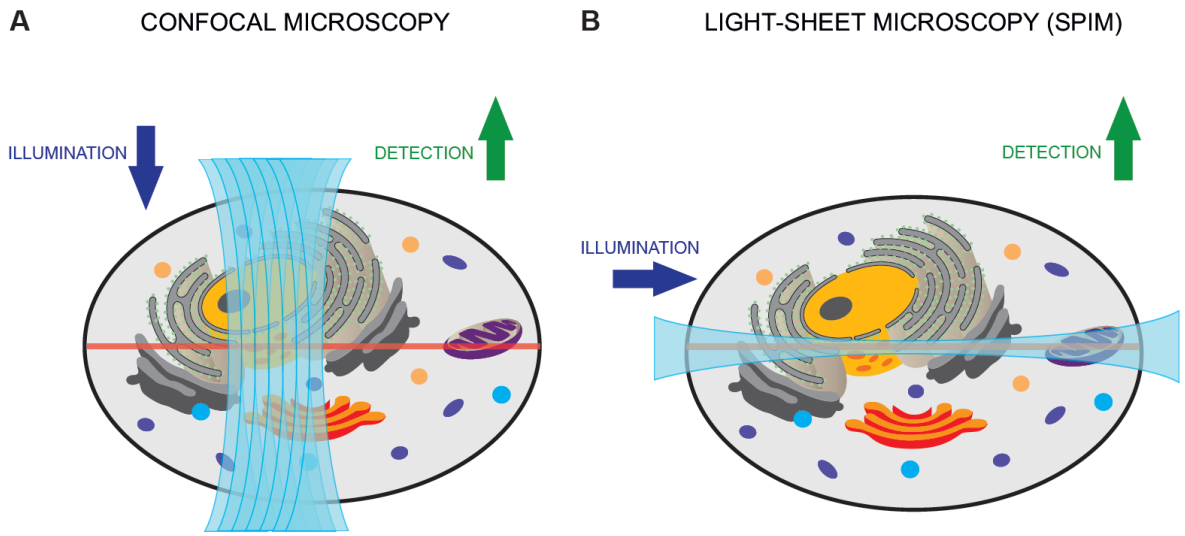

Figure 2.18: Comparison of the illumination and detection schemes of (A) confocal fluorescence microscopy and (B) single plane illumination microscopy. The red lines indicate the image plane of detection. The figure is adapted from [53].

3.2.1 SPIM SETUP

In this Thesis, I used a home-built dual color excitation and detection single plane illumination microscopy system based on the design in [71, 72] and built by Jan W. Krieger [53]. A blue 491 nm and a green 561 nm laser beam with two distinct laser beam expanders are combined by a dichroic mirror into a dual color excitation beam. The combined beam is then relayed by a telescope into a cylindrical lens followed by a projection objective, forming an approximately 1.3 µm thick ($1/e^2$-halfwidth) light sheet.

The sample is clamped and mounted from above at an angle slightly below 45° to the light sheet into the sample chamber filled with Hanks' solution. It is mounted on a xyz translation stage and placed at the intersection of the excitation and detection axes (*Figure 2.19*).

The sample fluorescence is collected perpendicular to the illumination by a water-dipping objective and corresponding tube lens. Fluorescence is split with an emission splitting system (DualView) into two spatially identical and spectrally distinct images. The two images are simultaneously projected side-by-side onto a 128x128 pixel EMCCD camera.

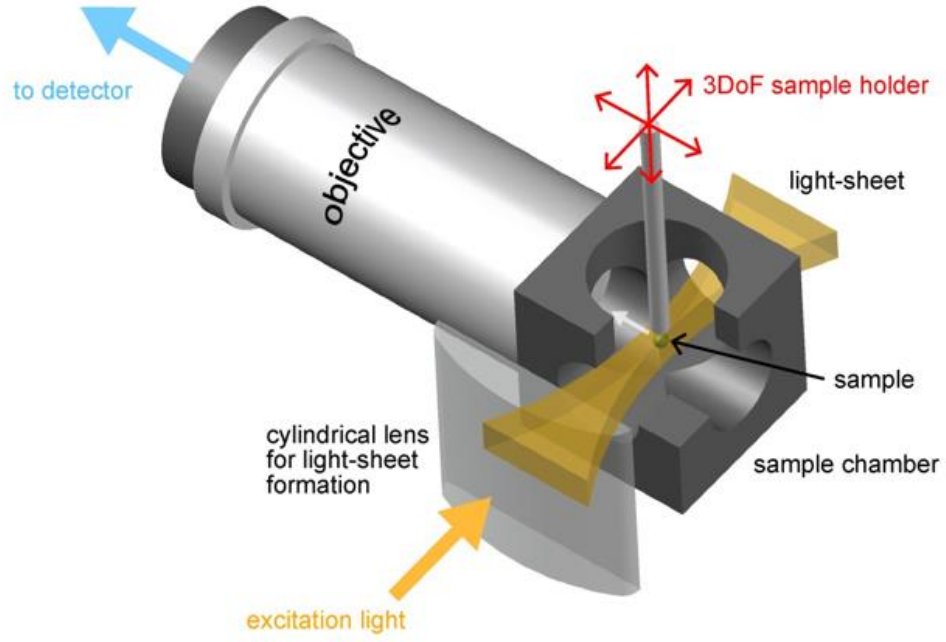

Figure 2.19: Principle of single plane illumination microscopy in a 3-dimensional view. The sample is mounted on a xyz translation stage from above into Hanks-filled sample chamber. A cylindrical lens is used to focus the excitation light in one direction and forming a light sheet. The fluorescence is collected perpendicular to the illumination by a water-dipping objective. The figure is adapted from [53].

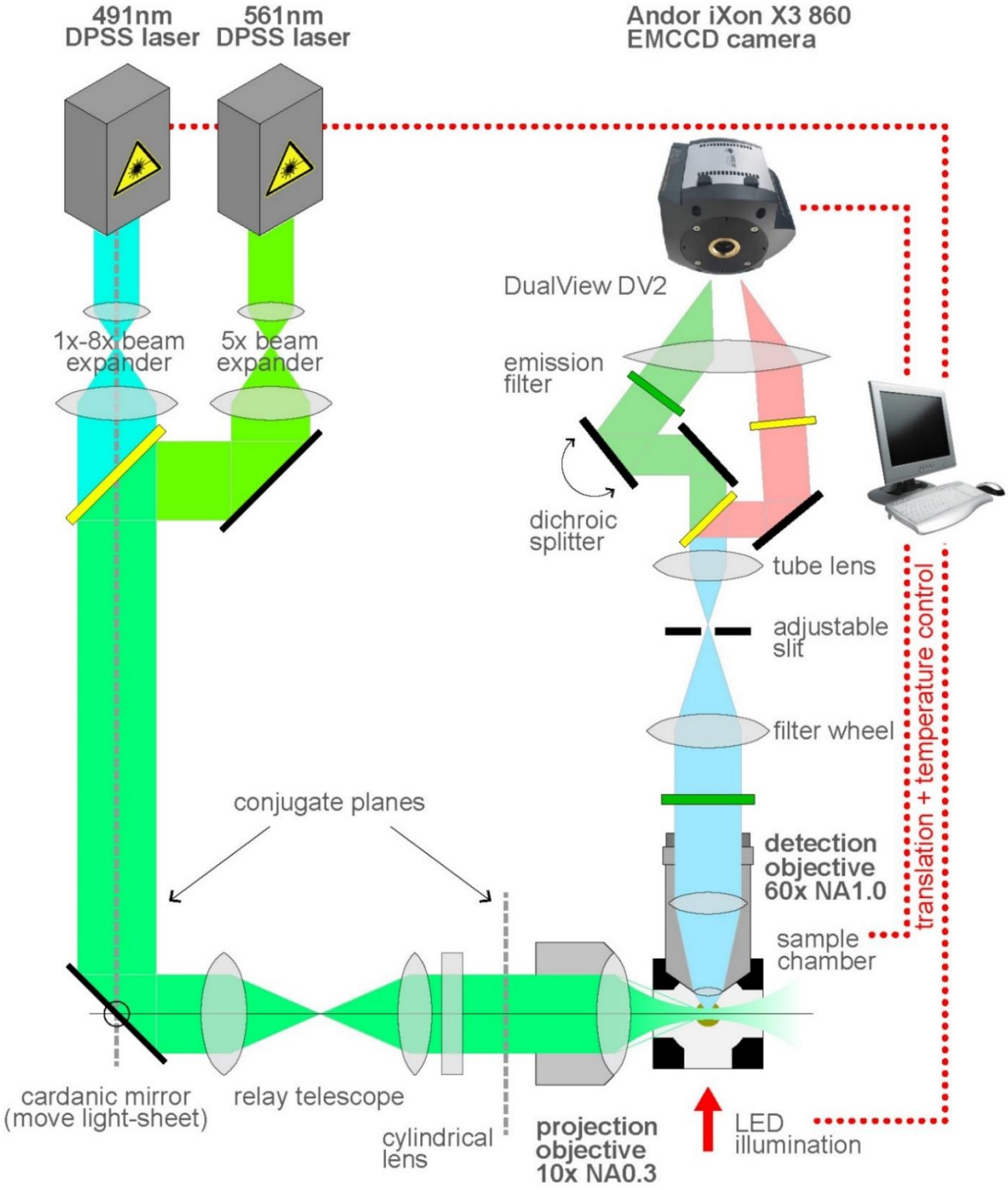

Figure 2.20: Schematic setup of dual-color SPIM microscope. The laser beams are combined by a dichroic mirror. A micrometer-thick light sheet is shaped by the combination of a cylindrical lens and a projection objective. A water dipping detection objective collects the fluorescence. The image splitter optics (DualView) separates the green and red fluorescence and focuses it on to an EMCCD camera. The figure is adapted from [53].

A detailed schematic of the optics of the SPIM microscope is shown in *Figure 2.20*. The figure illustrates the microscope from the top view. Photographs of the SPIM used in this Thesis are shown in *Figure 2.21*. It presents the sample chamber and the projection and detection objectives.

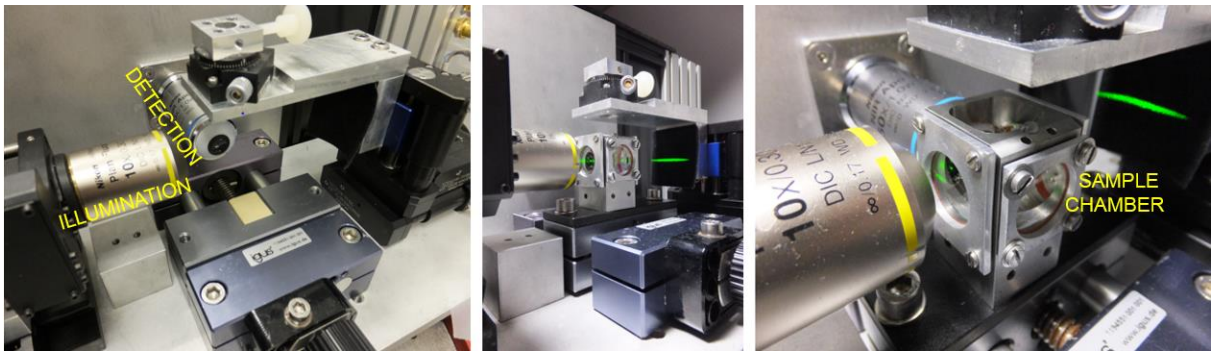

Figure 2.21: Photograph of the home-built dual color excitation and detection single plane illumination microscopy system. The figures show the perpendicular configuration of projection objective and the detection objective (left image). The sample chamber is fixed at the intersection of the illumination and the detection axes (middle and right image). A thin light sheet (green light) passes from the projection objective into the sample chamber and illuminates the sample.

3.2.2 SAMPLE PREPARATION AND MOUNTING

For the SPIM-FCCS measurements the cells are grown on little glass pieces. The glass pieces are cut with a steel glass cutter. The size of the piece has to be small enough to fit into the sample chamber. To remove any dirt, the pieces are first thoroughly washed with 70% ethanol, followed by the second wash with deionized water and are left to dry. At the end, the pieces were sterilized in an autoclave. During the measurement, a glass piece is clamped with tweezers and mounted from above into the sample chamber (*Figure 2.22*).

Figure 2.22: Cells are grown on small glass pieces, clamped with tweezers and mounted from above in the sample chamber.

The sample chamber is made out of stainless steel. It can be filled with up to 7 ml of solution, which can be exchange during the measurement. On each measuring day, the sample chamber has to be newly built. The dirty, used glass slips need to be exchanged with clean ones. The light sheet and the transmission light enter the sample chamber through the glass slips, thus the glass slips need to be clean. Between the glass slip and the sample chamber is a soft ring, which serves for a better seal and prevents any solution leakage.

Once the sample chamber is fixed, it is moved against the cone of the water dipping detection objective, using the xyz translational stage. The detection objective is then inside the sample chamber and in contact with the Hanks' solution (*Figure 2.23*).

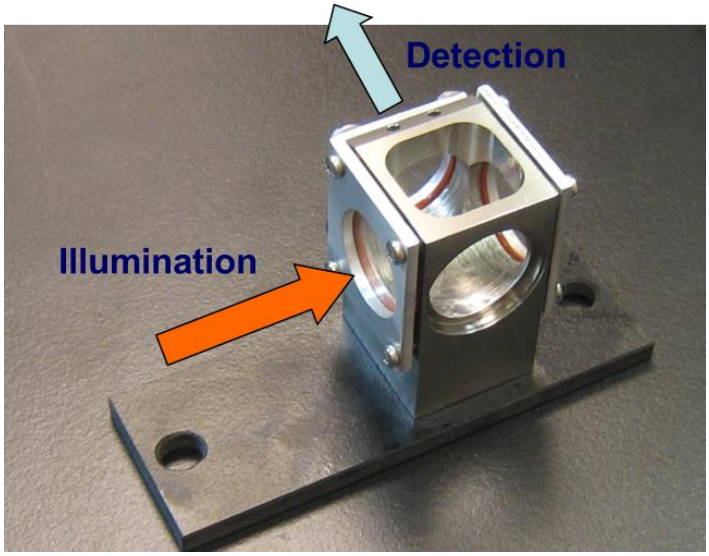

Figure 2.23: SPIM sample chamber. It is made out of stainless steel. On three sides it has glass windows and on one side it is pressed to the detection objective. The chamber is filled with Hanks' solution and the solution is mounted from above.

3.2.3 DETECTION

In SPIM-FCCS, the sample is excited with two overlapping light sheets of different wavelengths. The intensity fluctuations of the two fluorophores at the same spot of the sample are detected simultaneously at corresponding pixels and the two fluorescence channels are optically split to two half planes of the same sensor. The two images are simultaneously projected side-by-side onto a 128 x 128 pixels EMCCD camera (electron-multiplying charge-coupled device). The time resolution is determined by the speed of the recording camera.

EMCCD cameras proved to be the best choice in the sense of acquisition speed and sensitivity [102]. They have high detection efficiency with frame rates in the 1000 s^{-1} range and quantum efficiency of ~95%. The field of view is around 50 µm x 50 µm, which is sufficient to image HeLa cells with a typical diameter of 20 – 30 µm, while the pixel size is 400 nm x 400 nm. Significant increases in frame rate can be achieved by cropping the sensor and imaging only a smaller defined array size. For cell measurements a sub-region of 128 x 20 was selected. The EMCCD camera has been used as a detector for all SPIM-FCCS measurements in this thesis.

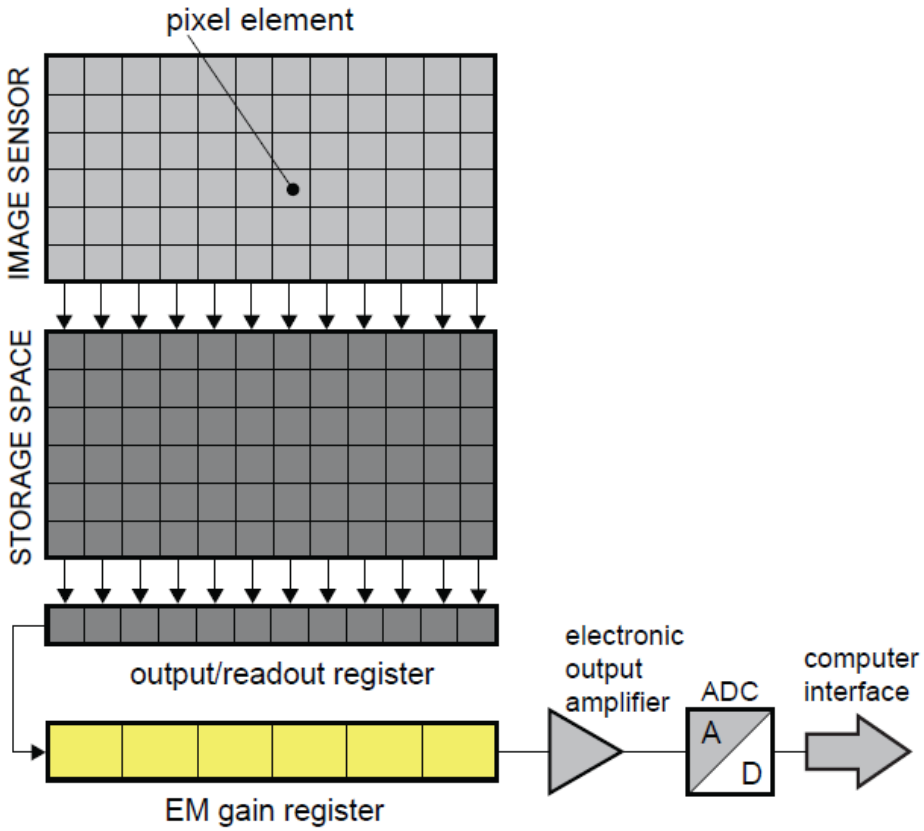

Figure 2.24: Schematic representation of the structure of a typical EMCCD image sensor. The charges are shifted downwards into an output/readout register. The signals are amplified by an external electronic current amplifier and before the amplifier is an on-chip gain to lift even very low signals well above the readout noise floor [79].

CCD cameras are imaging detectors that comprise of a 2-dimensional array of sensitive detectors, pixels. Photons that incident on the sensors are converted to electrons and stored within each pixel. The accumulated electrical charge depends on the amount of light that has fallen on the pixel. The charge is shifted downwards to the output/readout register. The charge is moved from each element of the array to the next and the content of the output register is

shifted horizontally out of the chip. The signals are amplified by an external electronic output amplifier and digitized with an ADC. The digitised photoelectron counts are then transmitted to the computer to be further processed [79].

Alike traditional CCD cameras, EMCCD cameras use an additional register between the readout register and the electronic output amplifier, the EM gain register. The electrons are multiplied by impact ionization similar like the avalanche photodiodes. Adding the EM register before external amplification lifts even the very low signals above the readout noise floor. This improves the detection contrast of weak signals and achieves detection of single photons while maintaining high quantum efficiency [79].

3.2.4 MEASUREMENT AND EVALUATION PIPELINE

Switch on procedure:

- Turn on the lasers 15-30 min before the measurement.
- Turn on the water cooling of the EMCCD camera.
- Exchange the dirty glass slips of the sample chamber with clean ones.
- Mount and fix the sample chamber. Move it against the cone of the water dipping detection objective and fix it with screws.
- Turn on the computer. Start *QuickFit 3.0* and SPIM control plug-in. Connect to all devices and the camera.
- Activate the joytick.

Calibration:

- Measure the laser power behind projection objective (between 60-100 W/cm^2 in each light sheet). This is a factor of 20 lower compared to the power density required by confocal FCCS. If we compare the total energy deposited in the cell either by acquiring a SPIM image over time *t*, or FCS data during the same time *t* per spot, the ratio of the total laser energies hitting the cell during the acquisition would be in first approximation equal to the ratio of the light sheet thickness to the total cell thickness in the z direction (5 µm), multiplied by the ratio of the power densities. Thus, the total laser power load in SPIM is about 100 times less than in an equivalent confocal scan. During the (shorter) acquisition, however, the total laser power in the

SPIM is higher, making photo-bleaching more prominent and a bleaching correction necessary.

- The sample chamber is filled with approximately 7 ml of Hanks' solution.
- Align the 488 nm and 561 nm light sheets with a mirror mounted at 45° to the detection objective. Set the light sheets to 1 mW, use a lamp and no filters to project the image onto the camera.
- Run the SPIM light sheet analysis evaluation in QF to check the overlay and position of the light sheets.
- Align the DualView optics with an EM-grid positioned parallel to the image plane. The grid is imaged on the camera using the LED. Images in the two color channels are aligned by maximizing the cross-correlation coefficient between the two images of the EM-grid. Accurate alignment of the two color channels is important to assure the two cross-correlated image pixels correspond to the same volume inside the measured sample.
- The longitudinal point spread functions are determined from the z-scan of 100 nm TetraSpec beads embedded in gel. Details are described in Chapter 3.2.5.
- The lateral point spread functions are determined by SPIM-FCS from the diffusion time of 100 nm TetraSpec beads diluted in water. Details are described in Chapter 3.2.5.
- Measure FCCS of 100 nm TetraSpec beads and 170bp DNA labeled with Alexa 488 and Alexa 594 in a sample bag. For illumination use both lasers, select a 128 x 20 pixels sub-region of the camera and acquire 100.000 frames. Evaluate the measured data in QF.

Live cell FCS measurements:

- The cells grown on little glass pieces are clamped with tweezers and positioned slightly below 45° to the light sheet.
- Find and select a transfected cell that is not too bright, but still visible in both channels and shows a typical shape of a HeLa cell.
- Focus the cell in the middle of the field of view.
- Select a 128 x 20 pixels sub-region of the camera and acquire 50.000 frames with a frame rate of approximately 1000 fps.

- During the acquisition, the camera automatically acquires an image series of 50.000 frames with the lasers turned off. Additionally, a before and after cell images are acquired to check if the cell has moved during the measurement.
- The EM gain is set to 300 for all the samples.
- After the measurements wash the sample chamber with 70% ethanol and clean the detection objective.

Data evaluation:

- Data evaluation is performed by the *QuickFit 3.0* software program.
- The measurements need to be sorted to exclude any errors or artifacts. If a cell has moved during the measurement, the data was discarded.
- Before analysis the background images are averaged and subtracted from the data images.
- Auto- and cross-correlation functions are fitted to a model function assuming two diffusing fluorescence components as described in Chapter 1.4.2. A model is fit to the average and their standard deviation is used for weighting.
- Set the initial parameters, like PSF sizes and cross-talk. A cross-talk correction is incorporated in a model fit.
- To reduce the complexity of the model, the concentrations are linked over all three curves during the fit.
- When all the values are set, fit all runs. Fit is performed for each pixel separately.
- The cells are masked with an intensity threshold to exclude pixels outside the cell or in very dark regions like the nucleolus.
- By color coding the diffusion coefficients and interaction, the parameter images are constructed.
- The amount of binding is defined as the relative concentration (*Equation 2.10*).

3.2.5 ALIGNMENT PROCEDURE

On each day of measurements, the SPIM setup has to be calibrated. The SPIM optics needs to be precisely aligned to ensure that the two cross-correlated image pixels correspond to the same volume inside the measured sample.

First, the light sheet is aligned. A mirror (*Figure 2.25 A*) is mounted on the translation stage and placed at 45° to the detection objective. The mirror is hanged from above into the sample chamber filled with Hanks' solution. With the mirror the light sheet can be directly projected onto the camera. Using the lamp and no filters, a direct image projection of the mirror can be seen. Dirt spots or scratches on the mirror are used to position the mirror in the middle of the field of view. Both lasers are set to 1 mW. First the blue laser (488 nm) is aligned and used as a reference. The formed light sheet is approximately 1.3 µm thick ($1/e^2$-halfwidth). The green laser (561 nm) is combined with the blue laser using a mirror and a dichroic beam combiner. The lasers are expanded with a beam expander before they are combined with the dichroic mirror. The lasers are positioned in the center of the field of view so the thicknesses of the light sheets are as small as possible and the side lobes of the light sheets are minimized.

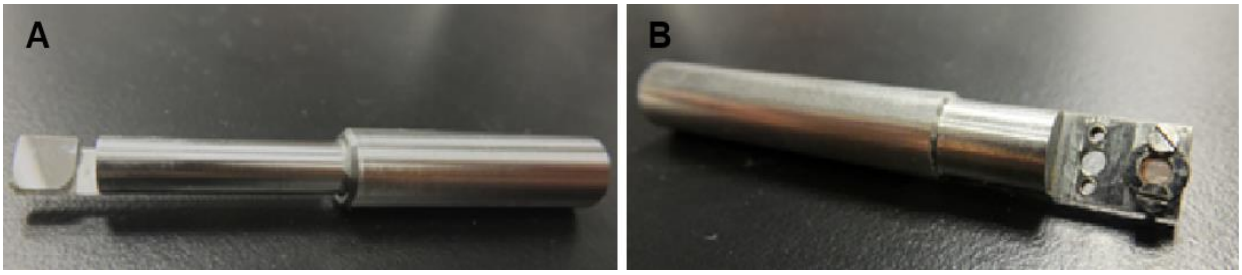

Figure 2.25: Photographs of (A) the mirror to align the light sheets and (B) the EM-grid to align the DualView optics. Both are fixed on the translation stage and hanged from above into the sample chamber.

To check the light sheet alignment, an x-stacks with 50 steps of 1 µm width are obtained. The stacks are acquired around the center position where the light sheet is the thinnest. The mirror can be scanned using the motorized translational stage. The tiff files are saved and imported to QF as a multi-image stack. Before the SPIM light sheet analysis, the borders of the image are masked. For precise alignment, the light sheets must have symmetrically positioned beam waists (*Figure 2.26*) and should overlap with <100 nm precision (*Figure 2.27*). A fine adjustment and precise overlay of the light sheets is crucial for accurate measurements.

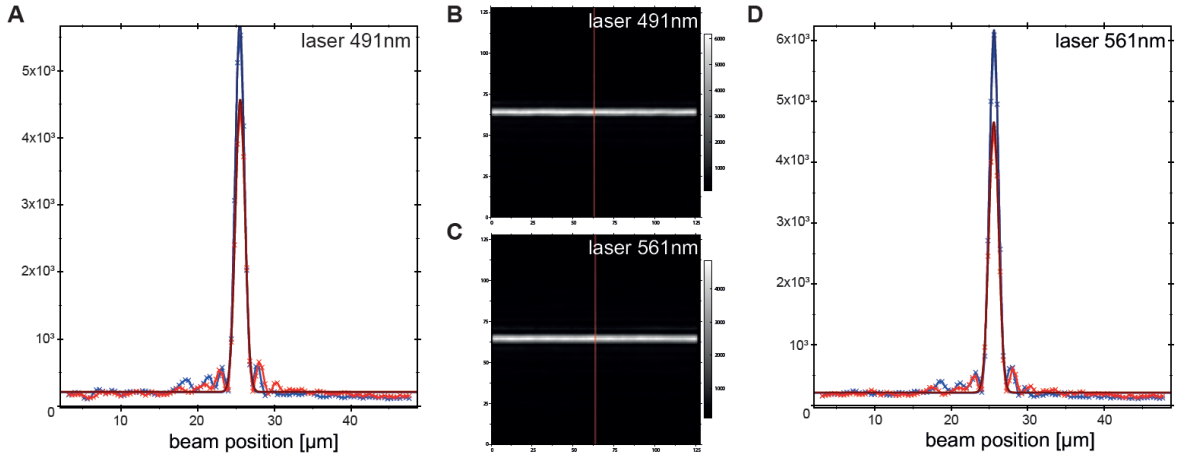

Figure 2.26: Light sheet alignment with the mirror. (B) and (C) show the blue and the green lasers position in the middle and imaged on the camera. (A) and (D) show the representative beam position, where the red lines are Gaussian fits to the light sheet data marked with blue.

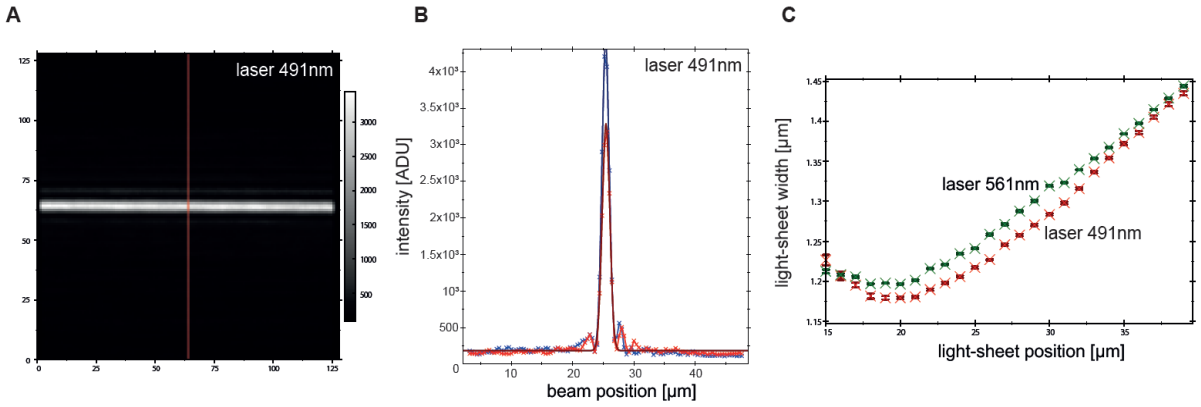

Figure 2.27: Light sheet analysis with the mirror. The blue and the green light sheets are evaluated to analyze the precise light sheet overlap (C).

Before each FCCS measurement, the DualView DV2 optics, which is used to split the detected fluorescence into two color channels, needs to be aligned. An electron microscopy grid (*Figure 2.25 B*) with 1500 or 2000 lines per inch is mounted from above into the sample chamber filled with Hanks' solution. The grid is mounted parallel to the image plane. Using the transmission illumination (LED light), the grid can be imaged by the camera. The grid is moved around until it is focused in the middle of FOV.

First, if necessary, the FOV blades are aligned like it is showed in *Figure 2.28 A*. The DV2 is then switched into the DualView mode (*Figure 2.28 B*) so it covers only the middle half of

the image. When it is centered, the beam splitter is inserted (*Figure 2.28 C*), which projects the half images into both color channels. To see the overlay clearly, the color is switched into the Matlab palette. The DV2 mirrors are adjusted so the green and the red channel image halves overlay as good as possible. Images in the two color channels are aligned by maximizing the cross-correlation coefficient between the two images of a calibration grid to about 0.98. Examples of a bad and a good alignment are shown in *Figures 2.28 D* and *E*.

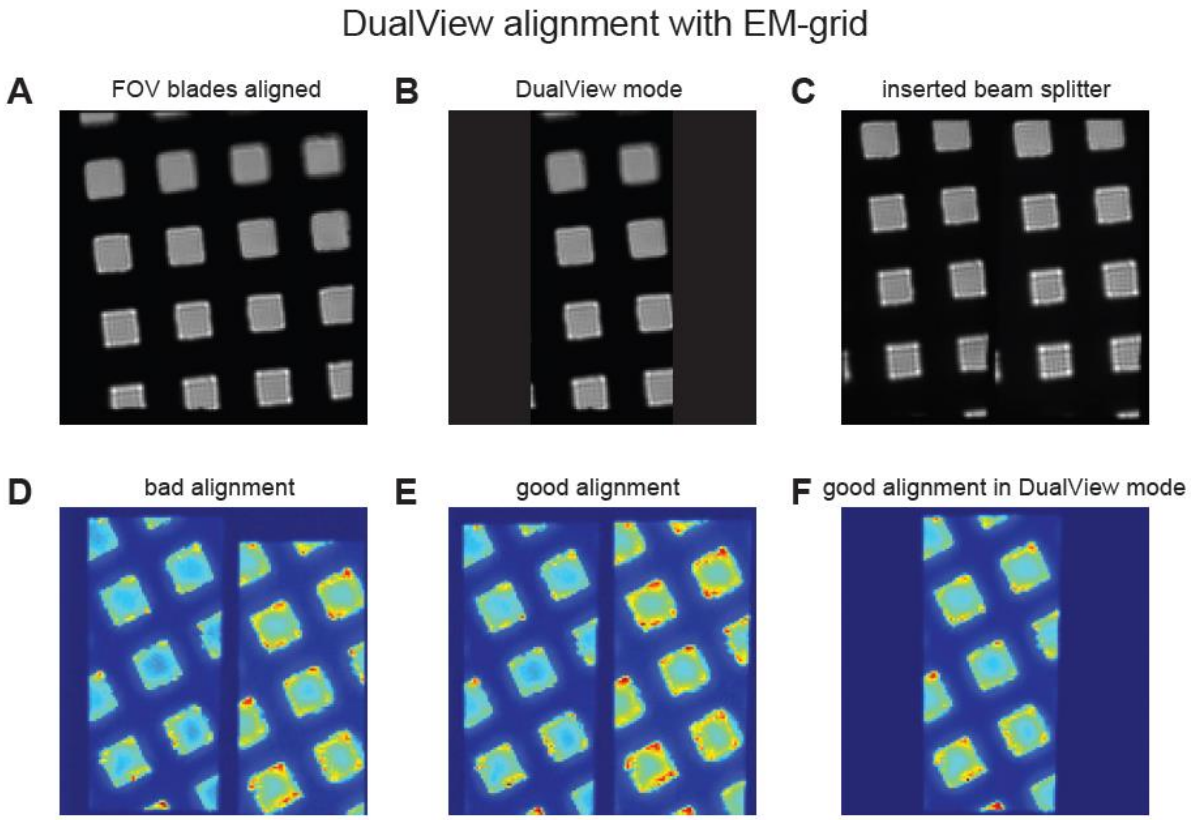

Figure 2.28: Alignment of DualView optics with EM-grid. The transmission image of the grid is projected onto the camera to prove that the image halves overlay as good as possible. (A) - (C) show different stages of the alignment, (D) shows a bad and (E) - (F) good alignments.

In SPIM-FCCS, the focus size of the detection/illumination optics is defined from the point spread functions (PSF). The longitudinal PSFs z_g and z_r are determined from the z-scan of 100 nm multi-fluorescent TetraSpec beads in gel. The lateral PSFs w_g and w_r are determined from the diffusion time of 100 nm multi-fluorescent TetraSpec beads in water measured by SPIM-FCS. The results were z_g=(1100±100) nm and z_r=(1200±100) nm for the longitudinal PSF and w_g=(610±50) nm and w_r=(620±50) nm for the lateral PSF, where g denotes the green and r the

red channel. The width of the pixel a is 400 nm and is determined by the size of the detector pixels. These results are later used for the SPIM-FCCS data evaluation.

For the bead scan, 100 nm TetraSpec beads are diluted in 0.5% Phytagel. 200 mg of gel is dissolved in 40 ml deionized water. 1 ml of gel is mixed with ~10 µl of beads. Around 400 µl of the mixture is draw up into the standard 1 ml syringe and left to thicken in the fridge. Before the z-scan measurement, around 0.5 – 1 cm of the gel is pressed out of the syringe and hanged above to a sample chamber filled with Hanks' solution (*Figure 2.29 A*). The gel is moved close to the detection objective so the light sheet illuminates inside the first 100 µm. It is left to hang for 15 – 20 min to stay still and to assure an accurate scan. With the blue laser set to 15 mW and the green set to 25 mW, 1000 steps with 0.1 µm width are obtained. To measure the longitudinal and lateral PSFs, a 3D Gaussian model function is fit to each bead in both color channels (*Figure 2.29 B* and *C*).

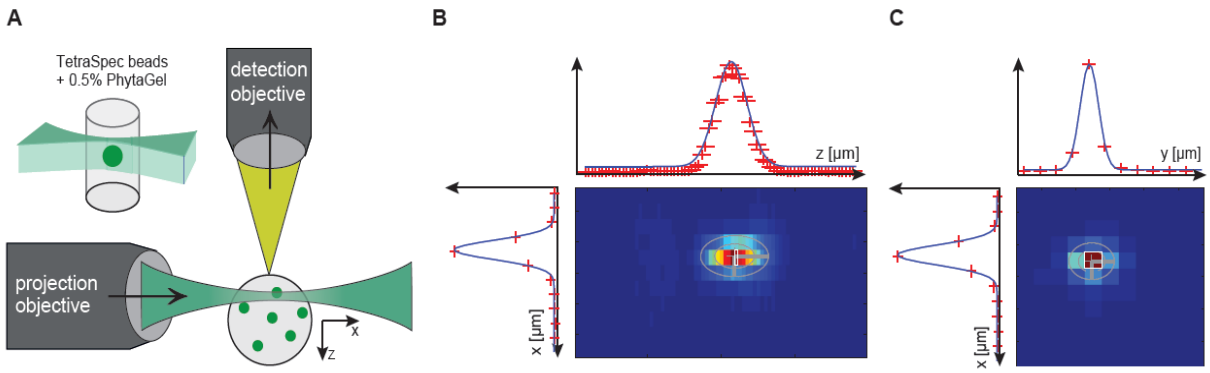

Figure 2.29: Determination of the longitudinal PSF from the z-scan of 100 nm TetraSpec beads in gel. (A) the position of the beads embedded in gel cylinder, (B) xz-cut and (C) xy-cut of the bead.

For the calibration of the PSF size w_g and w_r the multi-fluorescent TetraSpec beads in solution diluted to 0.5 nM were used. The pixel size of the camera a and magnification of the optical system are used to determine the absolute diffusion coefficient of the beads sample. This diffusion coefficient is used to estimate the PSF sizes. The beads are put into a sample bag made of a 25 µm thin plastic foil with the same refractive index as water. The sample bag is heat-sealed and closed on three sides. The bags are washed with 70% ethanol and deionized water. Around 30 µl of solution is filled into the bag and the forth side is heat-sealed to close the bag. The sample can be then stored in the fridge and re-used. Before the measurement, the sample is clipped with tweezers and hanged into the sample chamber filled with Hanks' solution. The

positon of the sample bag is close to the detection objective so the light sheet illuminates inside the first few 100 µm.

The raw SPIM-FCCS data is loaded in QF and auto-correlation functions are calculated for different binnings of the pixels (typically a binning between 1 and 5 was used). A diffusion coefficient is determined for each binning from a fit. Fits were performed for different w_g and w_r values (100 – 500 nm). Increasing the binning, w_g and w_r plotted against the pixel size assemble around the true diffusion coefficient. The average diffusion coefficient is fixed and finally, a good estimate of w_g and w_r can be determined (*Figure 2.30*).

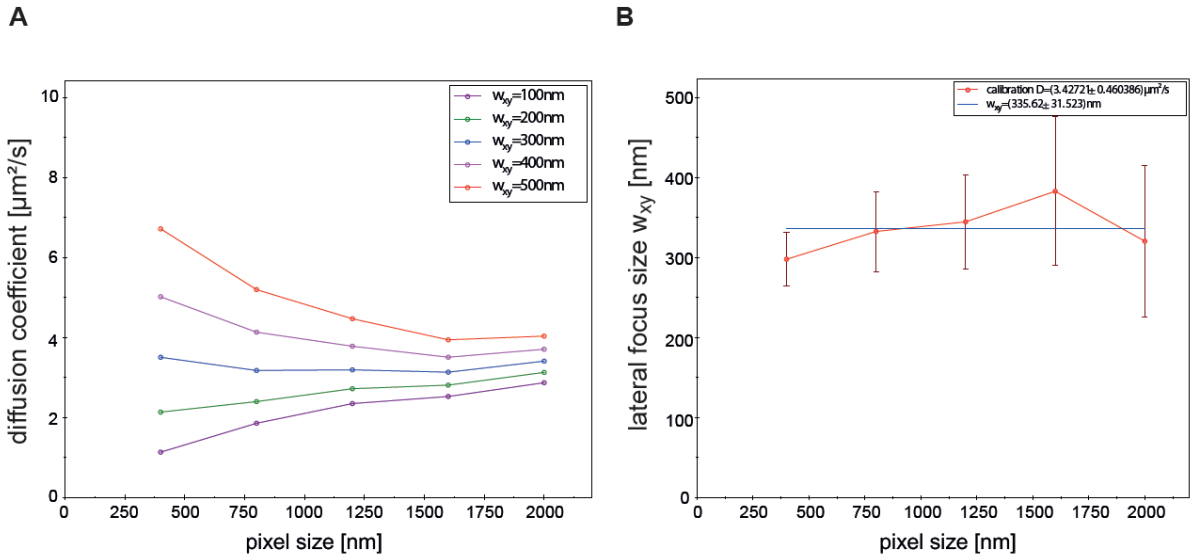

Figure 2.30: An example fit data from SPIM-FCS calibration using the 100 nm TetraSpec beads in solution. (A) fit results of diffusion coefficient *D* obtained with different pixel binning and for different fixed w_{xy}. (B) fit results for w_{xy} with fixed diffusion coefficient. The horizontal line is the average of all pixel binnings and results in w_{xy}=335 nm.

Additionally, to check the setup and validate SPIM-FCCS, a test SPIM-FCCS measurement with multi-fluorescent TetraSpec beads and double-stranded 170bp DNA labeled with Alexa 488 on one and Alexa 594 on the other end was performed. Both solutions were put in a sample bag, clipped with tweezers and hanged from above into the sample chamber. For both samples 100.000 frames were acquired. The auto- and cross-correlation functions for the multi-fluorescent in presented in *Figure 2.31 A*. The auto- and cross-correlation functions for the 170bp DNA are shown in *Figure 2.31 B*. The diffusion coefficients were D= (3.3±0.3) µm^2/s for the beads and D= (23±2) µm^2/s for the 170bp DNA. The amount of binding is determined from the cross-correlation amplitude, which was (0.95±0.1) for the beads and (0.63±5) for the 170bp DNA.

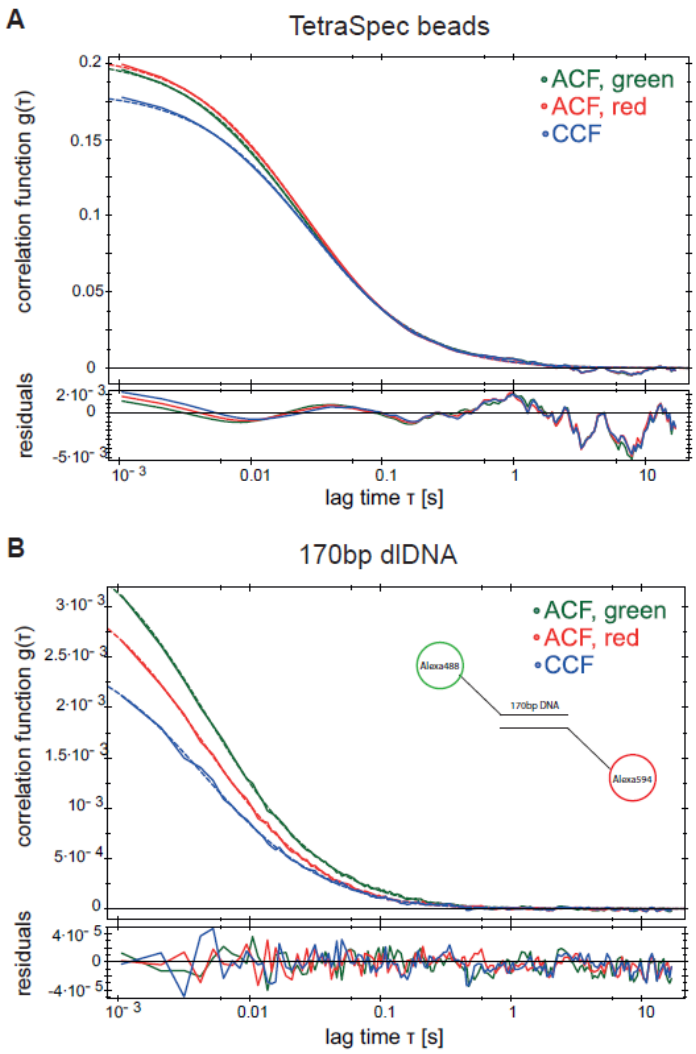

Figure 2.31: Auto-correlation functions obtained by SPIM *in-vitro* FCS measurement on (A) 100 nm multi-fluorescent TetraSpec beads ($D = 3.3\mu m^2/s$) and (B) double-stranded 170bp DNA labeled with Alexa 488 at one and Alexa 594 at the other end ($D = 21\mu m^2/s$). The graphs show the average over all pixels.

3.2.6 DATA EVALUATION

The intensity fluctuations of the two fluorophores at the same spot of a sample are detected simultaneously at corresponding pixels in the detector half planes. For each cell an image series of 50.000 frames with a frame rate of approximately 1000 fps was acquired using both lasers for illumination. The acquisition time typically lasted around 60 s. The full image is split into the green and red channels and the auto- and cross- correlations are calculated using a global fit model, fitting each pixel separately (*Figure 2.32*). By the global fitting approach, the optimum set of parameters is found, minimizing the least-squares deviations of the fit functions

from the measurements. The data was fitted with SPIM-FCS 2-component normal diffusion model implemented in QF software using the correlation functions describer in Chapter 1.4.2 (*Eq. 2.18 – 2.20)*, where the diffusion coefficients are specific to each detection channel and not to the species. The average over all pixels is first fitted to give initial values for further single pixel fits, which are repeated 3 – 5 times to assure all pixels have been appropriately fitted. The amount of binding is defined as the relative concentration p_{AB} (*Equation 2.10*). By color coding the diffusion component values or relative concentrations at each pixel, a parameter image can be constructed. If the cell has moved during the measurement, it has been removed for further evaluation. The cells were masked with a fluorescence intensity threshold to exclude pixels outside the cell or in very dark regions like the nucleolus. The cross-talk factor κ_{gr} between the green and the red color channel was determined on the day of the measurement. For eGFP only, the cross-talk was around 3 % and the cross-talk measured with c-Fos-eGFP only was between 5 and 8 %. The cross-talk correction was incorporated in a model fit.

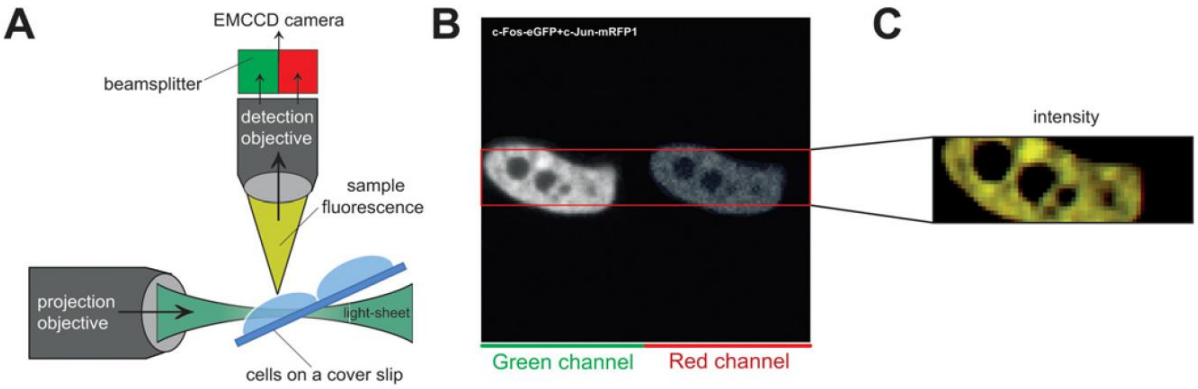

Figure 2.32: (A) SPIM-FCCS principle. The glass piece with adherent cells is positioned at an angle slightly below 45° to the light sheet. (B) an example of a SPIM-FCCS full-frame fluorescence image. The marked area indicates the measurement region (128x20). (C) the total intensity image obtained by combining the images in the green and red channels.

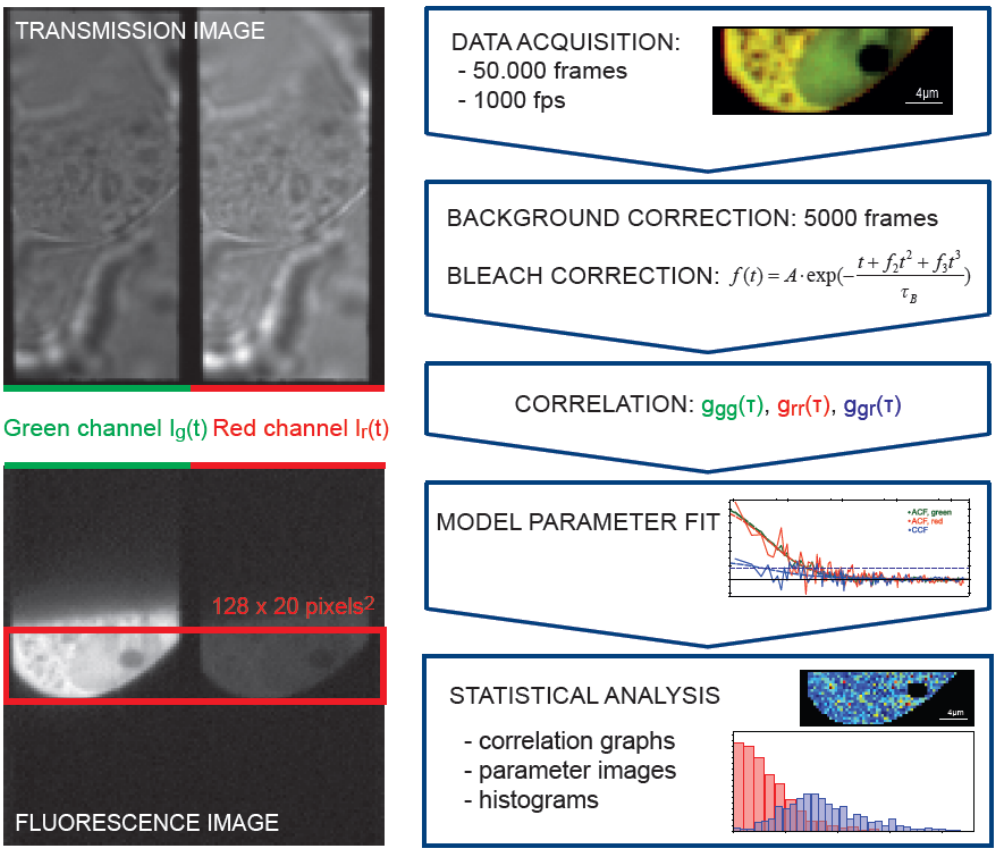

Figure 2.33: SPIM-FCCS data evaluation pipeline. First, image frames with additional background frames are acquired. If necessary a bleach correction is performed independently for each pixel. The measured data is correlated by calculating the auto- and cross-correlation functions and a model is fit to the correlation curves. Additionally, parameter images and histograms can be created.

Artifacts, such as background correction and photo-bleaching, need to be considered during the data fitting. The background signal was measured before each measurement by acquiring 5000 background frames without light sheet illumination and with the same camera settings as for the SPIM-FCCS cell data acquisition. The background images were then averaged and subtracted from the data images. Photo-bleaching is corrected independently for every pixel by normalizing the intensity with an exponential function (*Equation 2.25*) fitted to the pixel's intensity time trace [106]. The effect of different exponential function models used for bleach correction is shown in *Figure 2.34*.

$$f(t) = A \cdot exp\left[-\frac{t+f_2 t^2+f_3 t^3}{\tau_B}\right] \tag{2.25}$$

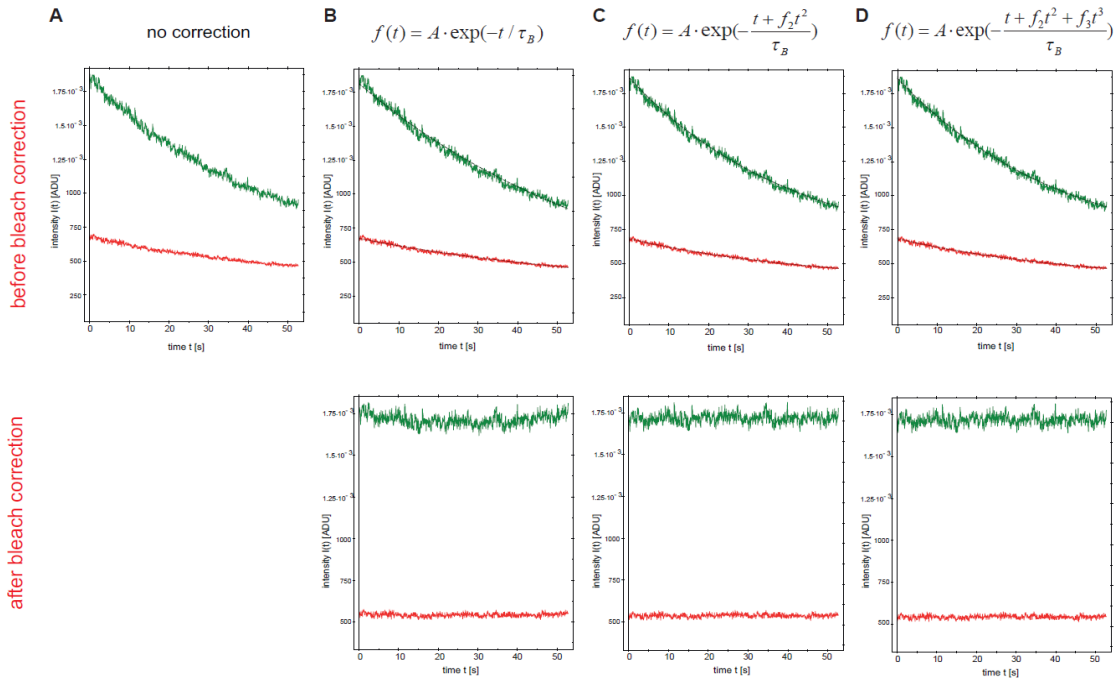

Figure 2.34: Intensity time traces for one pixel before (top) and after (bottom) bleach correction from c-Fos-eGFP and c-Jun-mRFP1 cell. (A) shows the intensity time trace without correction, (B-C) show intensity time traces with bleach correction fits using different exponential models.

3.3 CELL CULTURE

Adherent HeLa cells (provided by F. Rösl, DKFZ, Heidelberg) were grown in a phenol-free DMEM growth medium with 5% fetal calf serum and 1 % Glutamine at 37ºC in a 5% CO_2 humidified atmosphere. The cells are grown in the cell culture flasks and are passaged twice per week when they reach around 80% density. First, the growth medium is removed from the flask and the cells are washed with 5 ml of Hanks' balanced salts solution. To dissolve the cells from the culture flask bottom, 5 ml of Trypsin/EDTA solution is added and the cells incubated at 37ºC for about one minute. To stop the trypsinization process we add 10 ml of DMEM medium. The cells are then diluted (between 1:5 and 1:80) in a 10 ml fresh growth medium and seeded in a new cell culture flask depending on the requirements.

For confocal measurements the cells were seeded in a 60 mm petri dish on a 32 mm glass microscope slide. After two days, the cover glass was removed from the petri dish, washed with 37ºC warm Hanks' solution and transferred to a CHAMO measuring chamber [64, 65]. For SPIM measurements the cells were plated on small glass pieces in a 35 mm petri dish. The cells were then transfected one day before the measurement with a specific expression vector.

3.4 CELL TRANSFECTION

The mammalian expression vectors were transfected with FuGENE HD as proposed by the manufacturer. For confocal FCCS experiments the diluted cell suspension is seeded in a 60 mm petri dish on 32 mm cover slide two days before the measurements [64, 65]. For the SPIM-FCCS measurements, HeLa cells were plated and transfected on small glass pieces in a 35 mm petri dish 48h before the measurements. The cells were transfected 24h before the measurement with a specific expression vector [7, 16]. The transfection concentrations were the same for confocal and for the SPIM measurements, and are presented in *Table 4*.

Protein	**Plasmid**	**Amount of plasmid**	**Transfection**
c-Fos-eGFP and c-Jun-mRFP1	pSV-c-Fos-eGFP and pSV-c-Jun-mRFP1	1 – 1.5 µg	45 µl DMEM medium 4 µl FuGENE HD
c-FosΔΔ-eGFP and c-JunΔΔ-mRFP1	pSV-c-FosΔΔ-eGFP and pSV-c-Jun-ΔΔmRFP1	1 – 1.5 µg	“
eGFP-mRFP1 fusion protein	pSV-eGFP-mRFP1	100 ng	“
eGFP, mRFP1 monomers (IRES)	pIRES2-eGFP-mRFP1	140 ng	“
2x eGFP (dimer)	pCMV-2xGFP	50 ng	“
4x eGFP (tetramer)	pCMV-4xGFP	50 ng	“

Table 4: Transfection protocols of HeLa cells used for the confocal and SPIM measurements (for the standard 35 mm petri dish).

3.5 CELL CYCLE MEASUREMENTS

To be sure that the cells are in the G1, G2, S phase or mitosis, and to be sure the measurements are not performed on apoptotic cells, cells can be inhibited by means of chemicals in the respective cell cycle phase. In the G1 phase control mechanism ensures that everything is ready for DNA synthesis, and in S phase DNA replication occurs. To inhibit the cells in the G1/S phase, the cells are treated with Aphidicolin which inhibits the growth of eukaryotic cells. It especially prevents DNA chain elongation by inhibition of DNA Polymerase α, responsible for DNA replication, but leaves RNA and protein synthesis unaffected.

Aphidicolin was diluted in ethanol to reach 2.5 µg/ml concentration. It has been used to study interaction and mobility of transcription factors c-Fos and c-Jun in HeLa cells. On the first day the cells were seeded 1:5 in the morning (~4 flasks to have enough cells the next day). The cells were transfected on the same day, 5 h later, following the standard transfection protocol. 24 h after seeding the cells, they had to be synchronized. First the medium was removed and 5 ml of fresh medium added to the cells. The flask was shaken five times to inhibit the cells to move. The floating cells were removed from all the flasks and joined together in one. The amount of cells has to reach ~120.000 cells per petri dish. The cells were prepared in petri dishes for SPIM-FCCS measurements. 4 h later 2.5 µl Aphidicolin was added to the cells and the measurements performed 24 h later [7].

3.6 BIOLOGICAL PROCEDURES

For the propagation of plasmid DNA, the XL10-GOLD ultra-competent Escherichia coli (E.coli) cells have been used. In order to make larger quantities of plasmid DNA, this needs to be introduced into the bacteria. The process, where foreign DNA is introduced into a cell is transformation. To prepare the base for the growth and maintenance of E.coli in molecular microbiology procedures, the bacteria was grown in Luria-Bertani (LB) medium, and Agar plates were made from LB-Agar with 30 µg/ml Kanamycin and poured into 10cm petri dishes. After, the plasmid can be replicated.

The plasmid mini preparation kit (NucleoSpin®) was used to produce smaller amounts (10-30 µg) of plasmid DNA. For larger amounts (500 µg) of plasmid DNA, the plasmid maxi preparation kit (NucleoBond®) was used.

3.6.7 TRANSFORMATION

The newly constructed plasmids were transformed as follows:

10 µl of the XL10-GOLD ultra-competent E.coli cells (stored frozen at -80ºC) was left to thaw on ice and 100 ng of DNA was added. The cell suspension was left for 30 min on ice so the plasmids may enter the cells. After, they were stimulated through a heat shock for 40 s at 42ºC to activate the replication of plasmid DNA. After 2min cooling down on ice, 500 µl of SOC medium (high quality medium for bacteria) was added and the mixture put into 37ºC heating block for 1 h. The mixture must be shaken every 15min. During this time, the membrane closes. Finally, the mixture was poured onto an agar plate just to cover the surface of the petri dish. After a while, the mixture was gently scratched with a glass pipette, and left over night in the incubator. Only cells that contain the plasmid will be able to grow and form colonies. The next day, single colonies were picked with a pipette, and transferred and grown in medium with the appropriate antibiotic for further plasmid DNA preparation as described in the next two chapters.

3.6.8 PLASMID DNA MINI PURIFICATION

The plasmid mini preparation kit (NucleoSpin®) was used to produce smaller amounts (10 – 30 µg) of plasmid DNA. It was extracted from 5ml cultures for analysis of ligation and cloning. Preparation was carried out according to manufacturer protocol, described in *Table 5*.

3.6.9 PLASMID DNA MAXI PURIFICATION

To produce larger quantities of plasmid DNA (500 µg), the plasmid maxi preparation kit NucleoBond® PC500 was used. The procedure was followed as proposed by the manufacturer and described in the protocol in *Table 5*. The preparation is similar to the mini preparation, only the used buffer volumes are different. The DNA was bound to the column under low salt concentration and eluted under high salt concentrations.

	MINI plasmid DNA purification	**MAXI** plasmid DNA purification
Cultivate and harvest bacterial cells	Centrifugation: 4000x for 10 min at16ºC	Centrifugation: 5000x for 10 min at16ºC
Cell lysis	0.25 ml Buffer A1 0.25 ml Buffer A2 wait 3 min, room T 0.35 ml Buffer A3	24 ml Buffer S1 24 ml Buffer S2 wait 3 min, room T 24 ml Buffer S3 wait 5 min, room T
Equilibration of the column		7 ml Buffer N2
Clarification of the lysate	Centrifugation: 10.000x for 15 min	Folded filter
Binding	Load cleared lysate onto the column Centrifugation: 10.000x for 1 min	Load cleared lysate onto the column
Washing	0.7 ml Buffer A3	30 ml Buffer N3
Elution	0.5 ml Elution buffer AE	15 ml Buffer N5
Precipitation	0.75 ml Isopropanol Centrifugation: ≥10.000x for 30 min at 6ºC	11 ml Isopropanol Centrifugation: ≥10.000x for 30 min at 6ºC
Wash and dry DNA pellet		1 ml 70% ethanol Centrifugation: ≥10.000x for 10 min at 6ºC dry 10-20 min, room T
Reconstitute DNA		Appropriate volume of TE (tris + EDTA)

Table 5: Protocol for MINI and MAXI plasmid DNA purification as proposed by the Machnerey-Nagel.

III. RESULTS AND DISCUSSION

1 CONFOCAL MICROSCOPY

To assure that SPIM-FCCS is a reliable tool to measure mobility and molecular interactions, the SPIM-FCCS results have to be compared to some reference measurement technique. As the confocal microscopy FCCS is an established technique, it was used as a reference to which SPIM-FCCS measurements were compared.

Before each measurement, the confocal system was calibrated with Alexa 488 and Alexa 594 as described in Chapter 3.1.5. Examples of auto-correlation curves for Alexa 488 and Alexa 594 are shown in *Figure 2.16*. Knowing their diffusion coefficients, the size of the observation volume can be calculated and used for fitting cell FCS data. As the standard for maximum *in vitro* cross-correlation a 170bp DNA labeled with Alexa 488 and Alexa 594 on each end was used. Typical auto- and cross-correlation curves are presented in *Figure 2.17*.

1.1 CONTROL MESUREMENTS IN LIVE HeLa CELLS

The control measurements were performed with eGFP, mRFP1 monomers and the eGFP-mRFP1 fusion protein and respectively served as a reference for minimum and maximum interactions *in vivo*. The eGFP, mRFP1 monomer is a vector expressing the fluorescent proteins separately, but simultaneously in both, the red and the green channels. This assures that there is an equal amount of both proteins present in cells, but with no interaction occurring between them. The eGFP-mRFP1 fusion protein serves as a positive control for the maximum cross-correlation. The fluorescent proteins are connected by a short linker to assure the proteins are moving together.

Pointwise confocal FCCS measurements were performed at a room temperature on 20 HeLa cells expressing eGFP and mRFP1 monomers and on 20 HeLa cells expressing eGFP-mRFP1 fusion proteins. In each cell 6 rounds of 10 s in 4 – 5 selected points were measured. *Figure 3.1* shows examples of auto- and cross-correlation curves of eGFP-mRFP1 dimers (*Figure 3.1 A*) and eGFP, mRFP1 monomers (*Figure 3.1 B*). The auto-correlation functions were normalized

by the number of particles N for the green and the red channels, respectively. The cross-correlation function was normalized by the lower number of particles of one of the auto-correlation curves. The correlation functions were fitted with a global 2-component normal diffusion fit as described in Chapter 1.4.1 and yielded (mean±SD) diffusion coefficients for eGFP, mRFP1 monomers of (0.3±0.05) µm²/s for slow and (30±3) µm²/s for fast moving molecules and for eGFP-mRFP1 fusion protein of (0.3±0.05) µm²/s for slow and (20±3) µm²/s for fast moving molecules. The relative cross-correlation amplitude *q* obtained for the eGFP, mRFP1 monomers was (0.15±0.05). The relative cross-correlation amplitude *q* for eGFP-mRFP1 fusion protein was (0.45±0.05).

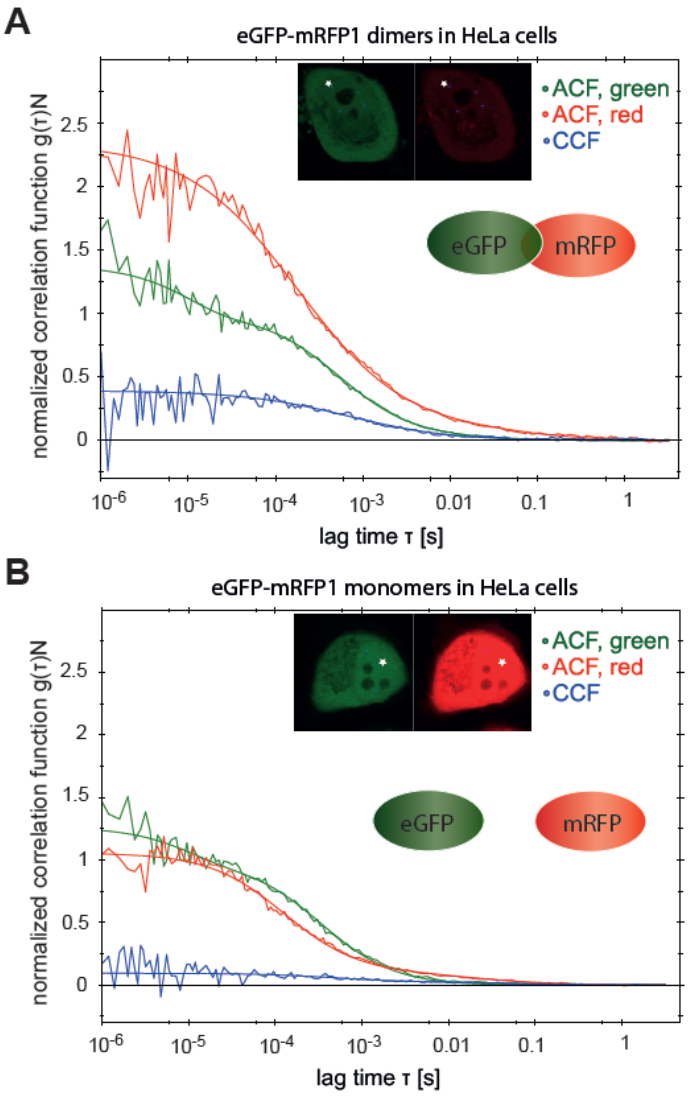

Figure 3.1: Auto- and cross-correlation functions obtained by confocal *in vivo* FCCS measurements on (A) eGFP-mRFP1 fusion protein and (B) eGFP and mRFP1 monomers. The point of measurement is indicated in cell images.

The results for the eGFP, mRFP1 monomers and eGFP-mRFP1 fusion protein well correlate with the previous work presented by N. Baudendistel et al. [7, 16]. The results they obtained are summarized in *Table 6*. The relative cross-correlation amplitude was (0.45±0.04) for the fusion protein and (0.13±0.03) for the monomers, which is very similar to my results. The cross-correlation amplitude of eGFP-mRFP1 fusion protein was taken as the reference level for complete dimerization in vivo and the cross-correlation amplitude for the separately expressed eGFP and mRFP1 proteins served as the reference for no interaction.

1.2 c-Fos AND c-Jun TRANSCRIPTION FACTORS

FCCS results on c-Fos-eGFP and c-Jun-mRFP1 using single-point measurements on a confocal setup have been presented before by N. Baudendistel [7, 16]. The findings demonstrated interaction of c-Fos-eGFP and c-Jun-mRFP1 in living HeLa cell nuclei. Here, I repeated the same measurements to verify the novel results obtained by the SPIM-FCCS.

I have conducted pointwise confocal FCCS measurements at a room temperature on 20 HeLa cells expressing c-Fos and c-Jun and 20 HeLa cells expressing c-Fos and c-Jun deletion mutants. All selected cells have equal level of fluorescence. As due to their NLS c-Fos and c-Jun are located only in the cell nuclei, measurements were performed in this area. Deletion mutants that are lacking dimerization and DNA-binding domains served as a negative control. The measurements were performed in 4 – 5 points in each cell. Data acquisition time consisted of 6 rounds of 10 s. *Figure 3.2* shows typical auto- and cross-correlation functions of confocal FCCS measurements of c-Fos-eGFP and c-Jun-mRFP1 (*Figure 3.2 A*) and its mutants (*Figure 3.2 B*). The auto-correlation functions were normalized by the number of particles N for the green and the red channels, respectively. The cross-correlation function was normalized by the lower number of particles of one of the auto-correlation curves. The correlation functions were fitted with a global 2-component normal diffusion fit as described in Chapter 1.4.1 and yielded (mean±SD) diffusion coefficients for c-Fos and c-Jun of (0.25±0.05) μm²/s for slow and (15±3) μm²/s for fast moving molecules. The fast component indicates freely diffusing proteins, whereas the slow component indicates that the AP-1 proteins are almost immobilized and that this complex might be associated with DNA. Control measurements performed with c-Fos and c-Jun deletion mutants yielded diffusion coefficients of (0.3±0.05) μm²/s for slow and (23±4) μm²/s for fast moving molecules.

The results about mobility of c-Fos-eGFP and c-Jun-mRFP1 can be well illustrated by histograms of slow and fast diffusion coefficients. *Figure 3.3* shows a histogram of slow and fast diffusion coefficients obtained from all c-Fos-eGFP cell measurements. The c-Jun-mRFP1 results obtained for all 20 cells are shown in *Figure 3.4*. The histogram presents a slow and a fast diffusion coefficient. The results were obtained from a 2-component normal diffusion fit and the average over all 20 measurements was calculated.

The relative cross-correlation amplitude *q* was used to measure the interaction between the proteins. The obtained *q* for the deletion mutants was (0.18±0.05), which was close to the minimal value (0.15±0.05) obtained for eGFP, mRFP1 monomers. The relative cross-correlation amplitude *q* for the c-Fos-eGFP and c-Jun-mRFP1 was (0.35±0.05), which indicates their dimerization, as the value for the eGFP-mRFP1 fusion protein was (0.45±0.05). The *in vivo* confocal FCCS results are summarized in *Table 6*.

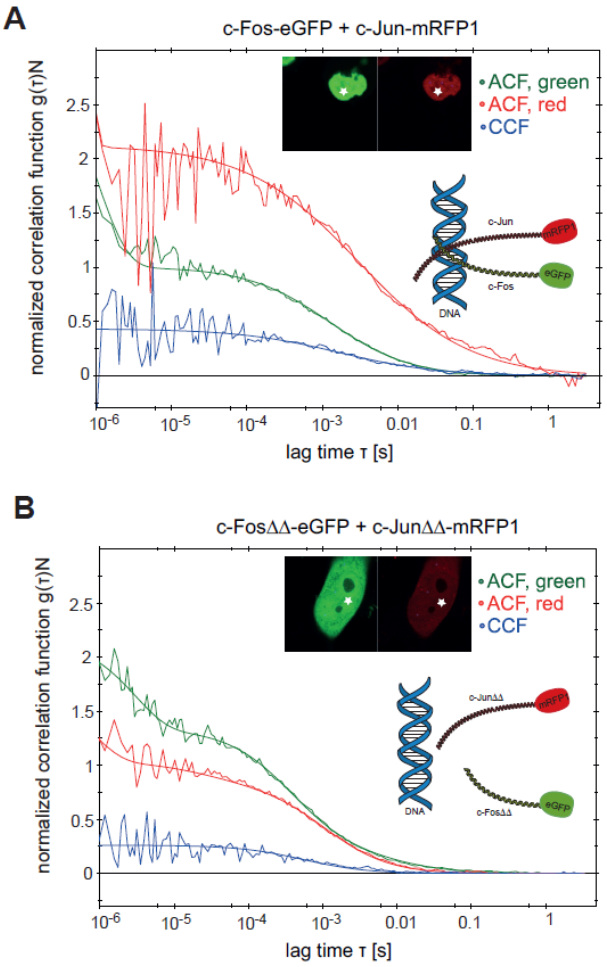

Figure 3.2: Auto- and cross-correlation functions obtained by confocal *in vivo* FCCS measurements on (A) AP-1 wild-type proteins c-Fos-eGFP and c-Jun-mRFP1 and (B) AP-1 deletion mutants c-FosΔdimΔDNA-eGFP and c-JunΔdimΔDNA-mRFP1. The point of measurement is indicated in cell images.

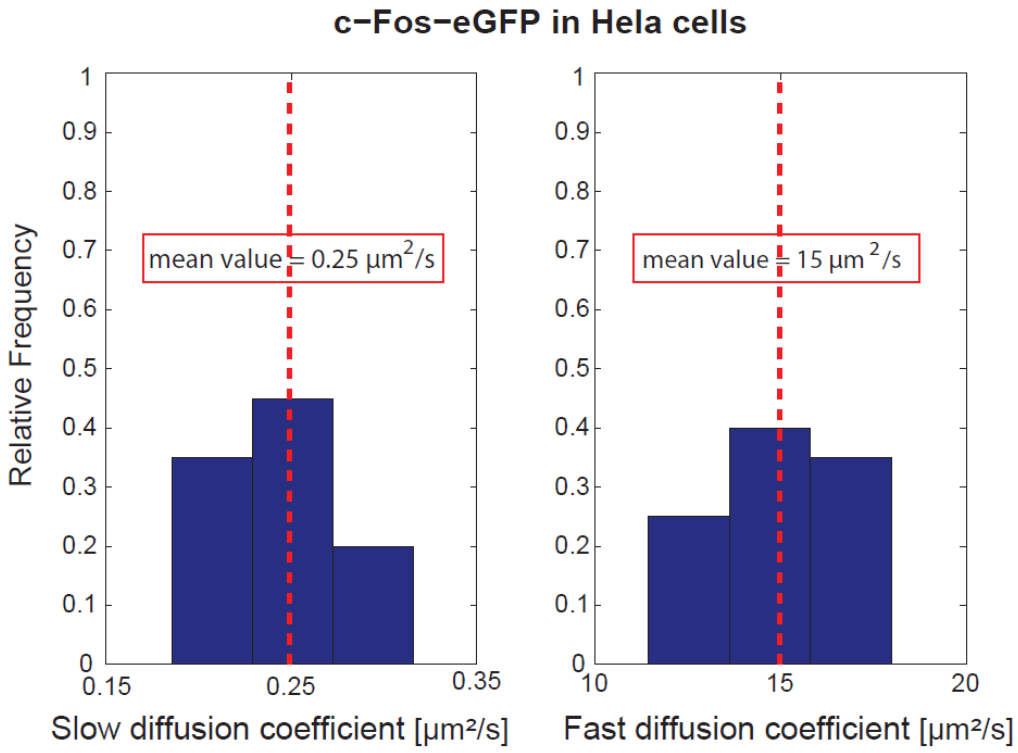

Figure 3.3: Confocal FCCS *in vivo* measurements of AP-1 wild type HeLa cell: histograms of slow and fast diffusion coefficient of c-Fos-eGFP for 20 measured cells.

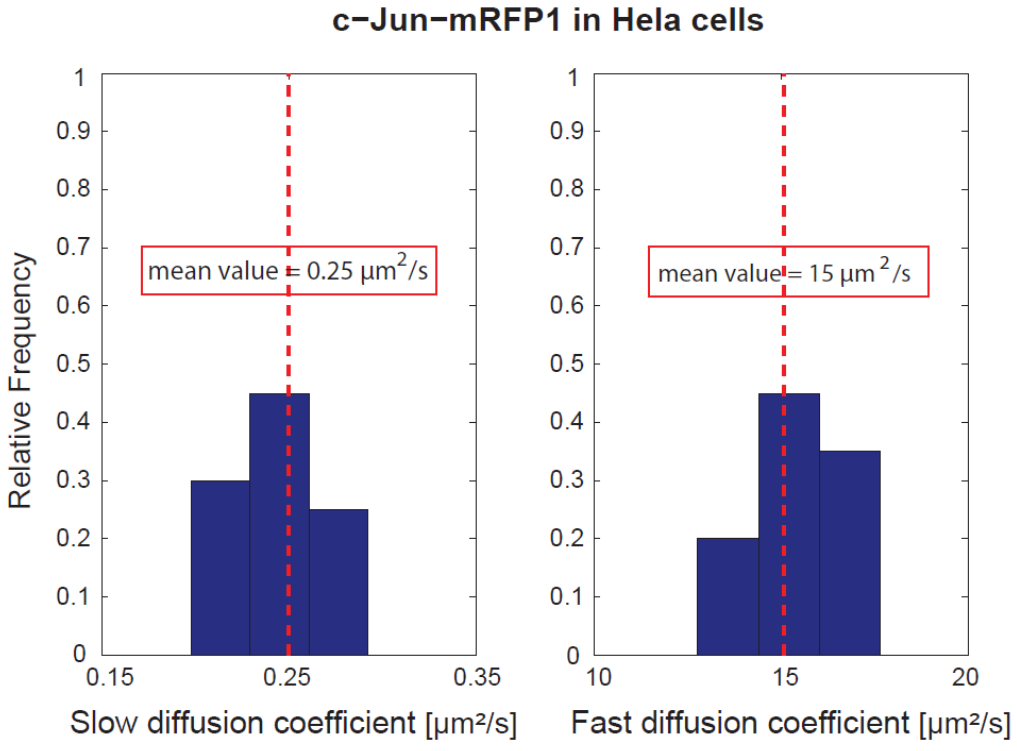

Figure 3.4: Confocal FCCS *in vivo* measurements of AP-1 wild type HeLa cell: histograms of slow and fast diffusion coefficient of c-Jun-mRFP1 for 20 measured cells.

	Confocal FCCS			Confocal FCCS [7, 16]		
CELLS	D_{fast} [μm²/s]	D_{slow} [μm²/s]	q	D_{fast} [μm²/s]	D_{slow} [μm²/s]	q
c-Fos-eGFP, c-Jun-mRFP1	15±3 15±3	0.25±0.05	0.35±0.05	9±3 11±5	0.18±0.06	0.31±0.06
c-FosΔΔ-eGFP, c-JunΔΔ-mRFP1	23±4 23±4	0.3±0.05	0.18±0.05	23±7 34±9	0.03±0.2	0.18±0.04
eGFP-mRFP1 fusion protein	20±3	0.3±0.05	0.45±0.05	19±7	0.03±0.2	0.45±0.04
eGFP, mRFP1 monomer protein	30±3	0.3±0.05	0.15±0.05	25±4	0.03±0.2	0.13±0.03

Table 6: Summary of the confocal FCCS results: (mean±SD) of diffusion coefficients D_{fast} and $D_{slow,}$ and relative cross-correlation amplitudes q obtained on confocal FCCS in this thesis and by [7, 16].

N. Baudendistel et al. [7, 16] were the first to use the c-Fos and c-Jun transcription factors system to demonstrate protein-protein interactions in live HeLa cells. For control measurements they used the c-Fos and c-Jun deletion mutants. The results they obtained are summarized in *Table 6*, which also shows the results that I have obtained. The relative cross-correlation amplitude was (0.31±0.06) for the c-Fos-eGFP and c-Jun-mRFP1, which is very similar to my results. Mine and N. Baudendistel et al. cross-correlation amplitudes clearly indicate c-Fos and c-Jun dimerization. The previous research resulted in relative cross-correlation amplitude of (0.18±0.04) for the deletion mutants, which is identical to my results. This indicates no dimerization between c-Fos and c-Jun taking into account the cross-correlation amplitude of (0.15±0.5) measured by eGFP, mRFP1 monomers serving as the negative control.

The fast and slow diffusion component from the c-Fos-eGFP and c-Jun-mRFP1 measurements that N. Baudendistel et al. [7, 16] obtained were also comparable to my results. The fast diffusion component that corresponds to freely diffusing c-Fos and c-Jun resulted in (9±3) μm²/s in the green and (11±5) μm²/s in the red channel. The slow diffusion component was (0.18±0.06) μm²/s in the green and (0.18±0.07) μm²/s in the red channel. The previous and my results indicate a strong retention or immobilization of the c-Fos and c-Jun transcription

factors. The slow diffusion component was higher than for the c-Fos and c-Jun deletion mutants, where the dimerization and DNA-binding domains were removed. The fast diffusion coefficient for the deletion mutants was (23±7) μm²/s in the green and (34±9) μm²/s in the red channel. This is also comparable to my results obtained for the c-Fos and c-Jun deletion mutants.

In summary, all results I have obtained by confocal FCCS measurements of c-Fos-eGFP and c-Jun-mRFP1, as well as for their deletion mutants in HeLa cells well agree with previously obtained results on these specimen. The presented results indicate that my confocal FCCS measurements can be used to verify the novel results of c-Fos-eGFP and c-Jun-mRFP1 obtained with the SPIM-FCCS and presented in this Thesis.

2 SINGLE PLANE ILLUMINATION MICROSCOPY

SPIM-FCS is a novel technique to monitor mobility and interaction in the whole image plane simultaneously and not just in one point like on conventional confocal FCCS. With SPIM-FCCS an image series is acquired. FCS is measured in every pixel of the camera and auto-correlation functions are calculated for each pixel separately. The cross-correlation functions are calculated between the corresponding pixels in two color channels. The fit is performed for each pixel separately, where diffusion coefficients are specific to each detection channel and not to the species. By color-coding the diffusion coefficients, number of particles, fraction of the slow diffusion coefficient or the relative concentrations at each pixel, corresponding maps can be constructed, showing the differences between different sites in the cell.

On each day of measurements, the SPIM microscope was calibrated following the procedure described in Chapter 3.2.5. First, a blue 491 nm and a green 561 nm laser sheets were aligned, following by the alignment of the red and green channels by maximizing the cross-correlation coefficient between the two corresponding images of a calibration grid. The lateral PSF was determined from the diffusion time of 100 nm TetraSpec beads by SPIM-FCS and the longitudinal PSF was determined from the z-scan of 100 nm TetraSpec beads in gel.

2.1 MOBILITY OF eGFP OLIGOMERS IN LIVE HeLa CELLS

To test the SPIM-FCS system, I measured the diffusion of eGFP oligomers in live HeLa cells. Because the diffusion coefficient of oligomers consisting of more monomer units will be lower than the diffusion coefficient of the oligomers consisting fewer monomer units, a correctly operating SPIM-FCS system should be able to detect differences in mobility. Additionally, the eGFP measurements were also performed to determine the cross-talk between the green and the red channel. Previous measurements on eGFP oligomers were performed using the confocal FCS where the diffusion properties were spatially resolved by multi-spot FCS measurements [64, 65]. In this Thesis I experimented with eGFP dimers and eGFP tetramers using 20 HeLa cells for measurements. For each measurement, a 64 x 20 pixels region of interest (ROI) of the camera sensor was selected and 100.000 frames were acquired.

Figure 3.5 shows the fit results for two representative cells. *Figures 3.5 A* and *B* present the intensity images, diffusion coefficients and number of particles maps for the eGFP dimer and tetramer, respectively. It can be noticed from the intensity images that the fluorescence ratio

between the nucleus and the cytoplasm decreases with the size of the oligomer. The eGFP tetramers are bigger than dimers and therefore cannot freely diffuse through the NPC from cytoplasm to the nucleus. This can be also noticed in the diffusion coefficient and number of particles maps in *Figure 3.5 A* and *B*. The diffusion coefficients and number of particles were defined for each pixel separately and the maps were created. The (mean±SD) diffusion coefficient of eGFP dimers was (31±10) μm²/s and of eGFP tetramers was (20±10) μm²/s. From the diffusion coefficient maps, no significant pattern within the cell could be visually observed. The diffusion coefficients were compared by creating histograms shown in *Figure 3.5 C* for the eGFP dimer and tetramer, respectively. The average diffusion coefficient was calculated for both proteins. For these two specific cells the average diffusion coefficients were 29 μm²/s and 21 μm²/s for the dimer and tetramer, respectively. The auto-correlation functions are presented in *Figure 3.5 D* for eGFP dimers in orange and eGFP tetramers in blue. They clearly indicate that the decay time increases with the size of the eGFP protein. These results clearly demonstrate the capability of the SPIM-FCS system.

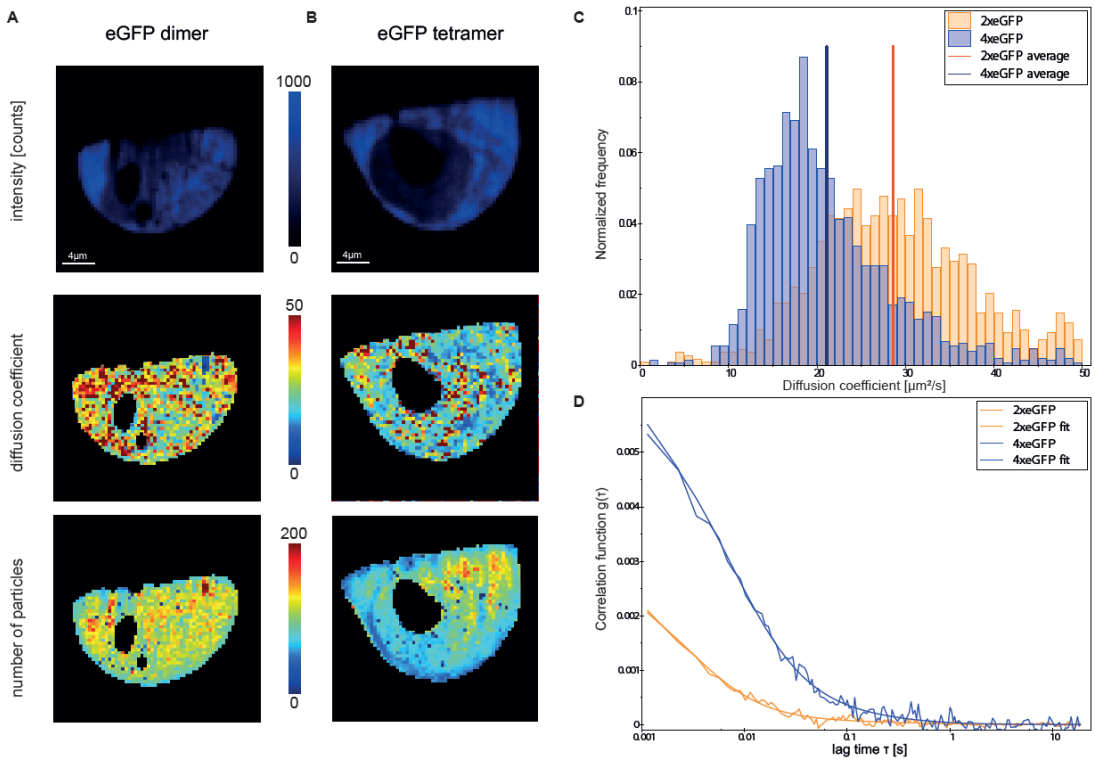

Figure 3.5: SPIM-FCS *in vivo* control measurement of the eGFP oligomers expressed in HeLa cells. The intensity image and color coded diffusion coefficients and number of particles maps for (A) eGFP dimer and (B) eGFP tetramer. (C) histogram of diffusion coefficients with averages and (D) auto-correlation functions and fits for the eGFP dimer (orange) and eGFP tetramer (blue).

The FCS measurements on eGFP oligomers have been done before by N. Dross et al. using a confocal microscope [64, 65]. Their results can be compared to the SPIM-FCS measurements on eGFP dimers and tetramers presented in this Thesis. They acquired between 30 – 50 localized FCS measurements per cell and constructed diffusion coefficient maps. Their FCS measurement positions were equally distributed over the entire cell. The acquisition length was reduced to 2 runs of 3 s and the diffusion coefficient was calculated for each point. Their maps showed regions of different diffusion times both in the nucleus and the cytoplasm. Similar structures could be noticed from the SPIM-FCS diffusion maps presented in *Figure 3.5*. The advantage of the SPIM-FCS is that the measurements are performed simultaneously in all pixels of the cell. The diffusion coefficients can be obtained for each pixel and the maps constructed more precisely than with the FCS measurements on confocal microscope.

They have obtained the diffusion coefficients for eGFP dimers in the range of 58 – 14.5 μm²/s with the average of 31 μm²/s. For the eGFP tetramers, they have obtained the diffusion coefficient in the range of 42 – 8 μm²/s with the average of 20.2 μm²/s. These averages are in perfect agreement with the averages I have obtained with SPIM-FCS.

2.2 CONTROL MEASUREMENTS IN LIVE HeLa CELLS

To further verify the SPIM-FCCS method, I have performed *in vivo* control measurements of eGFP and mRFP1 monomers and eGFP-mRFP1 fusion protein.

The eGFP, mRFP1 monomers were expressed in HeLa cells from a single plasmid constructed as described in 2.4 [7, 16]. This assured that both proteins were present equally in all cells. The eGFP-mRFP1 fusion protein is a vector with a short linker to separate the fluorophores. These constructs were used to obtain reference minimum and maximum relative concentrations p_{AB} *in vivo*, respectively, similarly as q values were obtained for these constructs by confocal FCCS.

I measured FCCS of eGFP and mRFP1 monomers and eGFP-mRFP1 fusion protein of 20 cells each. For each measurement I selected a 128 x 20 pixels large ROI and acquired 100.000 frames at a room temperature. For the auto- and cross-correlation data analysis a global fit was used. The data was fitted with the SPIM-FCS 2-component normal diffusion model as described in Chapter 1.4.2. It was assumed that the proteins have the same size and thus the same diffusion coefficients, therefore the three diffusion coefficients were linked together during the fit.

Figures 3.6 A, B and *C* show a typical intensity image and maps of the fast and slow diffusion coefficient components and relative concentrations for the negative and positive controls, i.e. monomers and fusion protein, respectively. Typical correlation functions and fits are shown in *Figures 3.6 D* and *E*. The (mean±SD) of the fast diffusion coefficient D_{fast}, obtained over 20 cell measurements, was (30±20) $\mu m^2/s$ for the eGFP-mRFP1 fusion protein and (38±15) $\mu m^2/s$ for the eGFP and mRFP1 monomers. The slow diffusion coefficient D_{slow} was (0.39±0.2) $\mu m^2/s$ for the fusion protein and (0.38±0.2) $\mu m^2/s$ for the monomers.

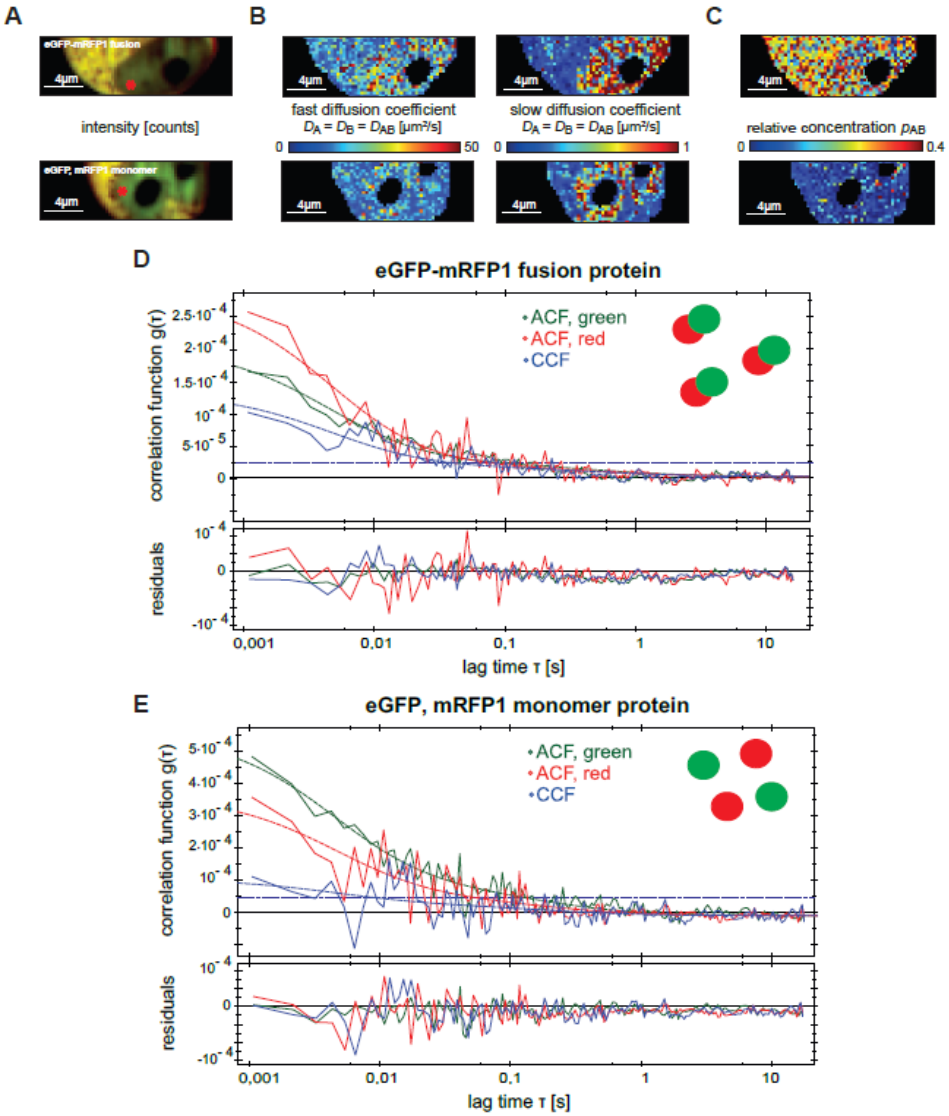

Figure 3.6: SPIM-FCCS *in vivo* control measurement of the eGFP-mRFP1 fusion protein (upper row) and eGFP and mRFP1 monomers (lower row) expressed in HeLa cells. (A), (B) and (C) the intensity image, slow and fast diffusion coefficient and relative concentration maps, respectively. (D) and (E) auto- and cross-correlation functions and fits for the fusion protein and the monomers, horizontal dashed lines indicate the cross-correlation explained by cross-talk.

The relative concentration p_{AB} was (0.29±0.15) for the fusion protein and served as a reference for complete dimerization *in vivo*. The separately expressed eGFP and mRFP1 gave a relative concentration p_{AB} of (0.08±0.08). This value was assumed as background due to spectral cross-talk between the channels and served as a reference for no interaction. The results for all 20 cells are presented in the Appendix (*Figures A1* and *A3*). For comparative purposes the histograms of relative concentrations for eGFP, mRFP1 monomers and eGFP-mRFP1 fusion protein are shown in histogram in *Figure 3.7*. It is evident that the relative concentrations for the fusion proteins peak around 0.2 and the relative concentrations for the monomers peak close to zero. The results are comparable to the confocal FCCS measurements on the same construct performed by N. Baudendistel et al. [7, 16].

In conclusion, the *in vivo* control measurements of eGFP and mRFP1 monomers and eGFP-mRFP1 fusion protein demonstrate the correct operation of the SPIM-FCCS method.

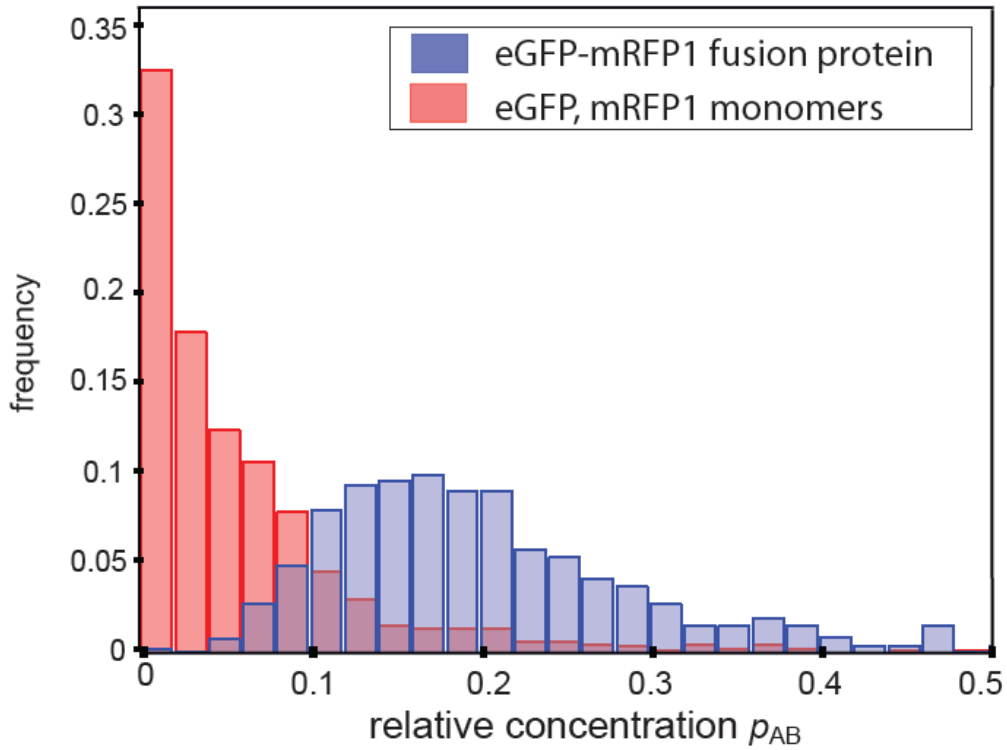

Figure 3.7: SPIM-FCCS *in vivo* measurements of eGFP-mRFP1 fusion protein and eGFP and mRFP1 monomers in HeLa cell: a histogram of relative concentration for the cells shown in *Figure 3.6*.

2.3 CHARACTERIZATION OF c-Fos AND c-Jun TRANSCRIPTION FACTORS

The transcription factors c-Fos and c-Jun have been described before in Chapters 4.1 and 4.2. I have performed SPIM-FCCS measurements at a room temperature on 20 HeLa cells expressing either c-Fos and c-Jun or their deletion mutants. The c-Fos and c-Jun are located only in the cell nuclei due to their nuclear localization sequence that is present in all full-length AP-1 proteins. The deletion mutants are lacking the dimerization and DNA-binding domains and serve as a negative control. They are distributed over the cytoplasm and the nucleus, as they are lacking the NLS. For each measurement I selected a 128 x 20 pixels ROI and acquired 100.000 frames. For the auto- and cross-correlation data analysis a global fit was used. The data was fitted with the SPIM-FCS 2-component normal diffusion model as described in Chapter 1.4.2.

SPIM-FCCS results of a typical HeLa cell with AP-1 wild type proteins c-Fos-eGFP and c-Jun-mRFP1 and one with deletion mutants are presented in *Figure 3.8*. The results for all 20 cells were similar and are shown in the Appendix (*Figures A5* and *A7*).

Figure 3.8 A shows the intensity images for the c-Fos-eGFP and c-Jun-mRFP1 (top) and the mutants (bottom). The upper image clearly indicates that c-Fos and c-Jun are localized only in the cell nucleus, while the mutants are distributed also in the cytoplasm. For the cells containing c-Fos-eGFP and c-Jun-mRFP1, the globally fitted diffusion coefficient was (0.28±0.1) μm²/s in the green and (0.3±0.1) μm²/s in the red channel for the slow and (18±10) μm²/s in the green and (23±6) μm²/s in the red channel for the fast component (*Table 7*). The diffusion maps (*Figure 3.8 B*) show the slow diffusive component represented formally by a diffusion coefficient. This should be taken as a phenomenological indication of mobility, since the actual random motion of proteins in the crowded intracellular environment is obviously more complex than can be described by one simple diffusion process. For the c-Fos-eGFP and c-Jun-mRFP1 mutants there is a lot of noise on the slow diffusion coefficient because of its much lower amplitude compared to the wild type.

As previously described [7, 16], I identified the slow diffusion coefficient with AP-1 proteins bound to immobile structures in the cell nucleus, most probably DNA. However, I also detected two diffusing components in the mutants with diffusion coefficients (0.38±0.2) μm²/s in the green and (0.4±0.2) μm²/s in the red channel for the slow, and (22±10) μm²/s in the green and (23±7) μm²/s in the red channel for the fast component. The slow component might therefore partially correspond to non-specifically trapped proteins.

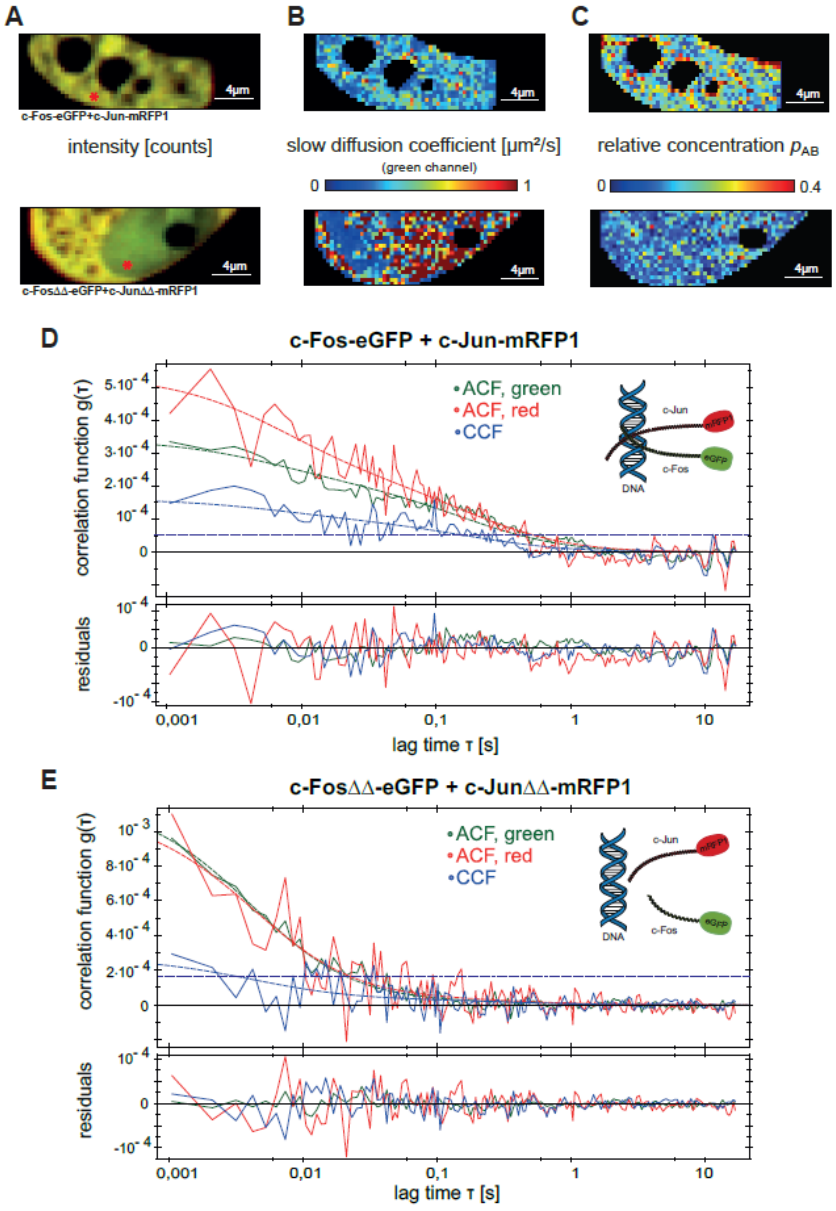

Figure 3.8: : SPIM-FCCS *in vivo* measurements of AP-1 wild type proteins and deletion mutants in HeLa cell. (A) intensity images, (B) diffusion coefficients and (C) relative concentration maps for AP-1 wild type proteins (top) and its mutants (bottom), respectively. (D) and (E) auto- and cross-correlation functions and fits, obtained for locations indicated by the red mark in the intensity images. The horizontal dashed lines indicate the cross-correlation explained by cross-talk.

The well-structured map of relative concentrations for the cell expressing c-Fos-eGFP and c-Jun-mRFP1 (*Figure 3.8 C* top) clearly indicates stronger interactions, while the map of the cell expressing deletion mutants (*Figure 3.8 C* bottom) is indicative of almost no interactions: this could be expected since their dimerization and DNA-binding domains were deleted. The small amount of interaction, i.e. low values of p_{AB} are the consequence of cross-correlation due

to cross-talk (horizontal lines marked in the correlation function graphs). The relative concentration p_{AB}, averaged over 20 cells, was (0.21±0.18) for the c-Fos-eGFP and c-Jun-mRFP1, and (0.13±0.07) for the deletion mutants.

Figures 3.8 D and *E* show auto- and cross-correlation functions obtained for locations indicated by the red mark in the intensity images. The cross-talk has been measured with c-Fos-eGFP only in HeLa cell and was between 5 and 8 %. The cross-talk correction was incorporated in the model fit. The cross-correlation explained by cross-talk is indicated in *Figures 3.8 D* and *E* by the horizontal dashed lines.

Additionally, c-Fos-eGFP was expressed together with c-Jun-mRFP1 deletion mutant in (*Figure 3.9 A*) and c-Jun-mRFP1 was expressed together with c-Fos-eGFP deletion mutant in HeLa cell (*Figure 3.9 B*). It can be seen in the intensity images that AP-1 transcription factors are located only in the nucleus. The relative concentration maps demonstrate that no interaction was measured between the AP-1 wildtype and the deletion mutants.

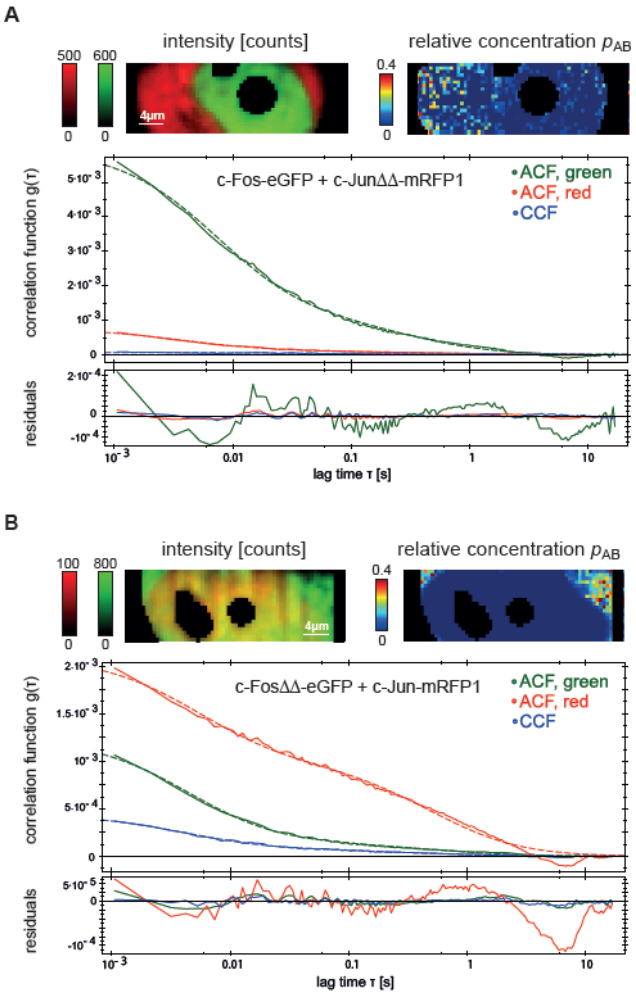

Figure 3.9: SPIM-FCCS *in vivo* measurements: auto- and cross-correlation functions and fits of (A) c-Fos-eGFP and c-JunΔΔ-mRFP1 and (B) c-FosΔΔ-eGFP and c-Jun-mRFP1 in HeLa cells.

The two histograms in *Figure 3.10* illustrate the difference in slow diffusion coefficients between the c-Fos-eGFP and c-Jun-mRFP1, and its mutants. The difference between the wildtype and the mutants is clearly demonstrated. The (mean±SD) of slow diffusion coefficients for all 20 cells expressing c-Fos-eGFP and c-Jun-mRFP1 are shown in *Figure 3.11*. The difference in fast diffusion coefficients between the c-Fos-eGFP and c-Jun-mRFP1, and its mutants is demonstrated in the two histograms in *Figure 3.12*. The (mean±SD) diffusion coefficients values of the fast component for all 20 c-Fos-eGFP and c-Jun-mRFP1 cells are shown in *Figure 3.13*. The two histograms in *Figure 3.14* illustrate the difference in the relative concentration p_{AB} between the c-Fos-eGFP and c-Jun-mRFP1, and its mutants. As already shown by the p_{AB} maps, the mutants exhibited no significant interaction. Figure 3.15 shows the (mean±SD) of relative concentration for all 20 c-Fos-eGFP and c-Jun-mRFP1 cells.

The slow and fast component diffusion coefficients, relative concentrations p_{AB} and relative cross-correlation amplitudes q, obtained by SPIM-FCCS and confocal FCCS, for the c-Fos-eGFP and c-Jun-mRFP1, their mutants, eGFP-mRFP1 fusion protein, and eGFP, mRFP1 monomers are summarized in *Table 7*. The values are averaged over 20 HeLa cell measurements each.

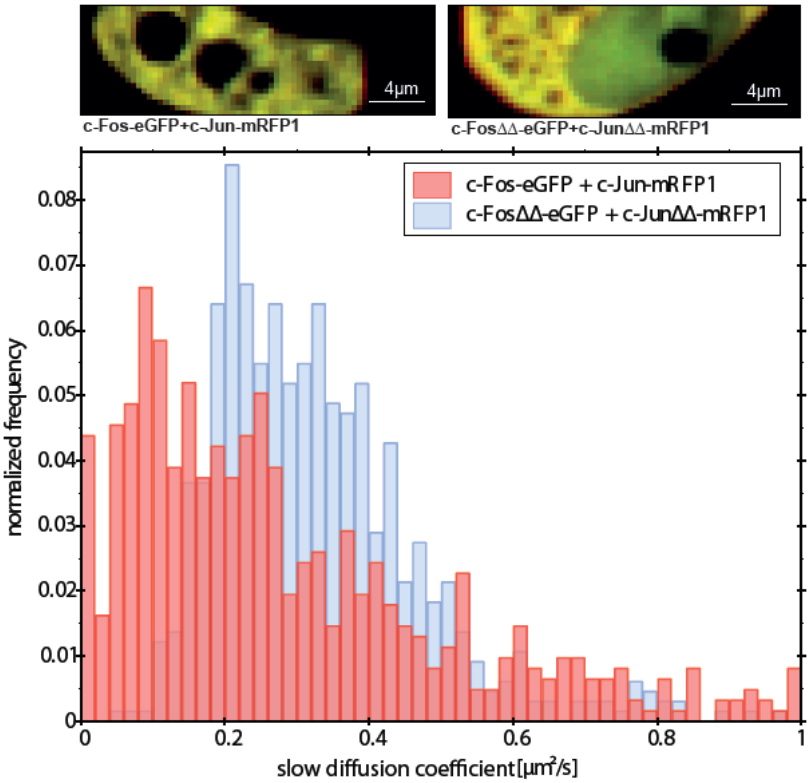

Figure 3.10: SPIM-FCCS *in vivo* measurements of AP-1 wild type proteins and deletion mutants in HeLa cell: a histogram of slow diffusion coefficient for the cells shown above.

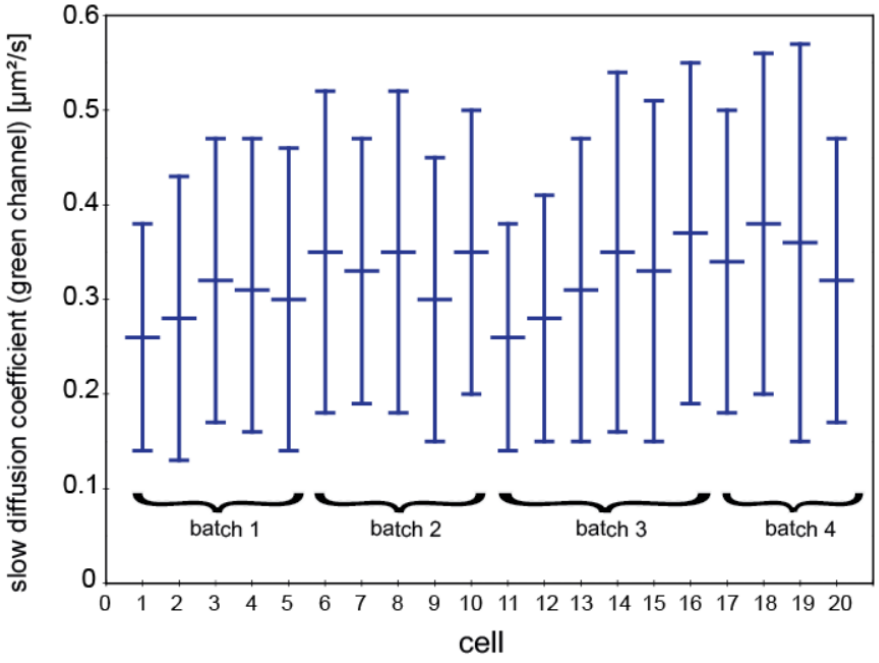

Figure 3.11: SPIM-FCCS *in vivo* measurements of AP-1 wild type proteins in HeLa cell: (mean±SD) of slow diffusion coefficient in the green channel for all 20 measured cells.

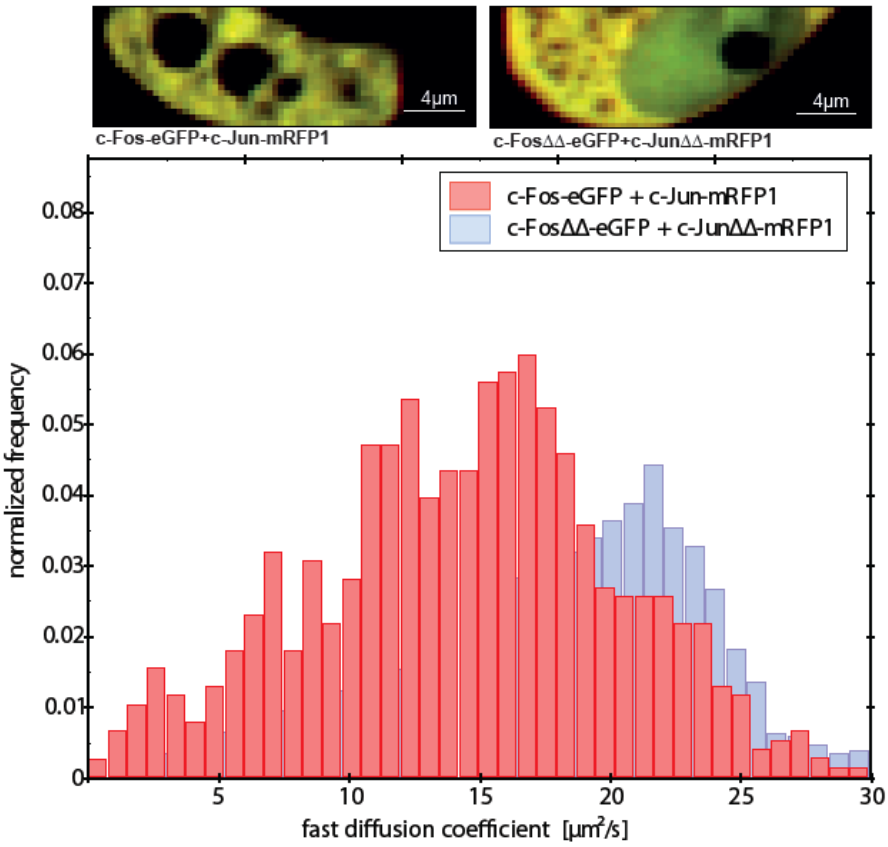

Figure 3.12: SPIM-FCCS *in vivo* measurements of AP-1 wild type proteins and deletion mutants in HeLa cell: a histogram of fast diffusion coefficient for the cells shown above.

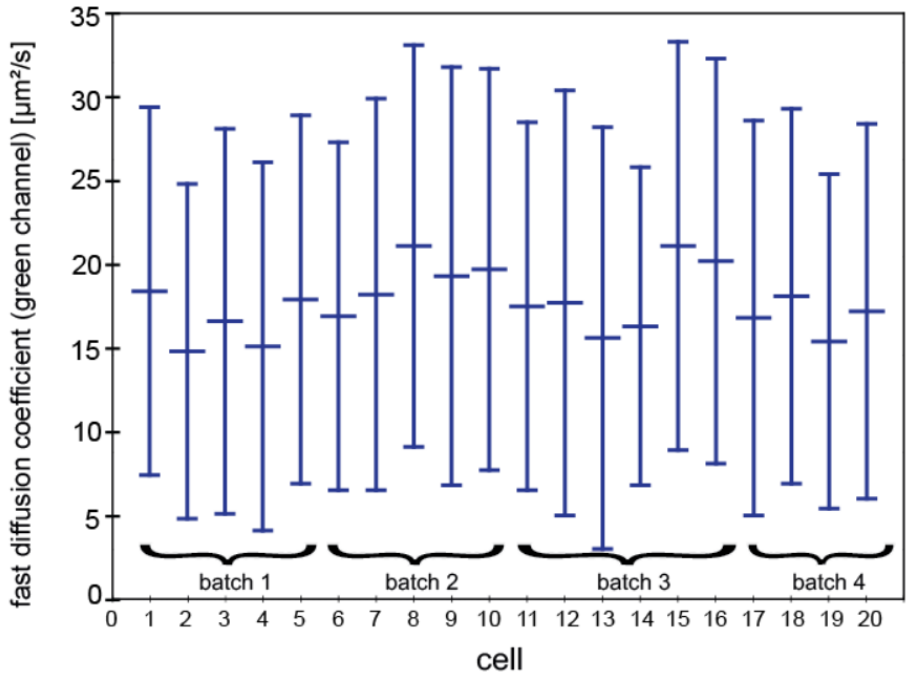

Figure 3.13: SPIM-FCCS *in vivo* measurements of AP-1 wild type proteins in HeLa cell: (mean±SD) of fast diffusion coefficient in the green channel for all 20 measured cells.

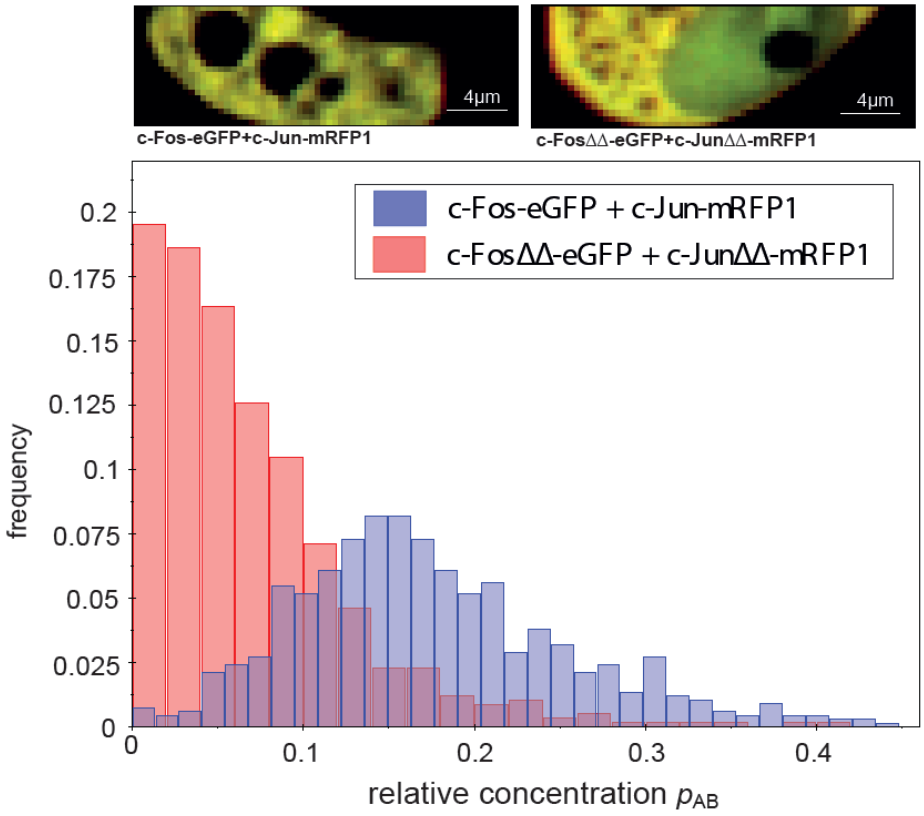

Figure 3.14: SPIM-FCCS *in vivo* measurements of AP-1 wild type proteins and deletion mutants in HeLa cell: a histogram of relative concentrations for the cells shown above.

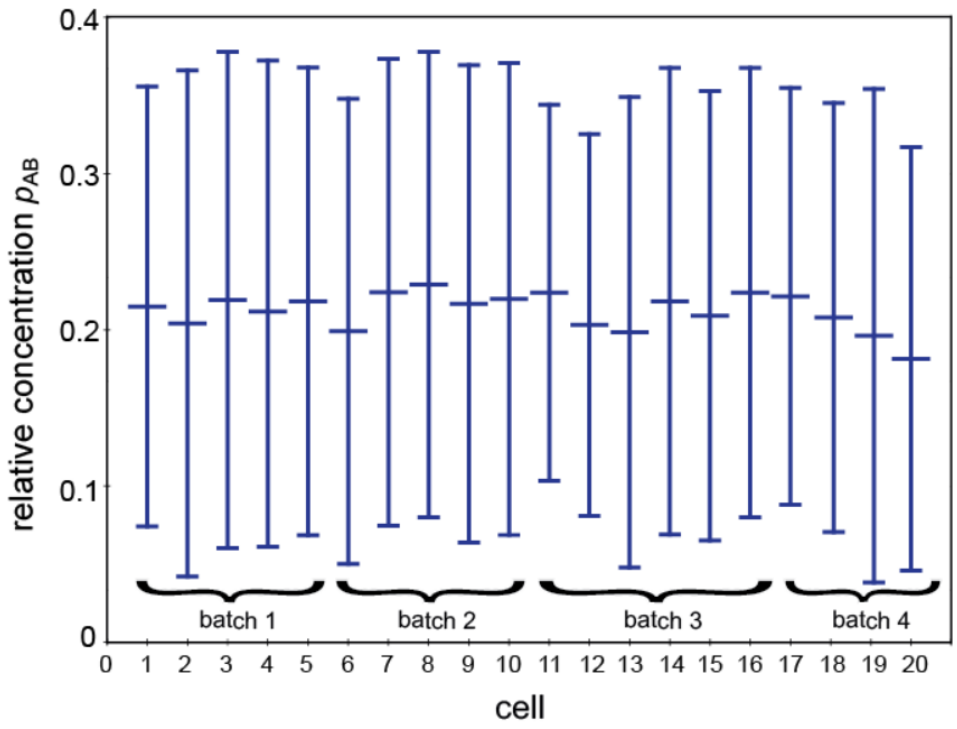

Figure 3.15: SPIM-FCCS *in vivo* measurements of AP-1 wild type proteins in HeLa cell: (mean±SD) of relative concentrations for all 20 measured cells.

I tried to infer a specific pattern of dimerization sites within a cell transfected with c-Fos-eGFP and c-Jun-mRFP1. *Figure 3.16* shows intensity images (*Figure 3.16 A*) and maps of the slow diffusion coefficient (*Figure 3.16 B*), fraction of the slow diffusion component (*Figure 3.16 C*) and the relative concentration p_{AB} (*Figure 3.16 D*) for five different cells. The maps reveal areas in the nucleus where c-Fos-eGFP and c-Jun-mRFP1 exhibit higher interaction and a lower diffusion coefficient (one such area is highlighted by an arrow in *Figures 3.16 B* and *D*), as well as areas of higher relative concentration and fraction of the slow diffusion component. Most of these areas are around the nuclear envelope and around the nucleolus. This finding may lead to the conclusion that c-Fos and c-Jun are associated with heterochromatin, which is located at the periphery of the nucleus and around the nucleolus. However, from the maps of the 20 analyzed cells, no other characteristic pattern of higher interaction areas could be established. The results for all measured cells are shown in Appendix (*Figure A7* and *A8*).

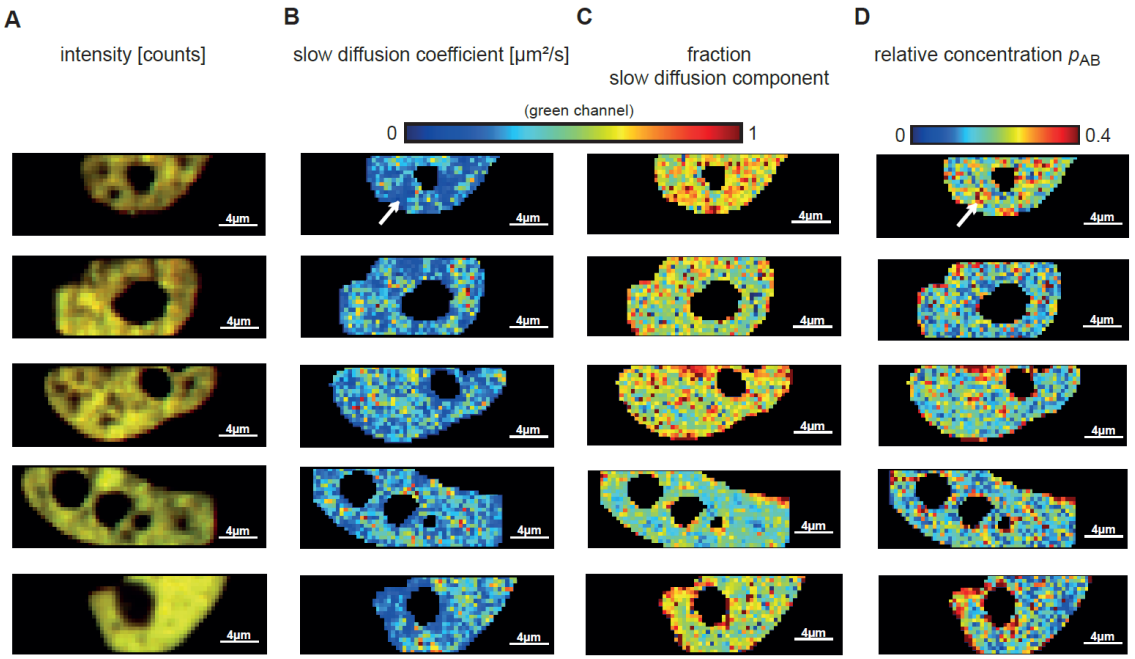

Figure 3.16: Typical SPIM-FCCS *in vivo* measurements of the AP-1 wild type proteins c-Fos-eGFP and c-Jun-mRFP1 in five cells. (A) intensity images, (B) slow component diffusion coefficient maps showing the diffusion coefficients across the cells, (C) fraction of the slow diffusion component and (D) relative concentration maps.

	SPIM-FCCS			**Confocal FCCS**		
CELLS	D_{fast} [µm²/s]	D_{slow} [µm²/s]	p_{AB}	D_{fast} [µm²/s]	D_{slow} [µm²/s]	q
c-Fos-eGFP, c-Jun-mRFP1	18±10 23±6	0.28±0.1 0.3±0.1	0.21±0.18	15±3	0.25±0.05	0.35±0.05
c-FosΔΔ-eGFP, c-JunΔΔ-mRFP1	22±10 23±7	0.38±0.2 0.4 ± 0.2	0.13±0.07	23±4	0.3±0.05	0.18±0.05
eGFP-mRFP1 fusion protein	30±20	0.39±0.2	0.29±0.15	20±3	0.3±0.05	0.45±0.05
eGFP, mRFP1 monomer protein	38±15	0.38±0.2	0.08±0.08	30±3	0.3±0.05	0.15±0.05

Table 7: Summary of the SPIM-FCCS and confocal FCCS results: (mean±SD) diffusion coefficients D_{fast} and D_{slow}, relative concentration p_{AB} (SPIM-FCCS) and relative cross-correlation amplitudes q (confocal FCCS). The SPIM-FCCS and confocal FCCS measurements, each obtained on different days, were averaged over 20 cells.

Visual inspection of the diffusion maps, like the ones in *Figure 3.16*, suggested a correlation between the relative concentration p_{AB} – indicating dimer formation – and the overall diffusion time, which appeared slower in the regions where strong dimerization occurred. To assess this effect quantitatively, I fixed both slow and fast diffusion coefficients to their average values across all pixels from the previous fit and fitted the data by varying only one parameter, the fraction of the slowly diffusing component. I then plotted the p_{AB} against the fraction of the slow component and fitted linear regression lines to the scatter plots for all 20 cells. *Figure 3.17* shows scatter plots for the five cells in *Figure 3.16*, while scatter plots for all 20 cells are presented in Appendix (*Figure A9*).

For 20 cell measurements, the Pearson correlation coefficient r ranged from r=0.54 to r=0.75. The significance of the correlation was checked with the p-value against the null hypothesis of no correlation, which for c-Fos-eGFP and c-Jun-mRFP1 was always $p < 0.001$. Thus the relative concentration and the fraction of the slow component are significantly correlated, strongly supporting the view that dimerization is a prerequisite for Fos/Jun binding.

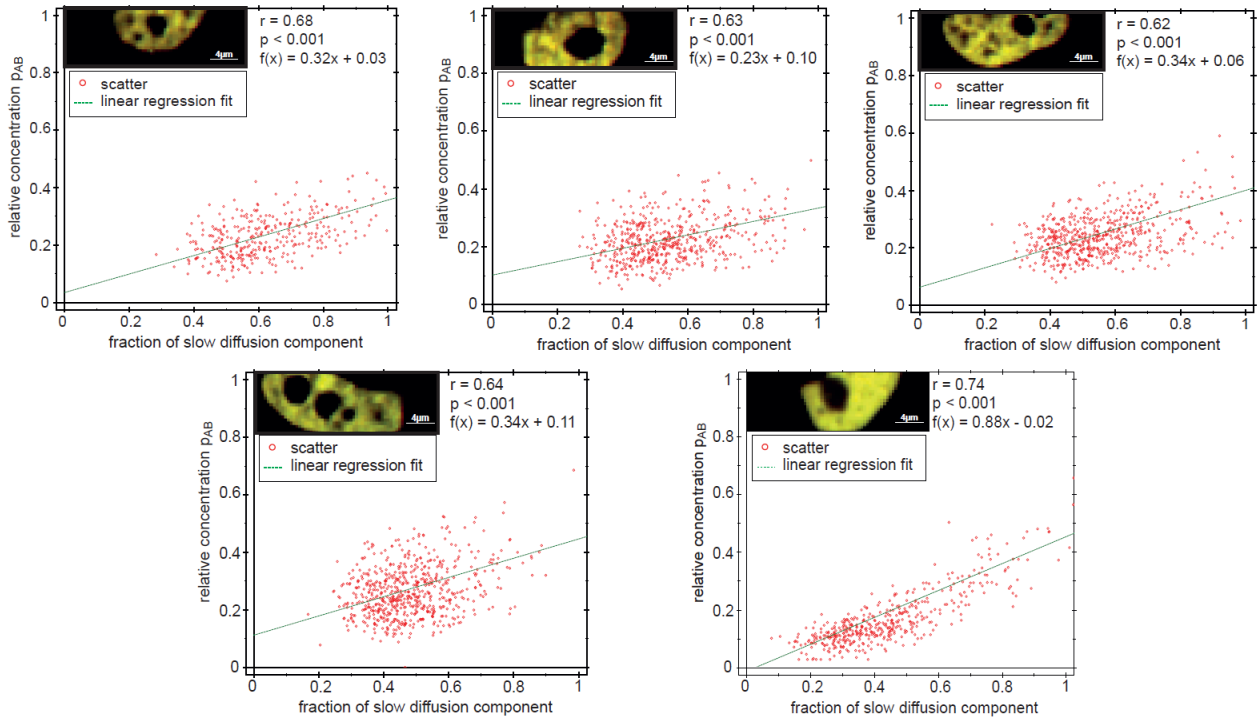

Figure 3.17: Scatter plots illustrating the relationships between relative concentrations and fraction of the slow diffusing component for the five cells shown in *Figure 3.16*.

As a control, I similarly analyzed the data from the c-Fos-eGFP and c-Jun-mRFP1 deletion mutants, eGFP and mRFP1 monomers and the eGFP-mRFP1 fusion protein. These constructs may either exhibit no interaction at all (deletion mutants and eGFP/mRFP1 monomers) or 100% interaction (fusion protein). Therefore, the relative concentration should not be correlated with the diffusion behavior. *Figure 3.18* presents the fraction of the slow diffusing component and relative concentrations in the form of scatter plots with a superimposed linear regression fit. The Pearson correlation coefficients were very low, indicating no significant correlation between the two parameters. Similar results were obtained for all measured cells and are presented in the Appendix (*Figures A2*, *A4*, and *A6*).

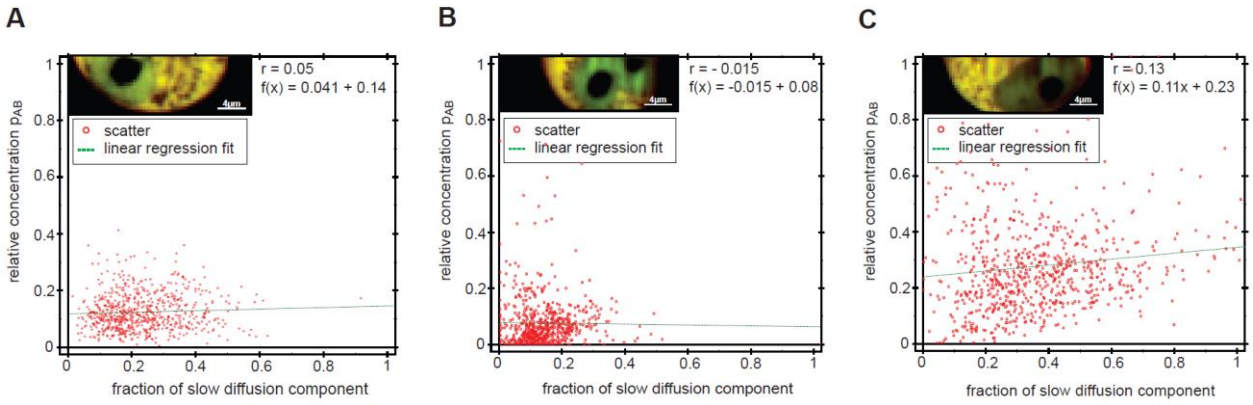

Figure 3.18: Scatter plots illustrating the relationships between relative concentration and fraction of the slow diffusing component. (A) c-FosΔdimΔDNA-eGFP and c-JunΔdimΔDNA-mRFP1, (B) eGFP and mRFP1 monomers and (C) eGFP-mRFP1 fusion protein expressed in HeLa cell.

2.4 c-Fos AND c-Jun TRANSCRIPTION FACTORS IN G1/S PHASE

Additional measurements were performed with c-Fos and c-Jun transcription factors in HeLa cells. The sample was treated with Aphidicolin as described in Chapter 3.5. Aphidicolin inhibits the growth of the cells and stops in the G1/S phase. The measurements were performed under the same conditions as the measurements on c-Fos and c-Jun without Aphidicolin. I acquired 100.000 frames for 20 different cells at a room temperature. The data was fitted with SPIM-FCS 2-component normal diffusion model.

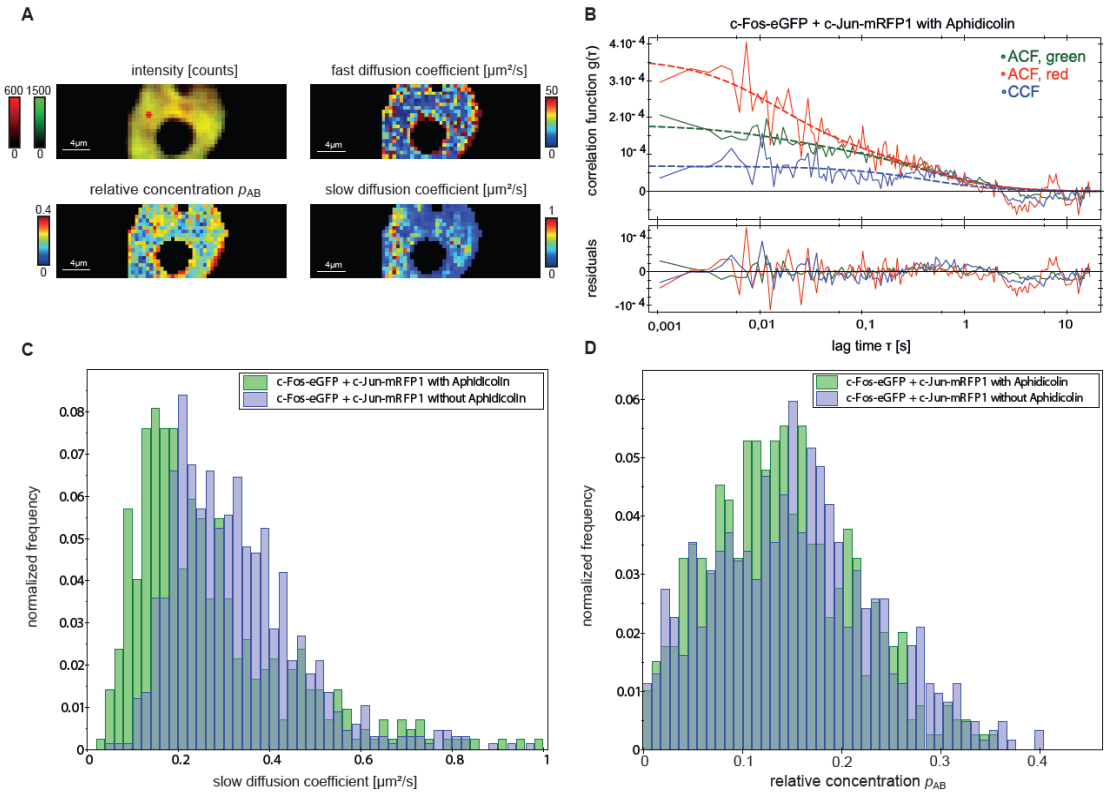

Figure 3.19: SPIM-FCCS *in vivo* measurements of AP-1 wild type proteins treated with Aphidicolin in HeLa cell. (A) intensity images, fast and slow diffusion coefficient maps and relative concentration map, (B) auto- and cross-correlation functions and fits, obtained for locations indicated by the red mark in the intensity image, (C) histogram of slow diffusion coefficient and (D) of relative concentration for AP-1 wild type with and without Aphidicolin.

Figure 3.19 A shows a typical intensity image, as well as maps of fast and slow diffusion coefficient components and relative concentration, respectively. The parameter images are comparable to those shown in *Figure 3.16* for the measurements without Aphidicolin. Typical auto- and cross-correlation functions and fits are shown in *Figure 3.19 B*. The (mean±SD) of the fast diffusion coefficient D_{fast}, obtained over 20 cell measurements, was (20±10) µm^2/s and (0.3±0.1) µm^2/s for slow diffusion coefficient D_{slow}. These results agree well with the values obtained from c-Fos and c-Jun measurements without Aphidicolin, which are summarized in *Table 7*. *Figure 3.19 C* shows a histogram of slow diffusion coefficient for a cell with and a cell without Aphidicolin treatment. It can be seen that there is not much difference in the diffusion coefficients. Additionally, the relative concentrations obtained from the same cells have been shown the histogram in *Figure 3.19 D*. The average relative concentration p_{AB} for c-Fos-eGFP and c-Jun-mRFP1 with Aphidicolin averaged over 20 cells was (0.20±0.16), while the average relative concentration for the c-Fos-eGFP and c-Jun-mRFP1 without Aphidicolin averaged over

20 cells was (0.21±0.18). Also here no significant differences can be noticed. The slight difference in the values could occur, because one small part of the measurements of c-Fos-eGFP and c-Jun-mRFP1 without Aphidicolin were performed while the cells were in the G2 phase or the mitosis.

2.5 CONTROL MEASUREMENTS IN LIVING MCF-7 CELLS

In addition to the *in vivo* control measurements with eGFP and mRFP1 monomers and eGFP-mRFP1 fusion protein expressed in HeLa cells, the applicability of SPIM-FCCS was tested with eGFP and mRFP1 monomers and eGFP-mRFP1 fusion protein in MCF-7 cells.

I measured and acquired FCCS for 20 cells. For each measurement I selected a 128 x 20 big sub-region of the camera and acquired 100.000 frames at a room temperature. For the auto- and cross-correlation data analysis, a global fit was used. The data was fitted with the SPIM-FCS 2-component normal diffusion model as described in Chapter 1.4.2. It was assumed that the proteins have the same size and thus the same diffusion coefficients, therefore the three diffusion coefficients were linked together during the fit.

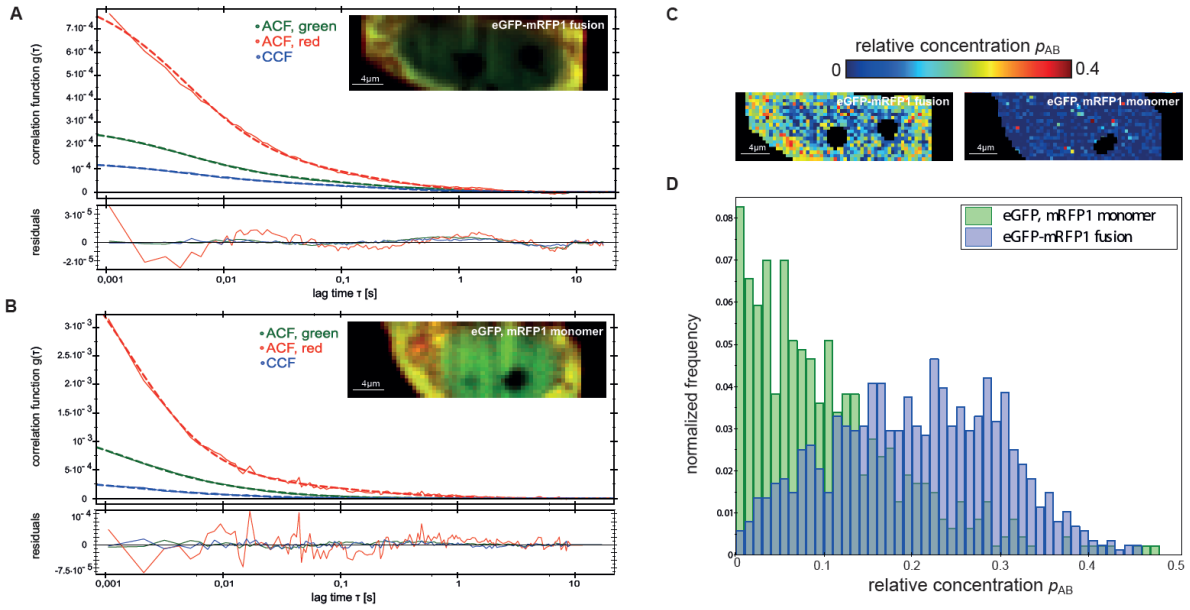

Figure 3.20: SPIM-FCCS *in vivo* control measurement of the eGFP-mRFP1 fusion protein and eGFP and mRFP1 monomers expressed in MCF-7 cells. (A) and (B) auto- and cross-correlation functions and fits for the fusion protein and the monomers, (C) the relative concentration maps and (D) histogram of relative concentration for the fusion protein and the monomers.

Figures 3.20 A and *B* show typical auto- and cross-correlation functions and fits for eGFP-mRFP1 fusion protein and eGFP and mRFP1 monomers expressed in MCF-7 cells, respectively. The (mean±SD) of the fast diffusion coefficient D_{fast}, obtained over 20 cell measurements, was (29±20) $\mu m^2/s$ for the eGFP-mRFP1 fusion protein and (39±15) $\mu m^2/s$ for the eGFP and mRFP1 monomers. *Figure 3.20 C* shows the relative concentration maps. The relative concentration p_{AB} was (0.28±0.15) for the fusion protein and the separately expressed eGFP and mRFP1 gave a relative concentration p_{AB} of (0.1±0.09). *Figure 3.20 D* presents a histogram of relative concentration for monomers and the fusion protein. The SPIM-FCCS results obtained for MCF-7 cells are comparable to the SPIM-FCCS results obtained for HeLa cells using the same construct.

3 SUMMARY

The aim of this Thesis was to measure mobility and interaction of c-Fos and c-Jun transcription factors within the whole cell nuclei. Dual-color fluorescence cross-correlation spectroscopy (FCCS) on single plane illumination microscope (SPIM) has proved to be a great method to spatially resolve the mobility and interactions of AP-1 transcription factors in living HeLa cells.

First, in addition to the *in vitro* calibration measurements, I applied the SPIM-FCCS method to several *in vivo* control measurements to validate the c-Fos and c-Jun results and prove the feasibility of the method. Chapter 2.1 presents the mobility of eGFP dimers and eGFP tetramers in HeLa cells. The results were compared to the previous measurements on eGFP oligomers using the confocal FCS [64, 65]. The negative and positive FCCS controls were performed with eGFP and mRFP1 monomers and eGFP-mRFP1 fusion protein, respectively. The results have been presented in Chapter 2.2.

Finally, SPIM-FCCS has been applied to c-Fos-eGFP and c-Jun-mRFP1 in HeLa cells. I obtained spatially resolved maps of mobility and interaction. I then plotted the relative concentration against the fraction of the slow diffusion component and found that strong interaction shows slow mobility. The association of AP-1 transcription factors and their binding to DNA has been verified by the confocal FCCS [7, 16] in Chapter 1.2. The results served as a reference to the SPIM-FCCS measurements.

Additional *in vivo* test measurements have been performed. In Chapter 2.4, the Hela cells with c-Fos and c-Jun have been treated with Aphidicolin to stop the growth of the cells in the G1/S phase. The results have been compared to the c-Fos and c-Jun measurements without

Aphidicolin. Chapter 2.5 presents the applicability of SPIM-FCCS with eGFP and mRFP1 monomers and eGFP-mRFP1 fusion protein in MCF-7 cells. The results have shown no significant difference in comparison to the measurements in HeLa cells.

The main findings are the following:

- c-Fos and c-Jun transcription factors are only localized in the cell nuclei, whereas their deletion mutants can be found also in the cytoplasm.
- The slow diffusion coefficients of c-Fos and c-Jun transcription factors refer to proteins bound to immobile structures in the cell nucleus, most probably DNA.
- The slow component might therefore partially correspond to non-specifically trapped proteins.
- The well-structured map of relative concentrations for the cell expressing c-Fos-eGFP and c-Jun-mRFP1 clearly indicates stronger interactions, while the map of the cell expressing deletion mutants is indicative of almost no interactions: this could be expected since their dimerization and DNA-binding domains were deleted.
- No interaction was measured between the AP-1 wildtype and the deletion mutants.
- Areas of higher relative concentration and fraction of the slow diffusion component of c-Fos and c-Jun can mostly be found around the nuclear envelope and nucleolus where heterochromatin is located.
- The relative concentration and the fraction of the slow component are significantly correlated, strongly supporting the view that dimerization is a prerequisite for Fos/Jun binding.
- The relative concentration and the fraction of the slow component are not correlated for the c-Fos and c-Jun deletion mutants, eGFP, mRFP1 monomers and eGFP-mRFP1 fusion protein.
- The measurements of c-Fos-eGFP and c-Jun-mRFP1 with or without Aphidicolin in HeLa cells show no significant difference.
- The SPIM-FCCS results obtained for c-Fos and c-Jun expressed in MCF-7 cells are comparable to the SPIM-FCCS results obtained for HeLa cells using the same construct.

IV. CONCLUSION

The aim of this Thesis was to study and characterize the mobility and interaction of c-Fos and c-Jun transcription factors in living cells using single plane illumination-cross correlation spectroscopy (SPIM-FCCS). Dual-color fluorescence cross-correlation spectroscopy on an in-house constructed SPIM-FCCS allowed us for the first time to measure the mobility and interaction of two proteins *in vivo* and simultaneously across an entire cell nucleus. The method provides rather detailed maps of diffusion coefficients and relative concentrations, indicating regions of slow and fast diffusion, and strong and weak interaction, within the live cell.

FCS is a well-established tool to study molecular motions and the extension to FCCS allows detecting biomolecular interactions. Two molecules are labeled with different fluorophores to distinguish them spectrally. They are excited by two focused laser beams and are characterized by an auto-correlation analysis to provide the information about the diffusion coefficients and concentrations. Cross-correlating the fluorescence fluctuations in the detection channels will reveal the interaction between the two molecules.

Here I used the SPIM-FCCS system to study the motion and interaction of the transcription factors c-Fos and c-Jun, which participate in the regulation of several cellular processes, including differentiation, proliferation, apoptosis and oncogenesis. Fos forms heterodimers with Jun-related proteins, whereas c-Jun forms homodimers and heterodimers with all Jun and Fos related proteins. Whether Fos can also form homodimers is still an unresolved issue.

Previous *in vivo* studies of the association of AP-1 transcription factors and their binding to DNA used single point confocal FCCS [7, 16]. They showed that c-Fos and c-Jun interact in living HeLa cells, using two autofluorescent protein tags. The disadvantage of confocal FCCS is that only a single measurement can be taken at a time, whereas to establish the spatially varying dynamics and interactions of proteins, experiments must be performed at many spots in parallel within the entire cell. SPIM-FCCS allows such measurements. Here, the confocal FCCS measurements were performed primarily as a reference to the results obtained with SPIM-FCCS.

SPIM uses a thin light sheet to illuminate the fluorescently labeled sample and simultaneously images all pixels in the two-dimensional field of view with a fast camera. As a detector I used a fast, high quantum efficiency EMCCD camera. Auto- and cross-correlation curves were obtained by fitting a global 2-component model, which yielded a fast and a slow

diffusion coefficient for each pixel. I obtained the relative concentration p_{AB} and presented the data as spatially resolved maps of c-Fos and c-Jun mobility and interaction. The diffusion coefficients for c-Fos-eGFP and c-Jun-mRFP1 were (18±10) μm²/s in the green and (23±6) μm²/s in the red channel for the fast and (0.28±0.1) μm²/s in the green and (0.3±0.1) μm²/s in the red channel for the slow diffusing component, which are comparable to the diffusing component measured by confocal FCCS. The slow diffusing component is associated with dimerization of transcription factors and their binding to DNA.

To validate the results on c-Fos and c-Jun proteins, I performed several controls. Confocal FCCS measurements at several spots of HeLa cells expressing either c-Fos-eGFP and c-Jun-mRFP1 or the mutants c-FosΔΔ-eGFP and c-JunΔΔ-mRFP1 resulted in correlation functions very similar to those obtained by SPIM-FCCS. Second, HeLa cells transfected with control vectors pSV-eGFP-mRFP1 (a fusion protein of the two dyes separated by a 7-AA linker), and pIRES2-eGFP-mRFP1 (expressing the dyes separately), gave the limits for the cross-correlation amplitudes in the case of 100% and 0% interaction. Finally, I performed SPIM-FCCS measurements with the mutants c-FosΔΔ-eGFP and c-JunΔΔ-mRFP1. In these mutants, where the dimerization and DNA-binding domains were deleted, I found no interaction and no DNA binding.

I found a significant spatial correlation in the SPIM-FCCS images between the fraction of the slow diffusion component (= DNA binding) and relative concentration p_{AB} (= dimerization), allowing us to map the diffusion properties and localization of c-Fos and c-Jun interactions and the regions of interactions between AP-1 transcription factors and DNA. The main results have partially presented in [107].

The SPIM-FCCS technique expands the repertoire of imaging tools with measurements of mobility and interaction of molecules in live cells. Besides that, the method might find use not only in cell biological studies, but could also be valuable for high-throughput detection of protein-drug interactions in live cells, since it would allow detection of the association and dissociation of target proteins [108] and as functional *in vivo* screening for inhibitor or enhancers of biomolecular interactions [109].

Appendix

1 IRES

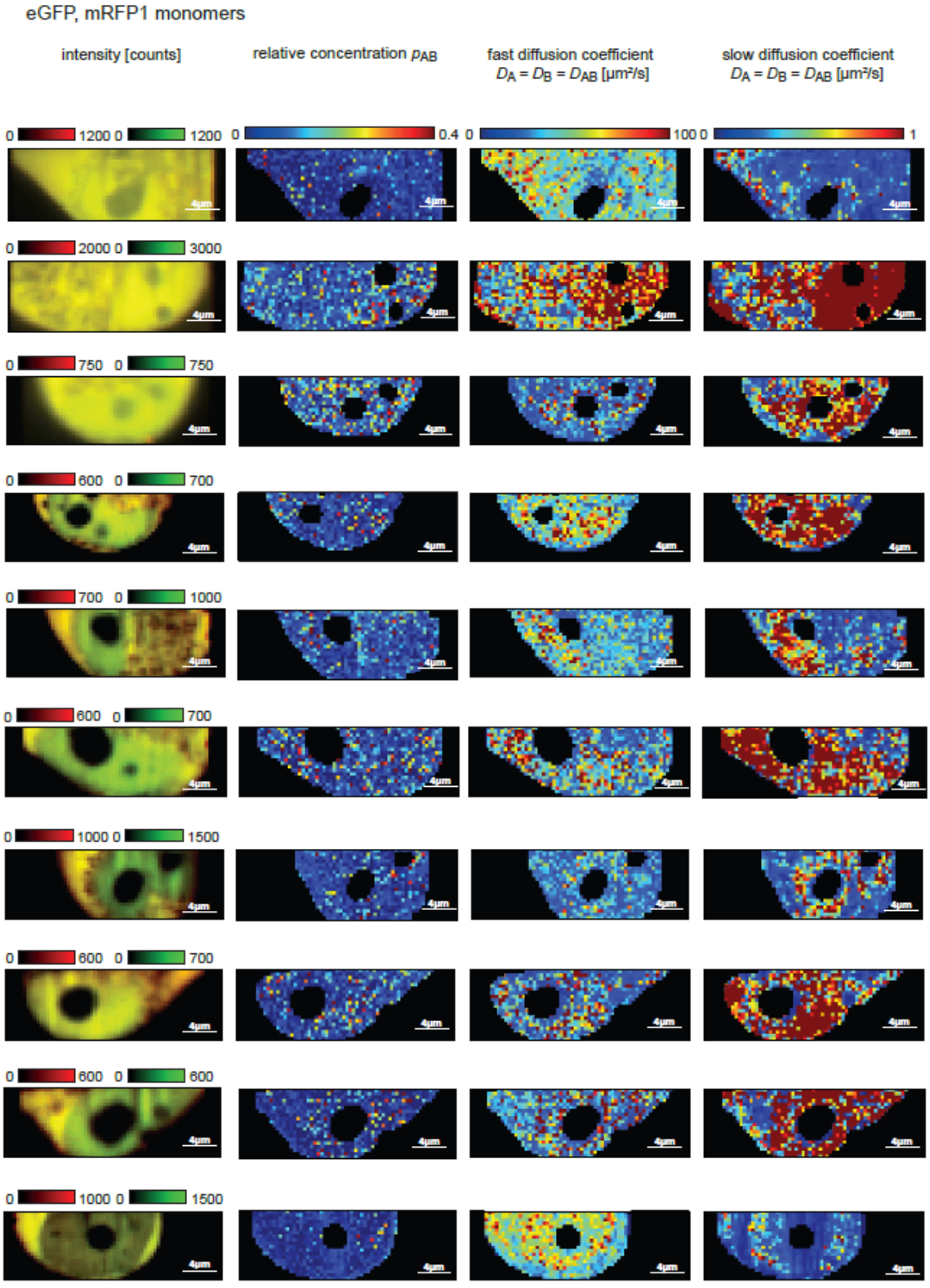

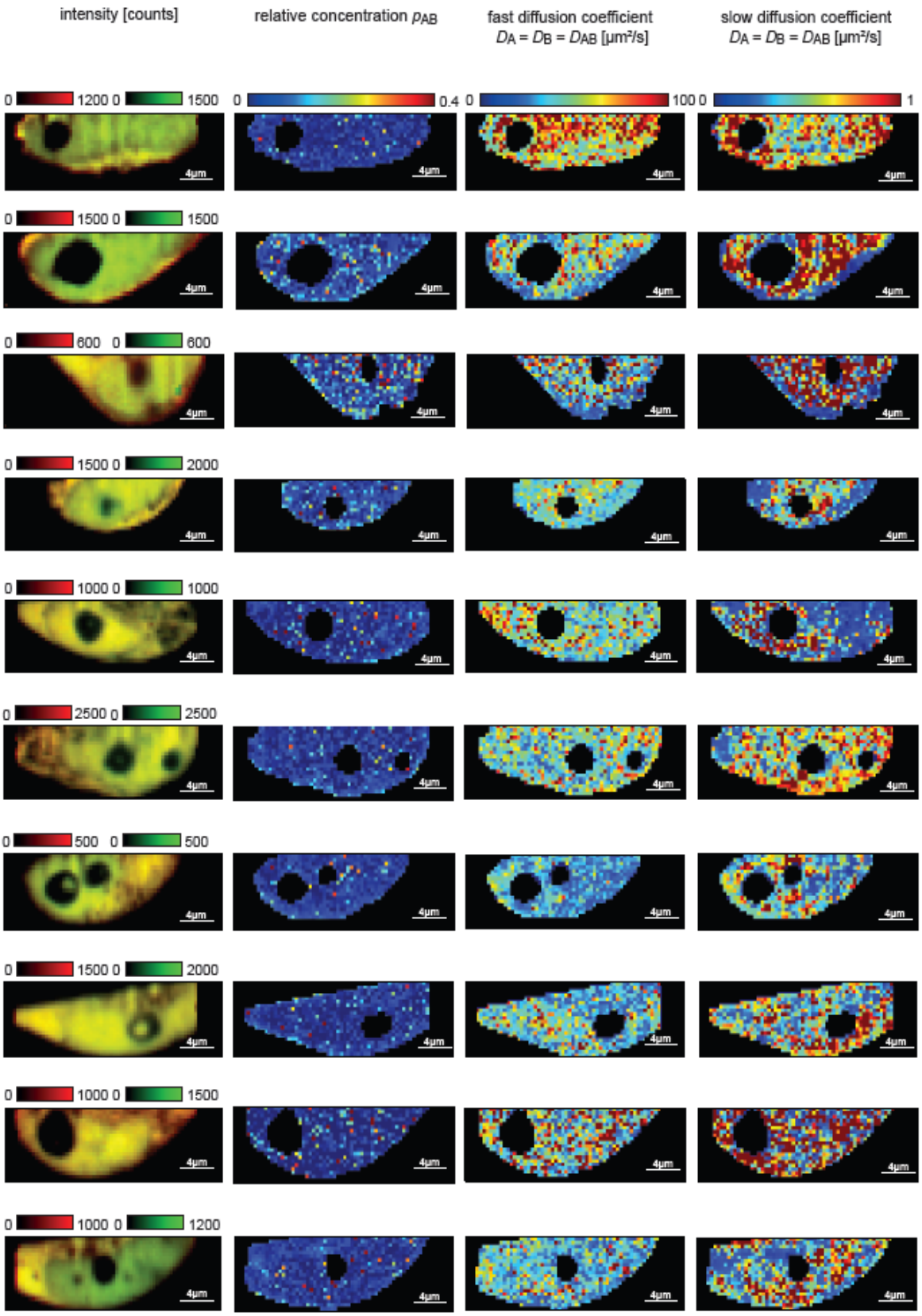

Figure A.1: SPIM-FCCS *in vivo* measurements of eGFP and mRFP1 monomer protein in HeLa cells: intensity images, relative concentration maps and fast and slow diffusion coefficients maps for all 20 measured cells.

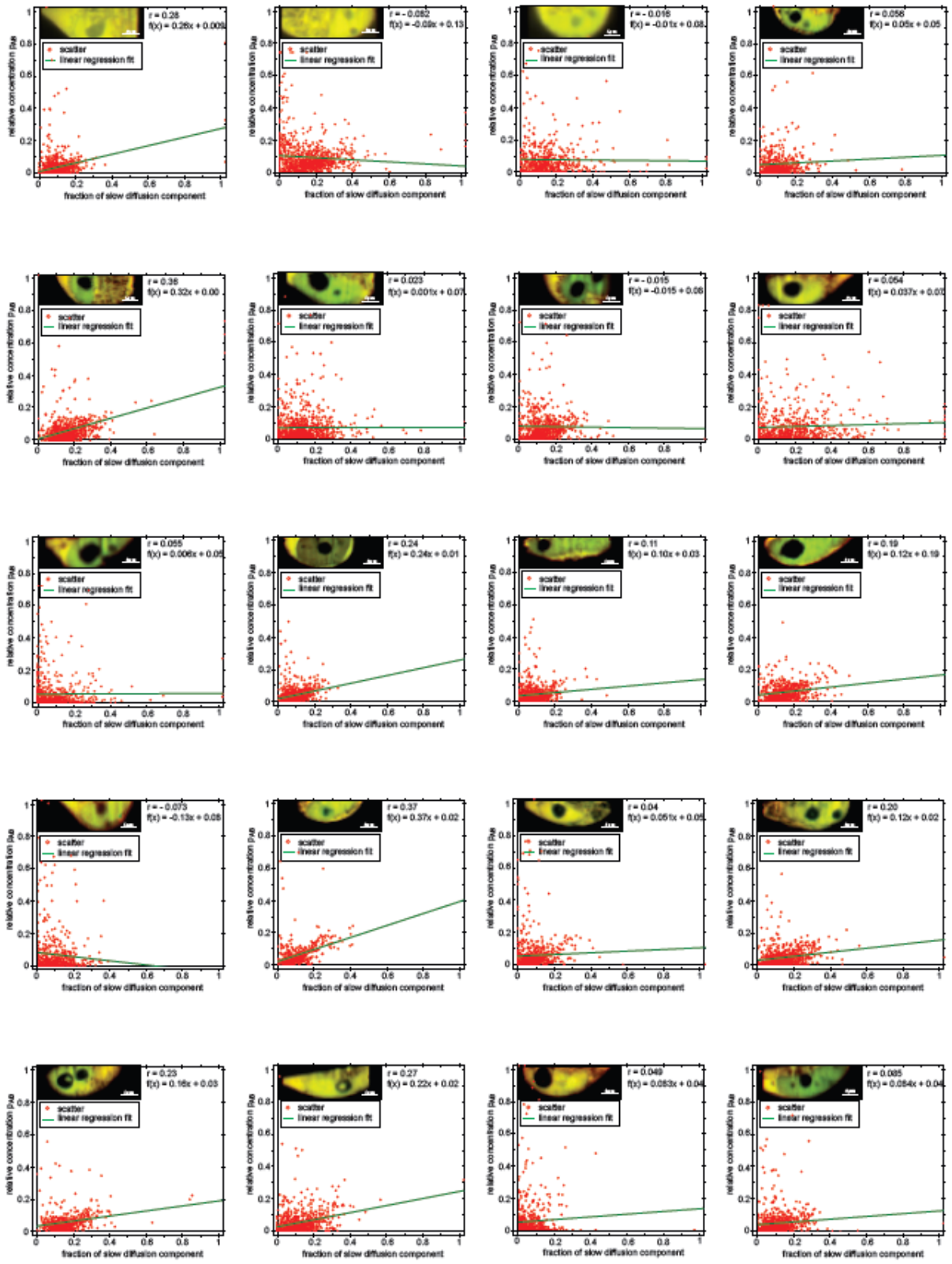

Figure A.2: Scatter plots illustrating the relationships between the fraction of the slow diffusing component, where D1 and D2 were fixed at average for the fit, and relative concentration p_{AB} of eGFP and mRFP1 monomer protein in HeLa cells for all 20 measured cells. Each graph shows a scatter plot where a point indicates values obtained at one pixel, and the linear regression fit.

2 FUSION

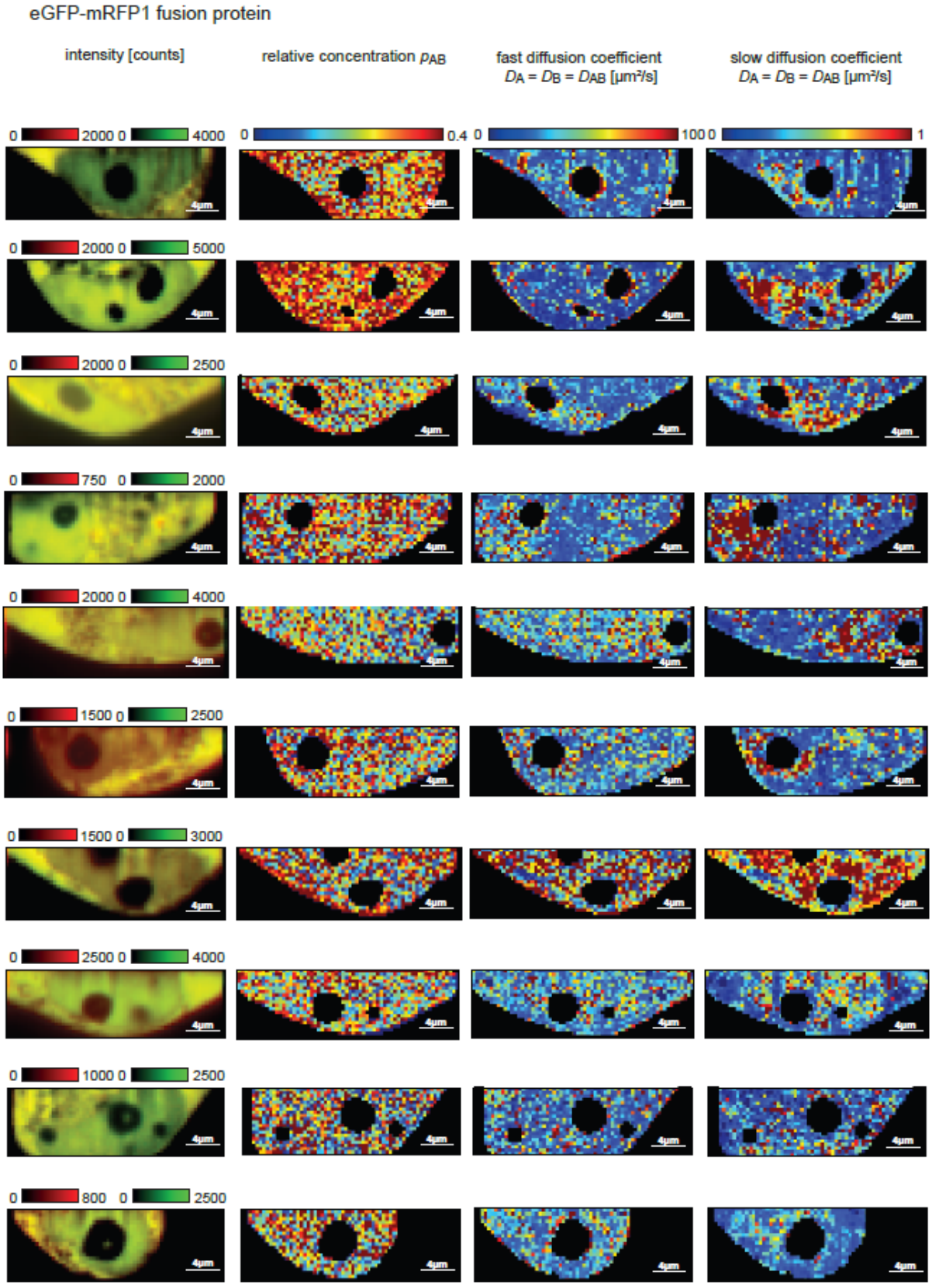
eGFP-mRFP1 fusion protein
intensity [counts]
relative concentration p_{AB}
fast diffusion coefficient
$D_A = D_B = D_{AB}$ [µm²/s]
slow diffusion coefficient
$D_A = D_B = D_{AB}$ [µm²/s]
0 2000 0 4000
0 0.4 0 100 0 1
0 2000 0 5000
0 2000 0 2500
0 750 0 2000
0 2000 0 4000
0 1500 0 2500
0 1500 0 3000
0 2500 0 4000
0 1000 0 2500
0 800 0 2500
4µm

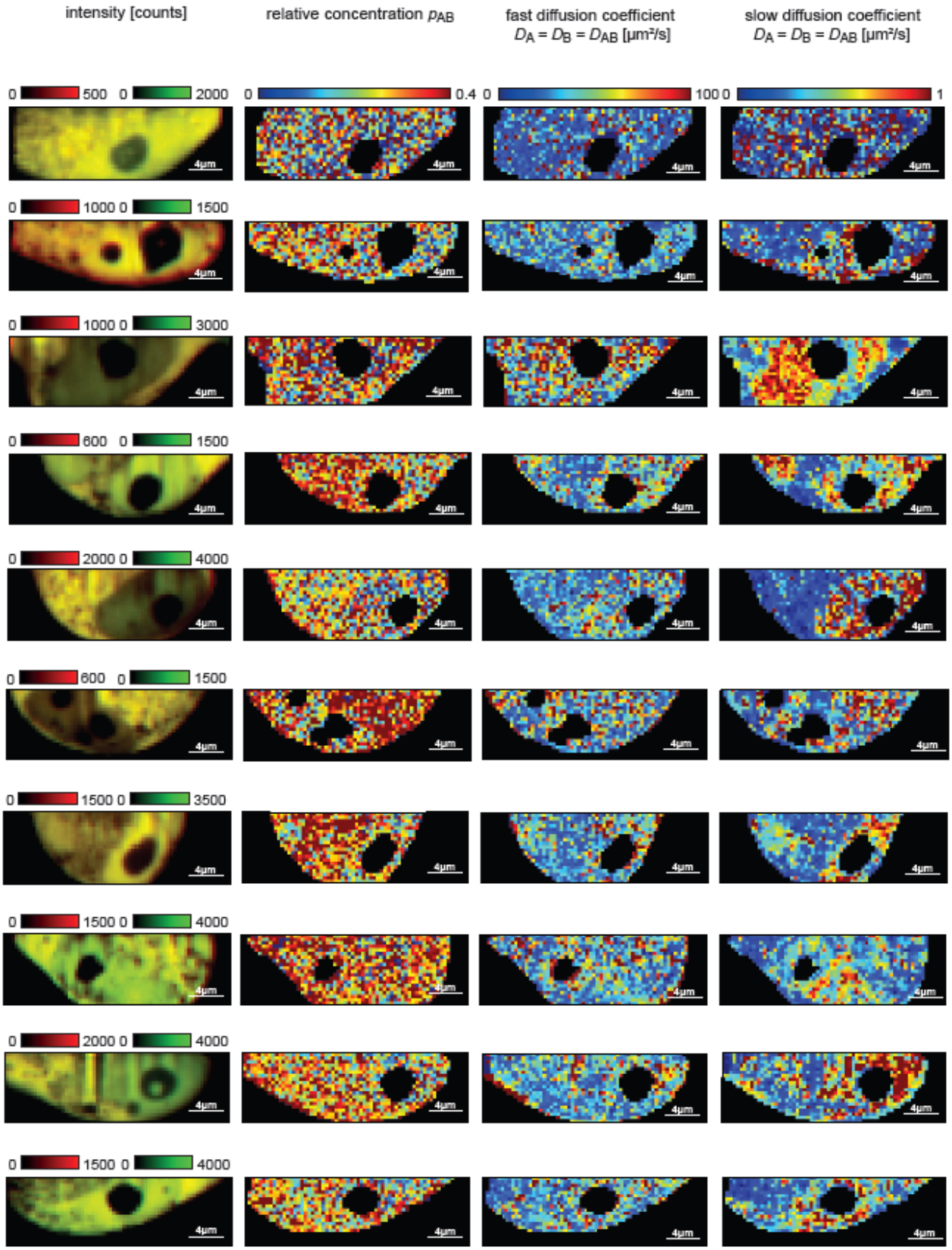

Figure A.3: SPIM-FCCS *in vivo* measurements of eGFP-mRFP1 fusion protein in HeLa cells: intensity images, relative concentration maps and fast and slow diffusion coefficients maps for all 20 measured cells.

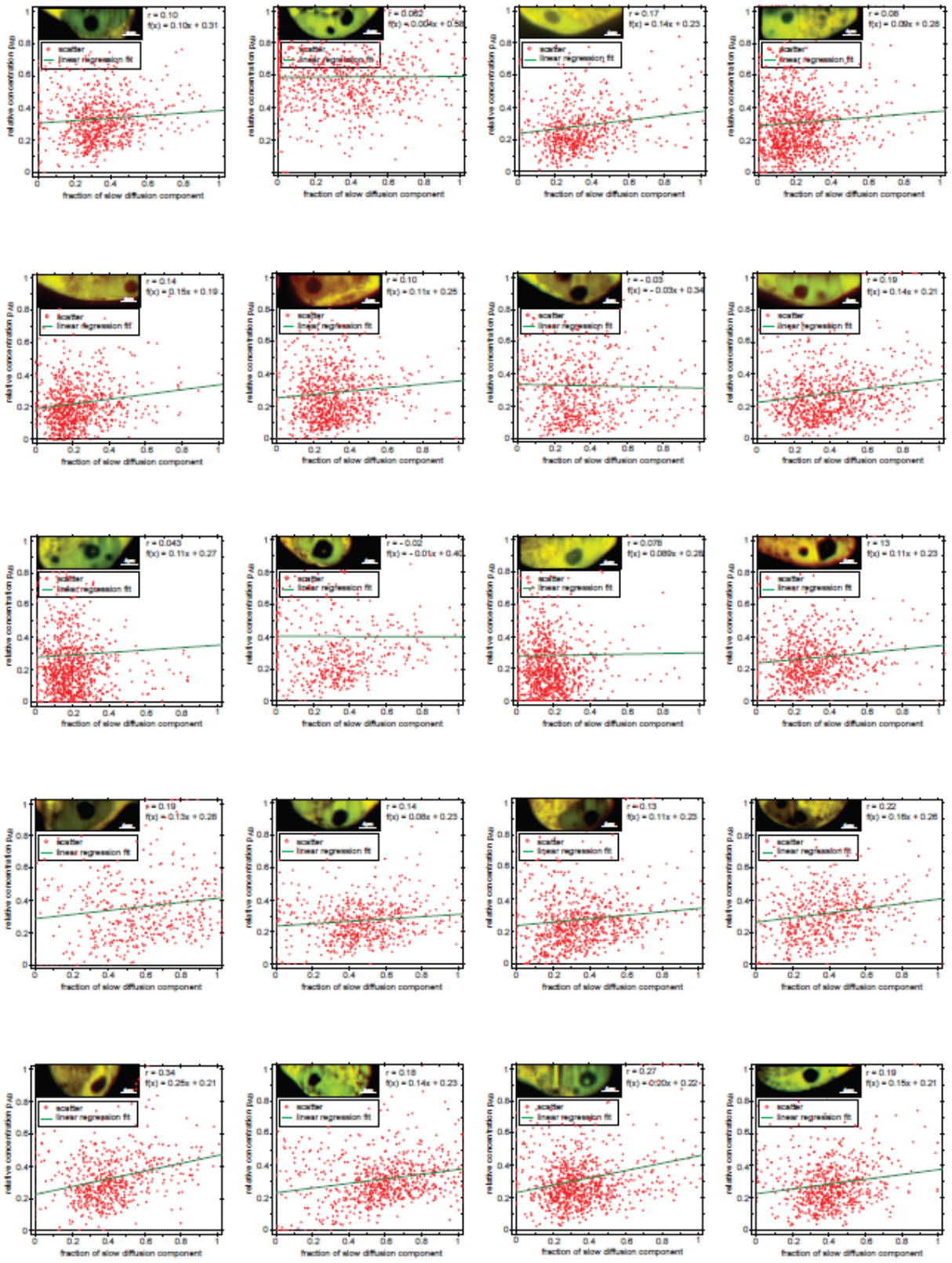

Figure A.4: Scatter plots illustrating the relationships between the fraction of the slow diffusing component, where D1 and D2 were fixed at average for the fit, and relative concentration p_{AB} of eGFP-mRFP1 fusion protein in HeLa cells for all 20 measured cells. Each graph shows a scatter plot where a point indicates values obtained at one pixel, and the linear regression fit.

3 MUTANTS

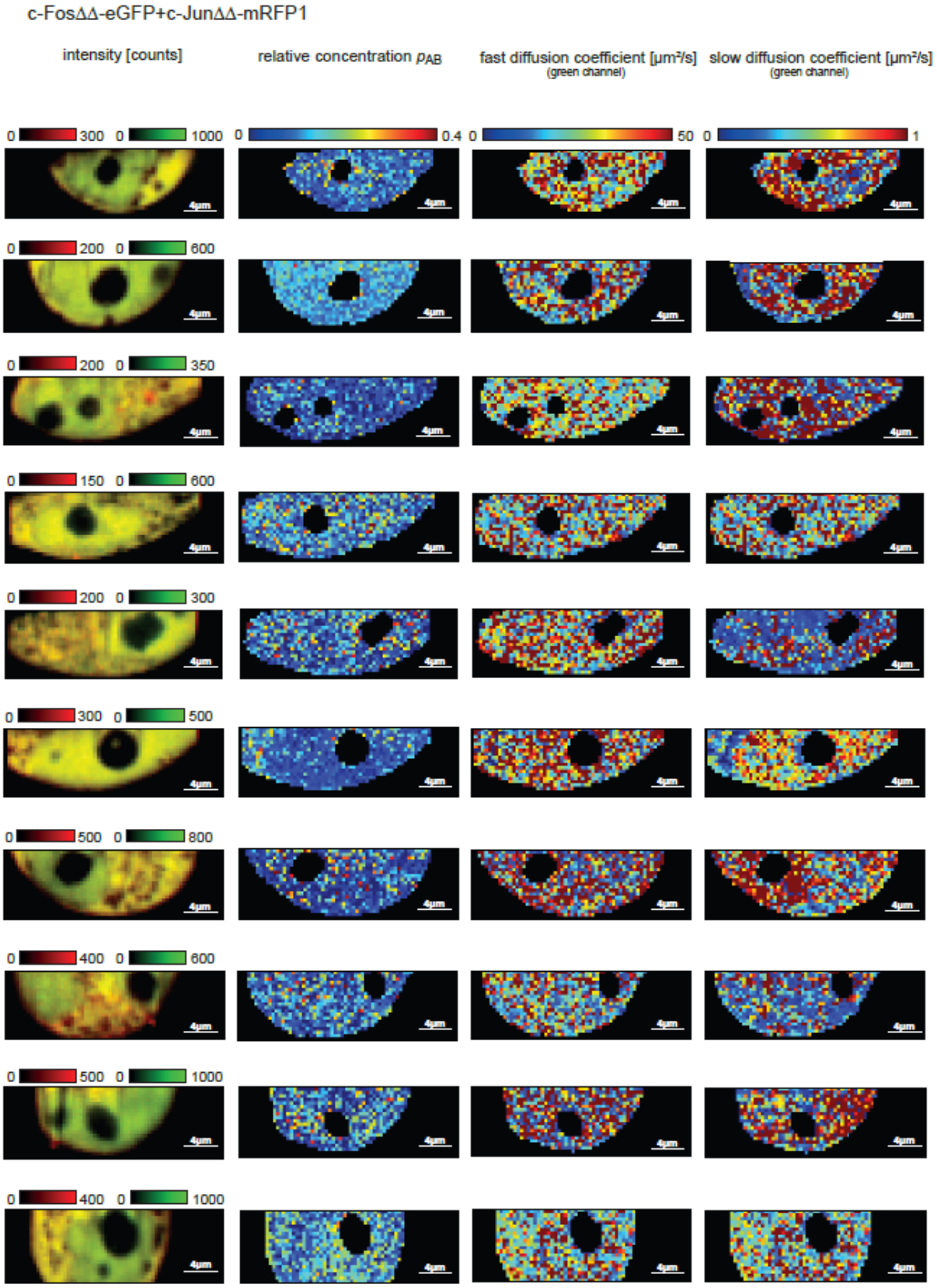
c-FosΔΔ-eGFP+c-JunΔΔ-mRFP1
intensity [counts]
relative concentration p_{AB}
fast diffusion coefficient [µm²/s] (green channel)
slow diffusion coefficient [µm²/s] (green channel)
0 300 0 1000
0 0.4 0 50 0 1
0 200 0 600
0 200 0 350
0 150 0 600
0 200 0 300
0 300 0 500
0 500 0 800
0 400 0 600
0 500 0 1000
0 400 0 1000
4µm

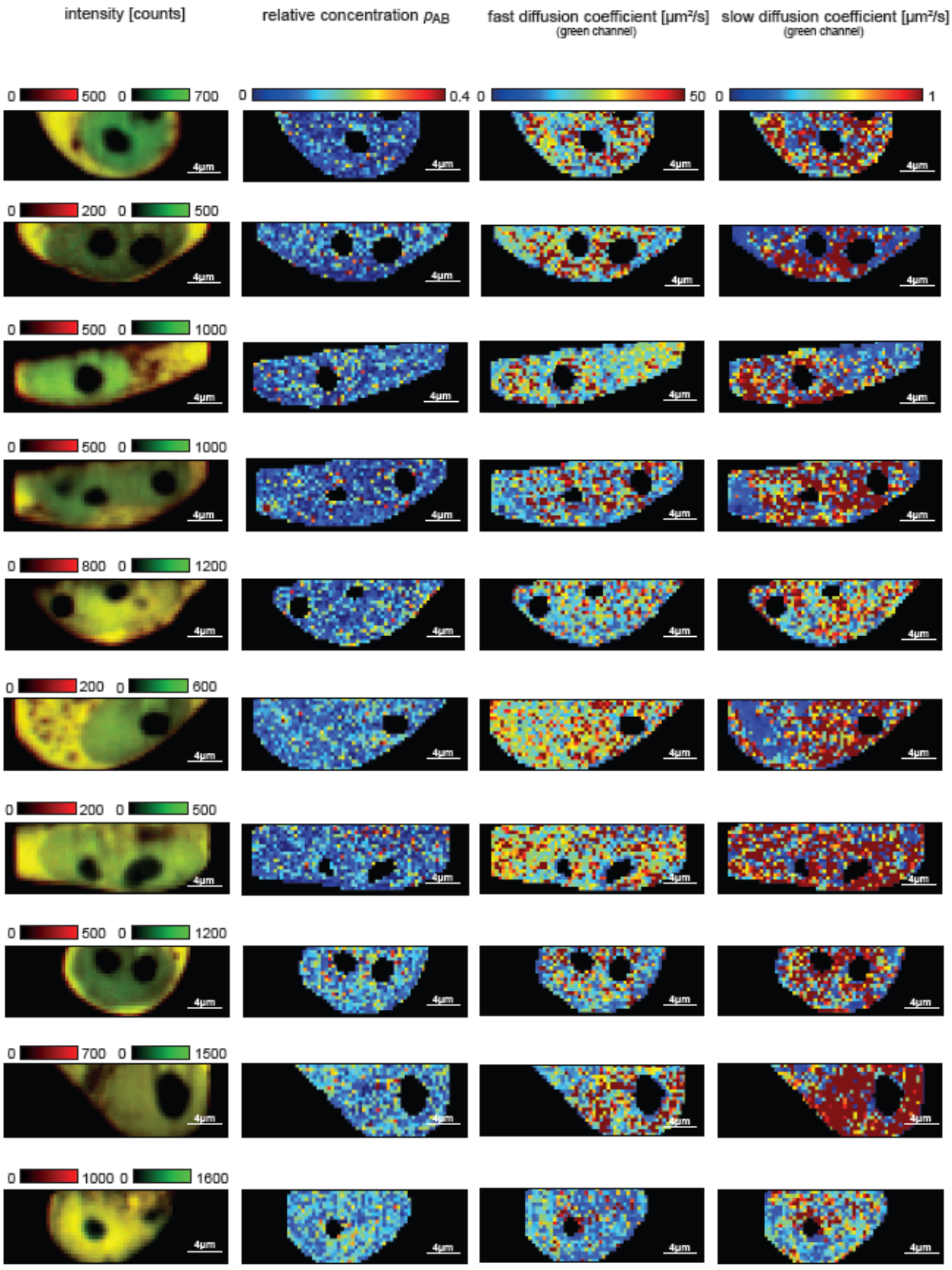

Figure A.5: SPIM-FCCS *in vivo* measurements of AP-1 deletion mutants c-FosΔdimΔDNA-eGFP and c-JunΔdimΔDNA-mRFP1 in HeLa cells: intensity images, relative concentration maps and fast and slow diffusion coefficients maps in the green channel for all 20 measured cells.

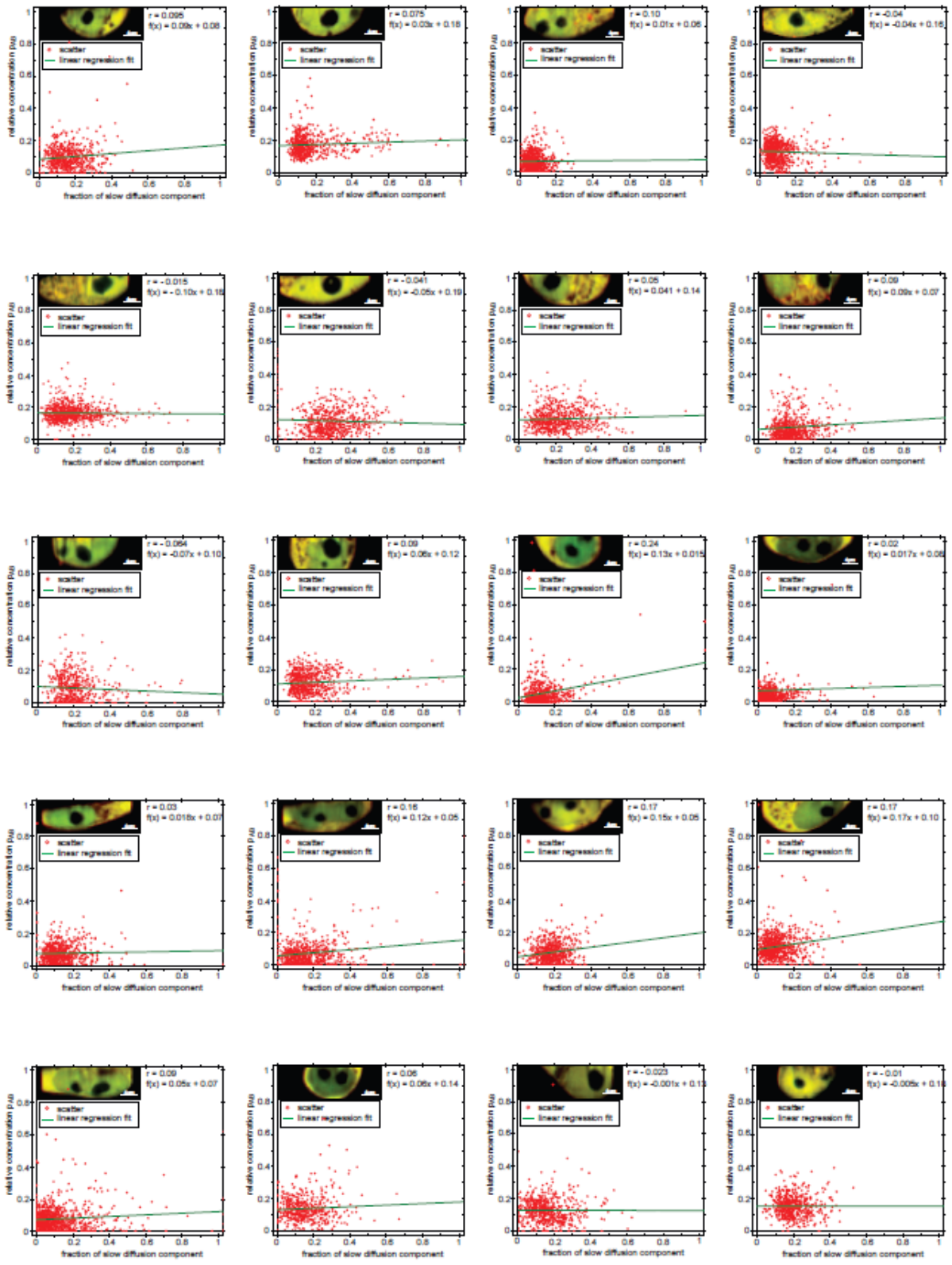

Figure A.6: Scatter plots illustrating the relationships between the fraction of the slow diffusing component, where D1 and D2 were fixed at average for the fit, and relative concentration p_{AB} of AP-1 deletion mutants c-FosΔdimΔDNA-eGFP and c-JunΔdimΔDNA-mRFP1 in HeLa cells for all 20 measured cells. Each graph shows a scatter plot where a point indicates values obtained at one pixel, and the linear regression fit.

4 AP-1

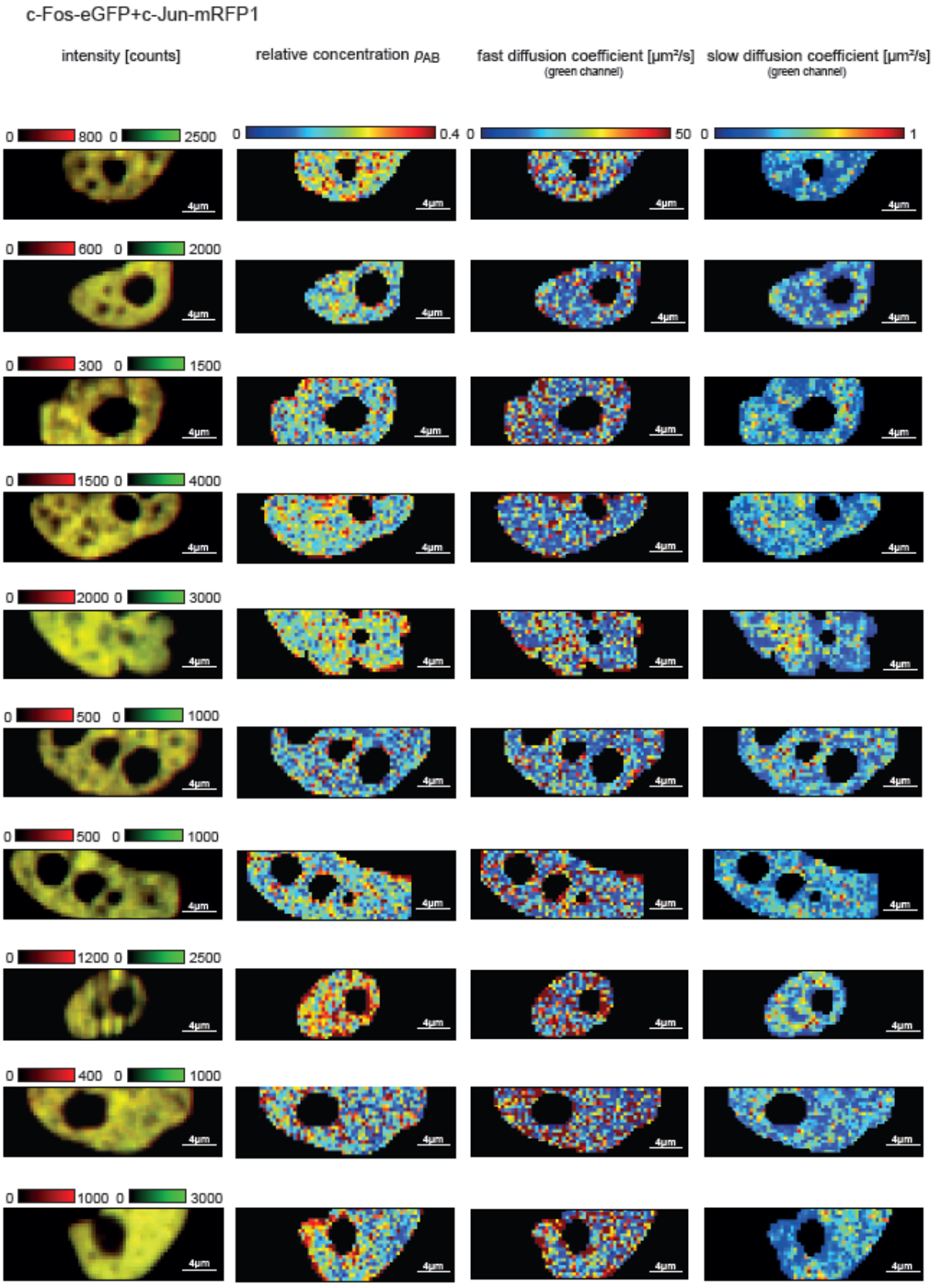
c-Fos-eGFP+c-Jun-mRFP1
intensity [counts]
relative concentration p_{AB}
fast diffusion coefficient [µm²/s] (green channel)
slow diffusion coefficient [µm²/s] (green channel)
0 800 0 2500
0 0.4 0 50 0 1
0 600 0 2000
0 300 0 1500
0 1500 0 4000
0 2000 0 3000
0 500 0 1000
0 500 0 1000
0 1200 0 2500
0 400 0 1000
0 1000 0 3000
4µm

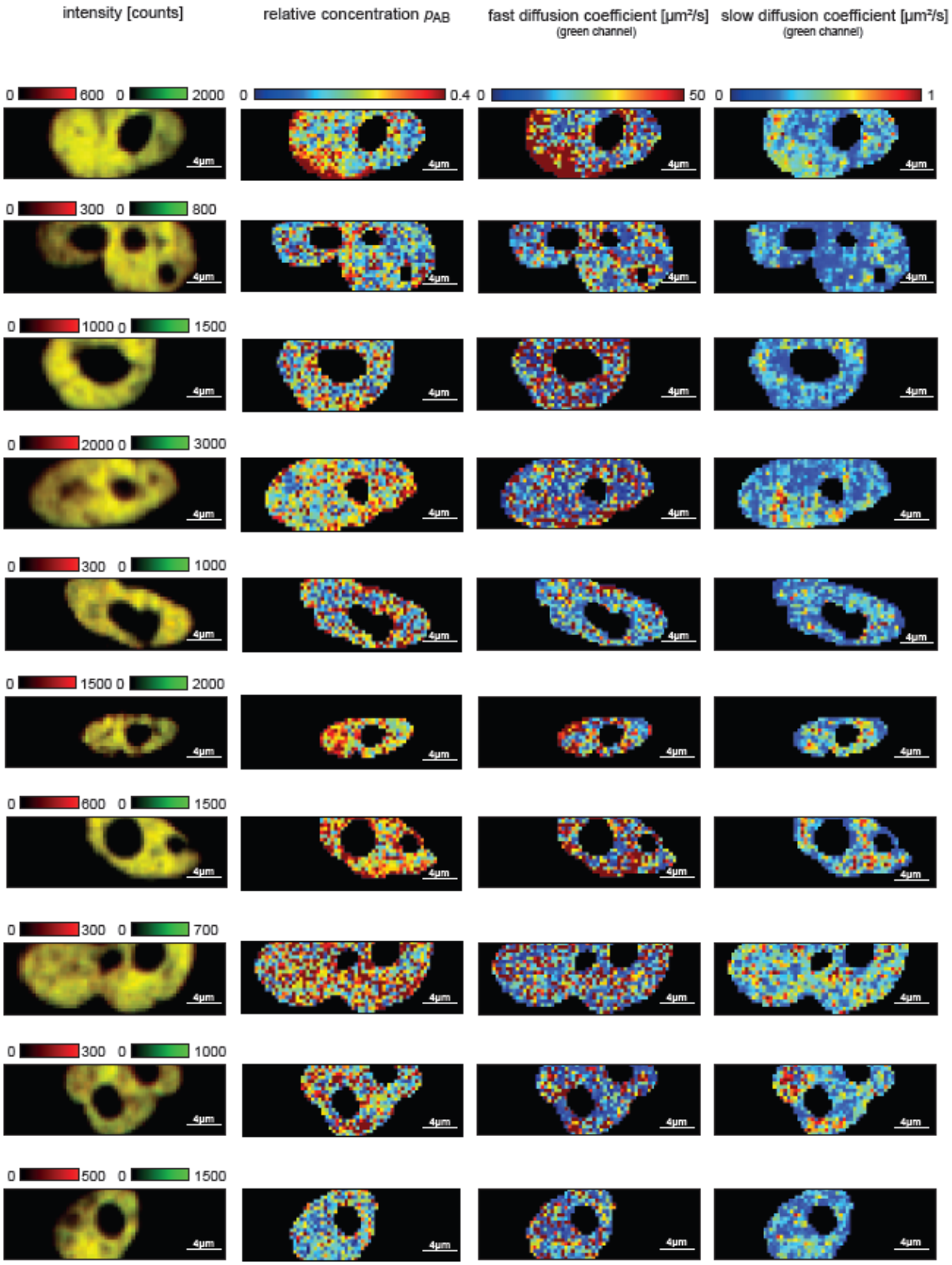

Figure A.7: SPIM-FCCS *in vivo* measurements of AP-1 wildtype proteins c-Fos-eGFP and c-Jun-mRFP1 in HeLa cells: intensity images, relative concentration maps and fast and slow diffusion coefficients maps in the green channel for all 20 measured cells.

c-Fos-eGFP+c-Jun-mRFP1

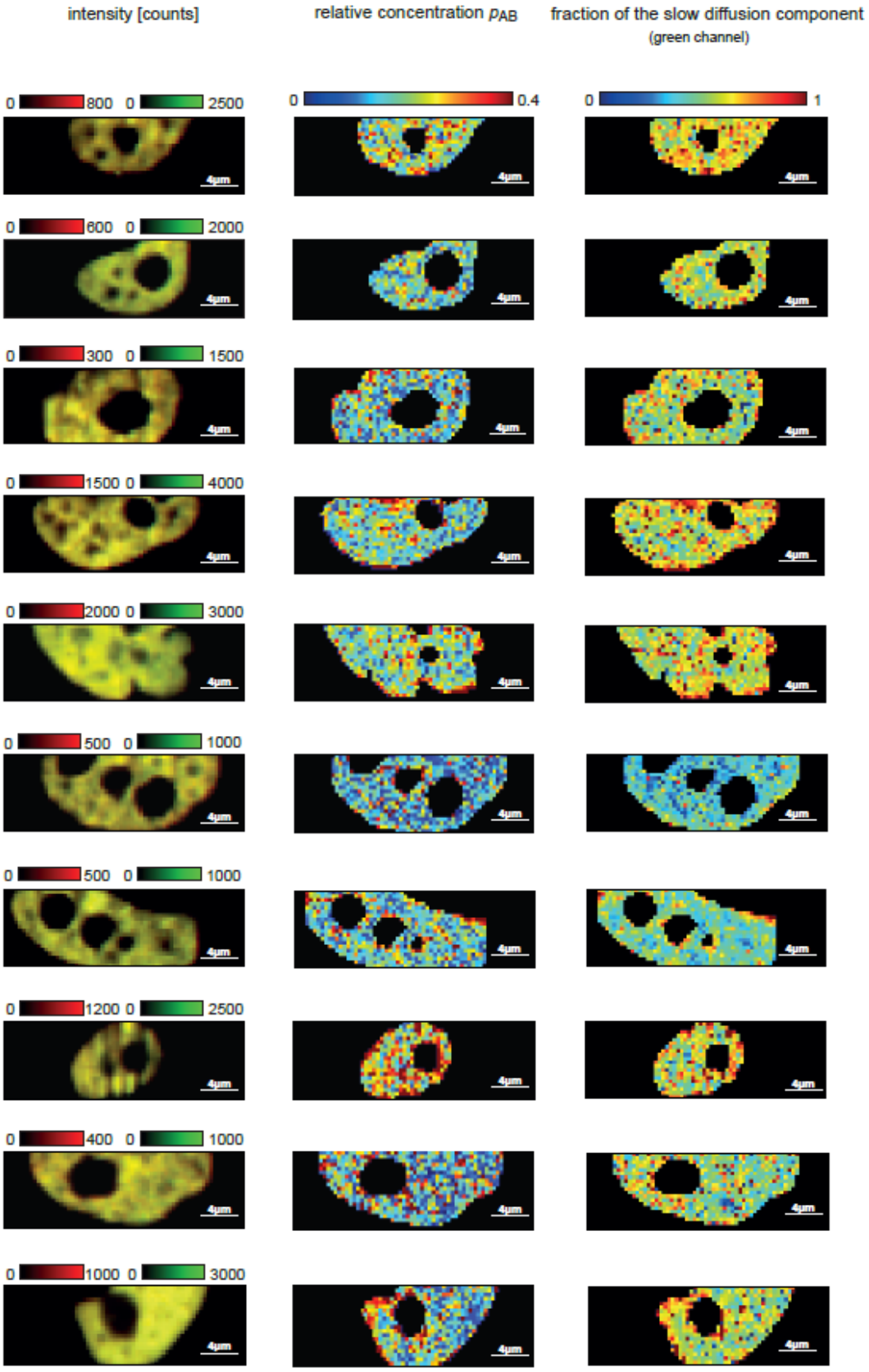

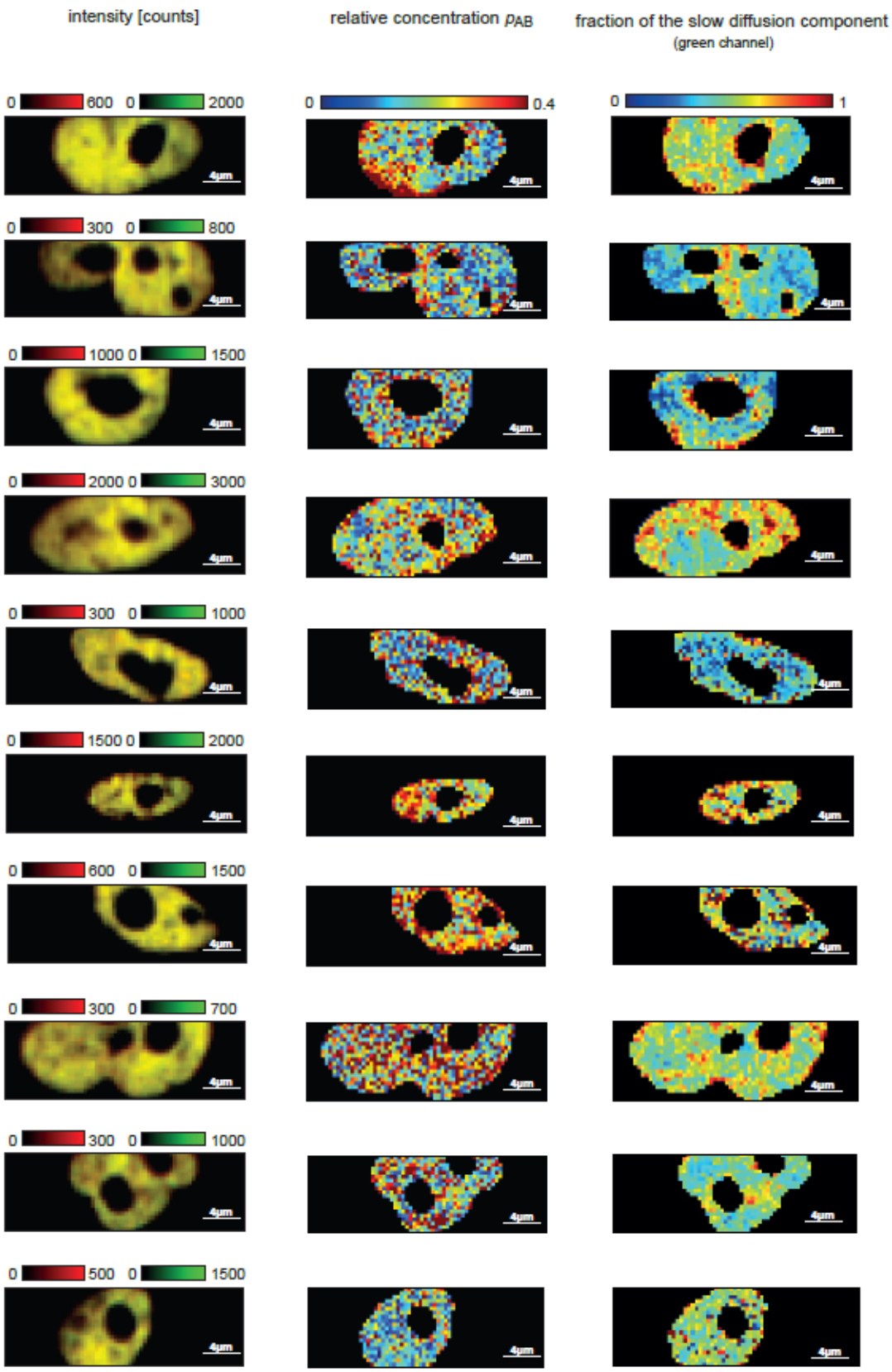

Figure A.8: SPIM-FCCS *in vivo* measurements of AP-1 wildtype proteins c-Fos-eGFP and c-Jun-mRFP1 in HeLa cells: intensity images, relative concentration maps and fraction of the slow diffusion component maps for all 20 measured cells.

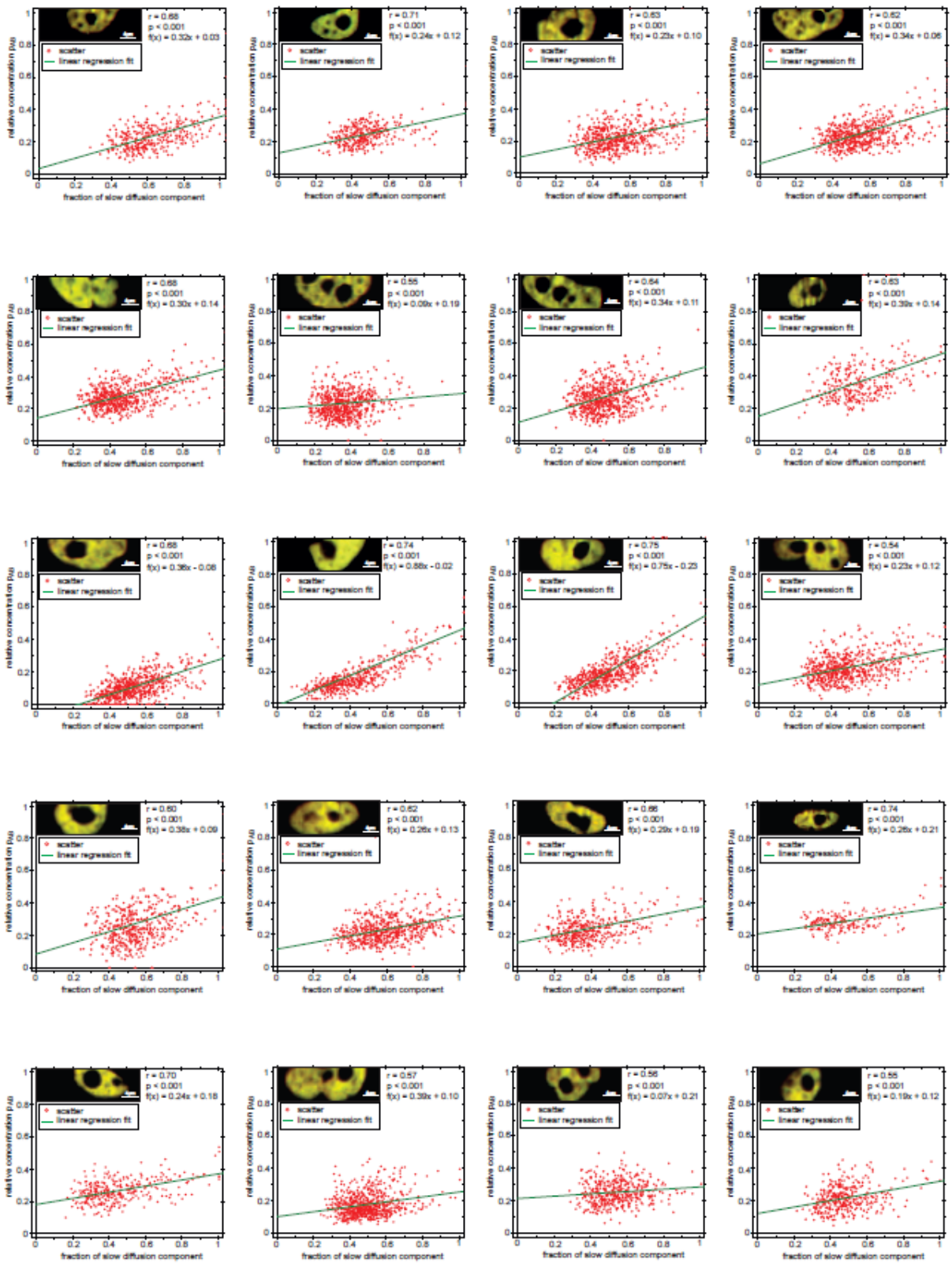

Figure A.9: Scatter plots illustrating the relationships between the fraction of the slow diffusing component, where D1 and D2 were fixed at average for the fit, and relative concentration p_{AB} of AP-1 wildtype proteins c-Fos-eGFP and c-Jun-mRFP1 in HeLa cells for all 20 measured cells. Each graph shows a scatter plot where a point indicates values obtained at one pixel, and the linear regression fit.

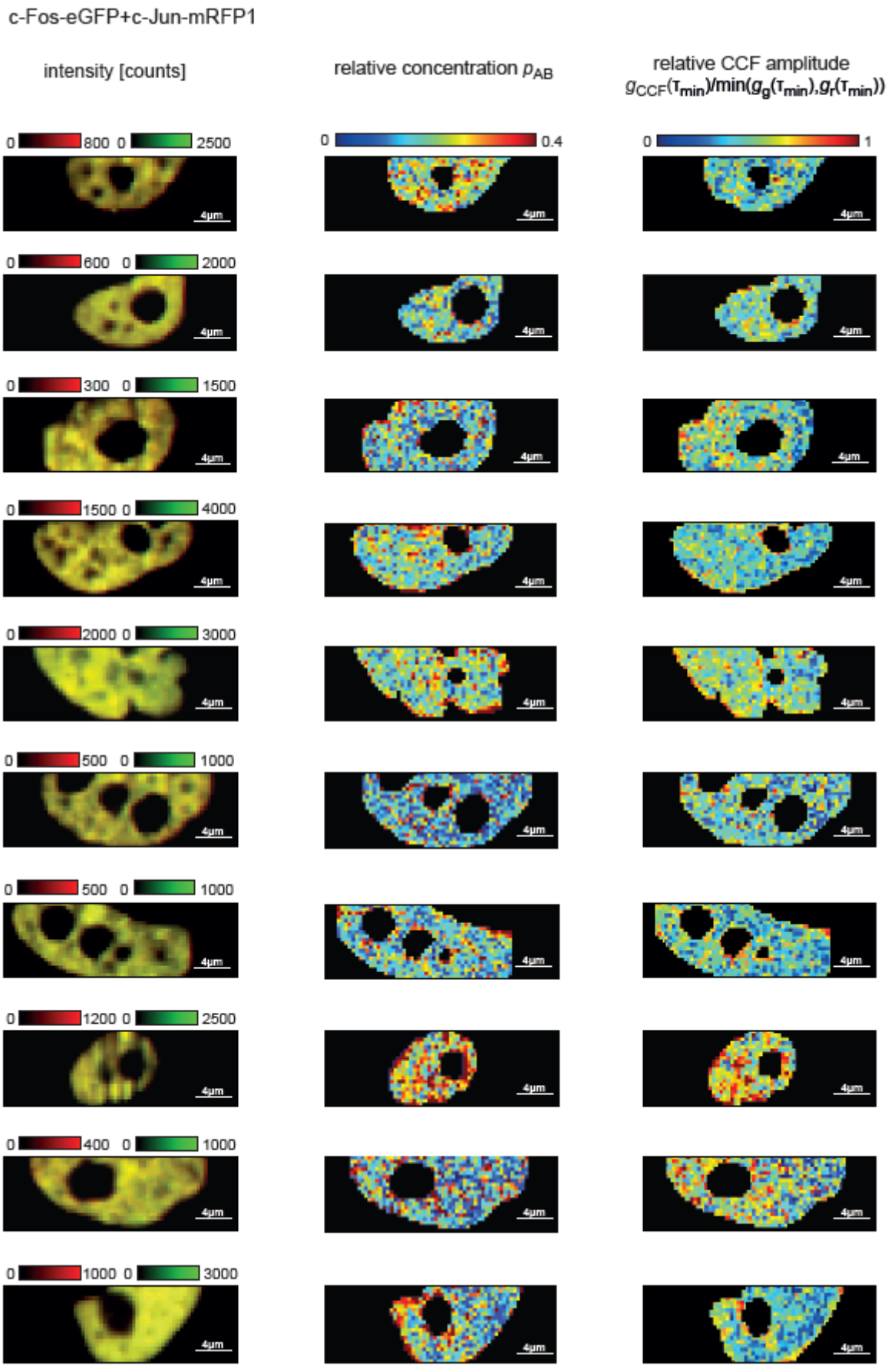
c-Fos-eGFP+c-Jun-mRFP1
intensity [counts]
relative concentration p_{AB}
relative CCF amplitude
$g_{CCF}(\tau_{min})/\min(g_g(\tau_{min}),g_r(\tau_{min}))$
0 800 0 2500
0 0.4
0 1
0 600 0 2000
0 300 0 1500
0 1500 0 4000
0 2000 0 3000
0 500 0 1000
0 500 0 1000
0 1200 0 2500
0 400 0 1000
0 1000 0 3000
4µm

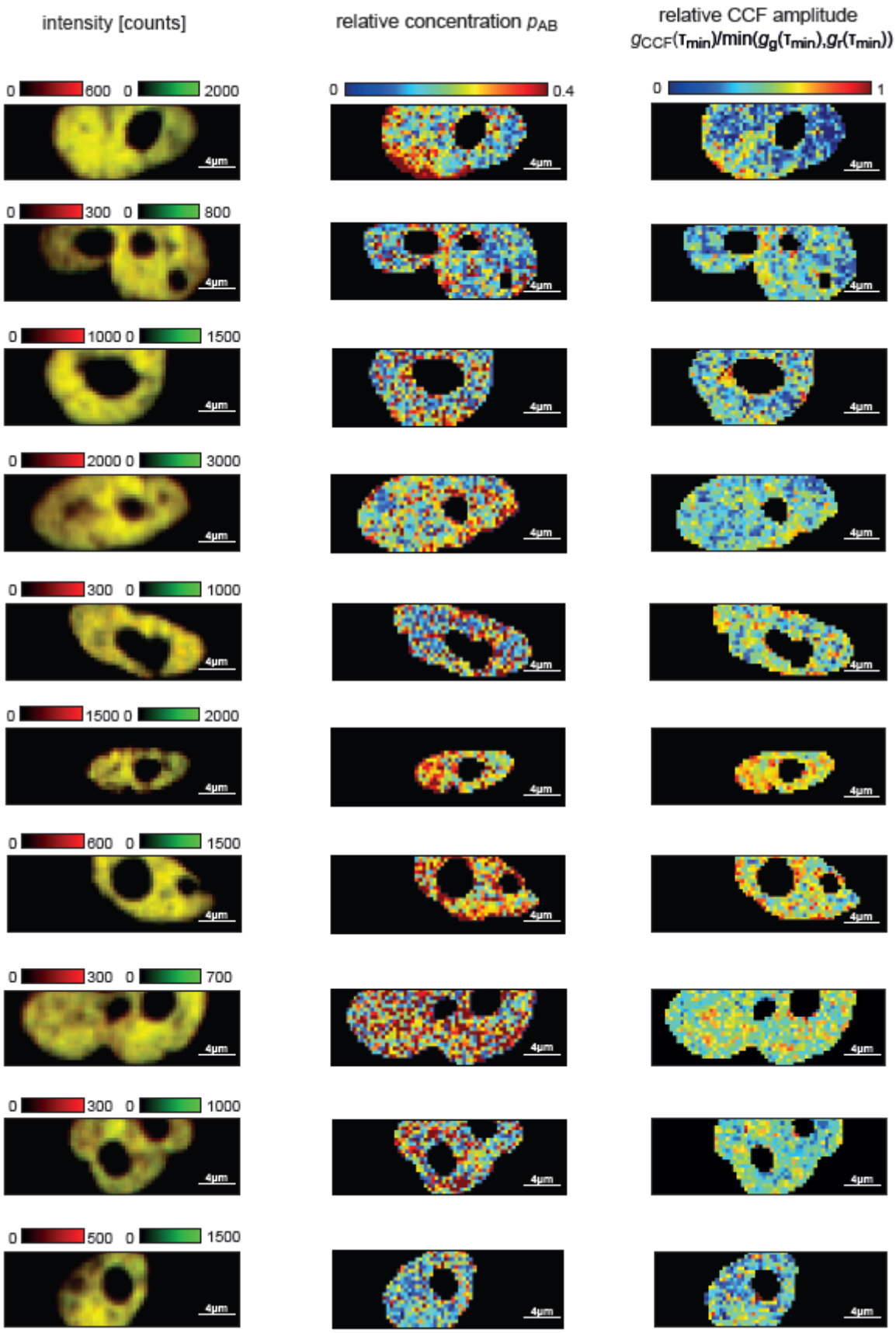

Figure A.10: SPIM-FCCS *in vivo* measurements of AP-1 wildtype proteins c-Fos-eGFP and c-Jun-mRFP1 in HeLa cells: intensity images, relative concentration maps and relative cross-correlation amplitude maps for all 20 measured cells.

References

[1] B. Alberts, A. Johnson, J. Lewis, M. Raff, K. Roberts and P.Walter (2008): Molecular biology of the cell, Garland Science, 5th edition

[2] T.M. Nordlund (2011): Quantitative understanding of biosystems: an introduction to biophysics, CRC Press

[3] Copyright 2008 from Molecular Biology of the Cell, 5th Edition by Alberts et al. Reproduced by permission of Garland Science/Taylor & Francis LLC

[4] F. Crick (1970): Central dogma of molecular biology. Nature, 227, 561-563

[5] T.R. Huges (2011): A handbook of transcription factors, Springer

[6] D.S. Latchman (1997): Transcription factors: an overview, The International Journal of Biochemistry and Cell Biology, 29(12), 1305-1312

[7] N. Baudendistel (2004): Zwei-Hybrid-Fluoreszenzkreuzkorrelationsspektroskopie: In vivo Characterisierung von Protein-Protein-Wechselwirkungen im AP-1 System, Doctoral thesis, University of Heidelberg,
http://archiv.ub.uni-heidelberg.de/volltextserver/5105/1/Diss_unibib.pdf

[8] J. Hess, P. Angel, M. Schorpp-Kistner (2004): AP-1 subunits: quarrel and harmony among siblings, Journal of Cell Science, 117(25), 5965-5973

[9] Y. Chinenov, T.K. Kerppola (2001): Close encounters of many kinds: Fos-Jun interactions that mediate transcription regulatory specificity, Oncogene, 20(19), 2438-2452

[10] P.K. Vogt (2002): Fortuitous convergances: the beginnings of Jun, Nature Reviews Cancer, 2(6), 465-469

[11] W.H. Landschulz, P.F. Johnson, S.L. McKnight (1988): The leucine zipper: a hypothetical structure common to a new class of DNA binding proteins, Science, 240(4860), 1759-1764

[12] R. Turner, R. Tjian (1989): Leucine repeats and an adjacent DNA binding domain mediate the formation of functional cFos-cJun heterodimers, Science, 243(4899, 1689-1694

[13] L. Patel, C. Abate, T. Curran (1990): Altered protein conformation on DNA binding by Fos and Jun, Nature, 347(6293), 572-575

[14] P.K. Vogt (2001): Jun, the oncoprotein, Oncogene, 20(19), 2365-2377

[15] H. van Dam, M. Castellazzi (2001): Distinct roles of Jun:Fos and Jun:ATF dimers in oncogenesis, Oncogene, 20(19), 2453-1464

[16] N. Baudendistel, G. Müller, W. Waldeck, P. Angel, J. Langowski (2005): Two-Hybrid Fluorescence Cross-Correlation Spectroscopy detects protein-protein interactions in vivo, ChemPhysChem, 6(5), 984-90

[17] G. Vámosi, N. Baudendistel, C.W. von der Lieth, N. Szalóki , G. Mocsár, G. Müller, P. Brázda, W. Waldeck, S. Damjanovich, J. Langowski, K. Tóth (2007): Conformation of the c-Fos/c-Jun complex in vivo: a combined FRET, FCCS, and MD-modeling study, Biophys J., 94(7), 2859-68

[18] M. Karin (1995): The regulation of AP-1 activity by mitogen-activated protein kinases, Journal of Biological Chemistry, 270(28), 16483-16486

[19] E. Shaulian, M. Karin (2001): AP-1 in cell proliferation and survival, Oncogene, 20(19), 2390-2400

[20] W. Lee, P. Mitchell, R. Tjian (1987): Purified transcription factor AP-1 interacts with TPA-inducible enhancer elements, Cell, 49(6), 741-752

[21] P. Angel, M. Imagawa, R. Chiu, B. Stein, R.J. Imbra, H.J. Rahmsdorf, C. Jonat, P. Herrlich, M. Karin (1987): Phorbol ester-inducible genes contain a common cis element recognized by a TPA-modulated trans-acting factor, Cell, 49(6), 729-739

[22] R. Eferl, E.F. Wagner (2003): AP-1: a double-edged sword in tumorigenesis, Nature Reviews Cancer, 3(11), 859-868

[23] P. Angel, M. Karin (1991): The role of Jun, Fos and the AP-1 complex in cell-proliferation and transformation, Biochimica et. Biophysica Acta, 1072(2-3), 129-157

[24] C.E. Malnou, F. Brockly, C. Favard, G. Moquet-Torcy, M. Piechaczyk, I. Jariel-Encontre (2010): Heterodimerization with different Jun proteins controls c-Fos intranuclear dynamics and distribution, The Journal of Biological Chemistry, 285(9), 6552-6562

[25] J.N. Glover, S.C. Harrison (1995): Crystal structure of the heterodimeric bZIP transcription factor c-Fos-c-Jun bound to DNA, Nature, 373(6511), 257-261

[26] D. Bohmann, T.J. Bos, A. Admon, T. Nishimura, P.K. Vogt, R. Tijan (1987): Human proto-oncogen c-jun encodes a DNA binding protein with structural and functional properties of transcription factor AP-1, Science, 238(4832), 1386-1392

[27] D.R. Cohen, P.C. Ferreira, R. Gentz, B.R. Franza Jr., T. Curran (1989): The product of a fos-related gene, fra-1, binds cooperatively to the AP-1 site with Jun: transcription factor AP-1 is comprised of multiple protein complexes, Genes and Development, 3(2), 173-184

[28] B.R. Franza Jr., F.J. Rauscher 3rd, S.F. Josephs, T. Curran (1988): The Fos complex and Fos-related antigens recognize sequence elements that contain AP-1 binding sites, Science, 239(4844), 1150-1153

[29] Y. Nakabeppu, K. Ryder, D. Nathans (1988): DNA binding activities of three murine Jun proteins: stimulation by Fos, Cell, 55(5), 907-915

[30] F.J. Rauscher 3rd, D.R. Cohen, T. Curran, T.J. Bos, P.K. Vogt, D. Bohmann, R. Tijan, B.R. Franza Jr. (1988): Fos-associated protein p39 is the product of the jun proto-oncogene, Science, 249(4855), 1010-1016

[31] F.J. Rauscher 3rd, L.C. Sambucetti, T. Curran, R.J. Distel, B.M. Spiegelman (1988): Common DNA binding site for Fos protein complexes and transcription factor AP-1, Cell, 52(3), 471-480

[32] M. Zerial, L. Toschi, R.P. Ryseck, M. Schuermann, R. Müller, R. Bravo (1989): The product of a novel growth factor activated gene, fos B, interacts with Jun proteins enhancing their DNA binding activity, EMBO Journal, 8(3), 805-813

[33] F.J. Rauscher 3rd, P.J. Voulalas, B.R. Franza Jr., T. Curran (1988): Fos and Jun bind cooperatively to the AP-1 site: reconstitution *in vitro*, Genes and Diversity, 2(12B), 1687-1699

[34] T.D. Halazonetis, K. Georgopoulos, M.E. Greenberg, P. Leder (1988): c-Jun dimerizes with itself and with c-Fos, forming complexes of different DNA binding affinities, Cell, 55(5), 917-924

[35] T. Smeal, P. Angel, J. Meek, M. Karin (1989): Different requirements for formation of Jun:Jun and Jun:Fos complexes, Genes and Development, 3(12B), 2091-2100

[36] J.J. Kohler, A. Schepartz (2001): Kinetic studies of Fos.Jun.DNA complex formation: DNA binding prior to dimerization, Biochemistry, 40(1), 130.142

[37] A. Morlon, P. Sassone-Corsi (2003): The LIM-only protein FHL2 is a seruminducible transcriptional coactivator of AP-1, Proceedings of the National Academy of Sciences of the United States of America, 100(7), 3977-3982

[38] K. McBride, F. Charron, C. Lefebvre, M. Nemer (2003): Interaction with GATA transcription factors provides a mechanism for cell-specific effects of c-Fos, Oncogene, 22(52), 8403-8412

[39] Y. Maki, T.J. Bos, C. Davis, M. Starbuck, P.K. Vogt (1987): Avian sarcoma virus 17 carries the jun oncogene, Proceedings of the National Academy of Sciences of the United States of America, 84(9), 2848-2852

[40] P.K. Vogt, T.J. Bos, R.F. Doolittle (1987): Homology between the DNA-binding domain of the GCN4 regulatory protein of yeast and the carboxyl-terminal region of a protein coded for by the oncogene jun, Proceedings of the National Academy of Sciences of the United States of America, 84(10), 3316-3319

[41] P. Angel, E.A. Allegretto, S.T. Okino, K. Hattori, W.J. Boyle, T. Hunter, M. Karin (1988): Oncogene jun encodes a sequence-specific trans-activation similar to AP-1. Nature, 332(6160), 166-171

[42] V. Adler, A. Polotskaya, F. Wagner, A.S. Kraft (1992): Affinity-purified c-Jun amino-terminal protein kinase requires serine/threonine phosphorylation for activity, Journal of Biological Chemistry, 267(24), 17001-17005

[43] P. Angel, K. Hattori, T. Smeal, M. Karin (1988): The jun proto-oncogene is positively autoregulated by its product, Jun/AP-1, Cell, 55(5), 875-885

[44] K. Hattori, P. Angel, M.M. Le Beau, M. Karin (1988): Structure and chromosomal localization of the functional intronless human JUN protooncogene, Proceedings of the National Academy of Sciences of the United States of America, 85(23), 9148-9152

[45] R. Wisdom, R.S. Johnson, C. Moore (1999): c-Jun regulates cell cycle progression and apoptosis by distinct mechanisms, The EMBO Journal, 18(1), 188-197

[46] M. Schreiber, A. Kolbus, F. Piu, A. Szabowski, U. Möhle-Steinlein, J. Tian, M. Karin, P. Angel, E.F. Wagner (1999): Control of cell cycle progression by c-Jun is p53 dependent, Genes and Development, 13(5), 607-619

[47] K. Milde-Langosch (2005): The Fos family of transcription factors and their role in tumourigenesis, European Journal of Cancer, 41(16), 2449-2461

[48] H. König, H. Ponta, U. Rahmsdorf, M. Büscher, A. Schönthal, H.J. Rahmsdorf, P. Herrlich (1989): Autoregulation of fos: the dyad symmetry element as the major target of repression, EMBO Journal, 8(9), 2559-2566

[49] P. Sassone-Corsi, L.J. Ransone, W.W. Lamph, I.M. Verma (1988): Direct interaction between fos and jun nuclear oncoproteins: role of the `leucine zipper´ domain, Nature, 336(6200), 692-695

[50] E. Tulchinsky (2000): Fos family members: regulation, structure and role in oncogenetic transformation, Histology and histopathology, 15(3), 921-928

[51] M. Piechaczyk, J.M. Blanchard (1994): c-fos proto-oncogene regulation and function, Critical Reviews in Oncology/Hematology, 17(2), 93-131

[52] J.W. Krieger, K. Tóth, J. Langowski (2014): Practical course Biophysics: Fluorescence Correlation Spectroscopy, http://www.dkfz.de/Macromol/teaching/files/fcs_practical.pdf

[53] J.W. Krieger (2014): Mapping diffusion properties in living cells, Doctoral thesis, University of Heidelberg,
http://archiv.ub.uni-heidelberg.de/volltextserver/17187/1/dissertation_final.pdf

[54] M. Weiss, M. Elsner, F. Kartberg, T. Nilsson (2004): Anomalous subdiffusion is a measure for cytoplasmic crowding in living cells, Biophysical Journal, 87(5), 3518-3524

[55] M. Wachsmuth, W. Waldeck, J. Langowski (2000): Anomalous diffusion of fluorescent probes inside living cell nuclei investigated by spatially-resolved fluorescence correlation spectroscopy, Journal of Molecular Biology, 298(4), 677-689

[56] T. Kühn, T.O. Ihalainen, J. Hyväluoma, N. Dross, S.F. Willman, J. Langowski, M. Vihinen-Ranta, J. Timonen (2011): Protein diffusion in mammalian cell cytoplasm, PLoS One, 6(8), e22962

[57] M. Weiss (2014): Crowding, diffusion, and biochemical reactions, International Review of Cell and Molecular Biology, 307, 383-417

[58] J.A. Dix, A.S. Verkman (2008): Crowding effects on diffusion in solutions and cells, Annual Review of Biophysics, 37:247-263

[59] D. Magde, E.L. Elson, W.W. Webb (1974): Fluorescence correlation spectroscopy. I. Conceptual basis and theory, Biopolymers, 13(1), 1-27

[60] D. Magde, E.L. Elson, W.W. Webb (1974): Fluorescence correlation spectroscopy. II. An experimental realization, Biopolymers, 13(1), 29-61

[61] R. Rigler, Ü. Mets, J. Widengren, P. Kask (1993): Fluorescence correlation spectroscopy with high count rate and low background: analysis of translational diffusion, European Biophysical Journal, 22(3), 169-175

[62] K. Bacia, P. Schwille (2007): Fluorescence correlation spectroscopy, Methods Molecular Biology, 398, 73-84

[63] G. Vámosi, S. Damjanovich, J. Szöllosi, G. Vereb (2009): Measurement of molecular mobility with fluorescence correlation spectroscopy, Current Protocols in Cytometry, 2(2.15), 1-19

[64] N. Dross, C. Spriet, M. Zwerger, G. Müller, W. Waldeck, J. Langowski (2009): Mapping eGFP oligomer mobility in living cell nuclei, PLoS ONE 4, e5041

[65] N. Dross (2009): Mobilität von eGFP-Oligomeren in lebenden Zellkernen, Doctoral thesis, http://archiv.ub.uni-heidelberg.de/volltextserver/10470/1/Dross_Mobilitaet_von_eGFP_Oligomeren_in_lebenden_Zellkernen.pdf

[66] P. Schwille, F.J. Meyer-Almes, R. Rigler (1997): Dual-color fluorescence cross-correlation spectroscopy for multicomponent diffusional analysis in solution, Biophysical Journal, 29(1), 74-85

[67] K. Bacia, S.A. Kim, P. Schwille (2006): Fluorescence cross-correlation spectroscopy in living cells, Nature Methods, 3(2), 83-89

[68] G. Vámosi, A. Bodnár, G. Vereb, A. Jenei, C.K. Goldman, J. Langowski, K. Tóth, L. Mátyus, J. Szöllösi, T.A. Waldmann, S. Damjanovich (2004): IL-2 and IL-15 receptor alpha-subunits are coexpressed in a supramolecular receptor cluster in lipid rafts of T cells, Proc. Natl. Acad. Sci. USA, 101(30), 11082-11087

[69] X. Ma, S. Ahmed, T. Wohland (2011): EGFR activation monitored by SW-FCCS in live cells, Frontiers in Bioscience (Elite Edition), 22-32

[70] T. Wohland, X. Shi, J. Sankaran, E.H.K. Stelzer (2010): Single plane illumination fluorescence correlation spectroscopy (SPIM-FCS) probes inhomogeneous three-dimensional environments, Optics Express, 18(10), 10627-10641

[71] K. Greger, J. Swoger, E.H.K. Stelzer (2007): Basic building units and properties of a fluorescence single plane illumination microscope, Review of Scientific Instrumentation, 78(2), 023705

[72] J. Huisken, J. Swoger, F. Del Bene, J. Wittbrodt, E.H.K. Stelzer (2004): Optical sectioning deep inside live embryos by selective plane illumination microscopy, Science, 305(5686), 1007-1009

[73] J. Capoulade, M. Wachsmuth, L. Hufnagel, M. Knop (2011): Quantitative fluorescence imaging of protein diffusion and interaction in living cells, Nature Biotechnology, 29(9), 835-839

[74] P. Brazda, J.W. Kriger, B. Daniel, D. Jonas, T. Szekeres, J. Langowski, K. Tóth, L. Nagy, G.Vámosi (2014): Ligand binding shifts highly mobile retinoid x receptor to the chromatin-bound state in a coactivator-dependent manner, as revealed by single-cell imaging, Molecular and Cellular Biology, 34(7), 1234-1245

[75] J.W. Krieger, A.P. Singh. C.S. Garbe, T. Wohland, J. Langowski (2014): Dual-Color Fluorescence Cross-Correlation Spectroscopy on a Single Plane Illumination Microscope (SPIM-FCCS), Optics Express, 22(3), 2358-75

[76] A.P. Singh, T. Wohland (2014): Applications of imaging fluorescence correlation spectroscopy, Current Opinion in Chemical Biology, 20, 29-35

[77] M. Sauer, J. Hofkens, J. Enderlein (2011): Handbook of fluorescence spectroscopy and imaging, Wiley-VCH

[78] A.R. Hibbs (2004): Confocal microscopy for biologists, Kluwer Academic/Plenum Publishers

[79] C. Gell, D. Brockwell, A. Smith (2008): Handbook of single molecule fluorescence spectroscopy, Oxford

[80] J.W. Krieger, K. Tóth, J. Langowski (2014): Practical course Biophysics: Absorption and fluorescence spectroscopy,
http://www.dkfz.de/Macromol/teaching/files/fluorescence_practical.pdf

[81] U. Kržič (2009): Multiple-view microscopy with light-sheet based fluorescence microscope, Doctoral thesis,
http://archiv.ub.uni-heidelberg.de/volltextserver/9668/1/Uros_Krzic_PhD_Thesis_Heidelberg_University_July_2009_v40.pdf

[82] P.R. Selvin, T. Ha (2008): Single molecule techniques: a laboratory manual, Cold Spring Harbor laboratory press

[83] J.B. Pawley (2006): Handbook of biological confocal microscopy, Springer, 3rd edition

[84] K. Bacia, P. Schwille (2007): Practical guidelines for dual-color fluorescence cross-correlation spectroscopy, Nature Protocols, 2(11), 2842-2856

[85] X. Ma, Y.H. Foo, T. Wohland (2014): Fluorescence cross-correlation spectroscopy (FCCS) in living cells, 1076, 557-573

[86] E. Haustein, P. Schwille (2007): Fluorescence correlation spectroscopy: novel variations of an established technique, Annual Review of Biophysics and Biomolecular Structure, 36, 151-169

[87] R. Macháň, T. Wohland (2014): Recent applications of fluorescence correlation spectroscopy in live systems, FEBS Letters, 588(19), 3571-3584

[88] L.C. Hwang, T. Wohland (2007): Recent advances in fluorescence cross-correlation spectroscopy, Cell Biochemistry and Biophysics, 49(1), 1-13

[89] J. Langowski (2008): Protein-protein interactions determined by fluorescence correlation spectroscopy, Methods Cell Biology, 85, 471-484

[90] K. Bacia, P. Schwille (2003): A dynamic view of cellular processes by in vivo fluorescence auto- and cross- correlation spectroscopy, Methods, 29(1), 74-85

[91] J.W. Krieger, J. Langowski (2014): *QuickFit 3.0* (Beta, SVN: 3157, build date: 2014-04-11): A data evaluation application for biophysics, http://www.dkfz.de/Macromol/quickfit/

[92] J. Widengren, R. Rigler, Ü. Mets (1994): Triplet-state monitoring by fluorescence correlation spectroscopy, Journal of Fluorescence, 4(3), 255-259

[93] O. Krichevsky, G. Bonnet (2002): Fluorescence correlation spectroscopy: the technique and its applications, Reports on Progress in Physics, 65, 251-297

[94] O. Shimomura, F.H. Johnson, Y. Saiga (1962): Extraction, purification and properties of aequorin, a bioluminescent protein from the luminous hydromedusan, Aequorea, Journal of Cellular and Comparative Physiology, 59(3), 223-239

[95] R.Y. Tsien (1998): The green fluorescent protein, Annual Review of Biochemistry, 67(1), 509-544

[96] R.E. Campbell, O. Tour, A.E. Palmer, P.A. Steinbach, G.S. Baird, D.A. Zacharias, R.Y. Tsien (2002): A monomeric red fluorescent protein, Proceedings of the National Academy of Sciences, 99(12), 7877-7882

[97] J.J.M Landry, P.T Pyl, T. Rausch, T. Zichner, M.M.Tekkedil *et.al* (2013): The genomic and transcriptomic landscape of HeLa cell line, G3, 3(8), 1213-1224

[98] H.D. Soule, J. Vazquez, A. Long, S. Albert, M. Brennan (1973): A human cell line from a pleural effusion derrived from a breast carcinoma, Journal of the National Cancer Institute, 51(5), 1409-1416

[99] M. Wachsmuth (2001): Fluorescence fluctuation microscopy: design of a prototype, theory and measurements of the mobility of biomolecules in the cell nucleus, Ph.D. thesis, Ruprecht-Karls-Universität, Heidelberg

[100] M. Tewes, J. Langowski (2001): Fluorescence correlation spectroscopy module for a microscope, European patent no. 0941470

[101] N. Dross, J. Langowski, C. Spriet (2008): Messkammer fuer mikroskopische Beobachtungen und Messungen, DE 20 2008 010 895.0, DPMA, utility model, Germany

[102] A.P. Singh, J.W. Krieger, J. Buchholz, E.Charbon, J. Langowski, T. Wohland (2013): The performance of 2D array detectors for light sheet based fluorescence correlation spectroscopy, Optics Express, 21(7), 8652-68

[103] S. Cova, M. Ghioni, A. Lacaita, C. Samori, F. Zappa (1996): Avalanche photodiodes and quenching circuits for single-photon detection, Applied Optics, 35(12):1956

[104] Z. Petrášek, P. Schwille (2008): Precise measurement of diffusion coefficients using scanning fluorescence correlation spectroscopy, Biophysical Journal, 94(4), 1437-1448

[105] J.M. Nitsche, H.C. Chang, P.A. Weber, B.J. Nicholson (2004): A transient diffusion model yields unitary gap junctional permeabilities from images of cell-to-cell fluorescent dye transfer between Xenopus oocytes, Biophysical Journal, 86(4), 2058-2077

[106] J. Ries, S. Chiantia, P. Schwille (2009): Accurate determination of membrane dynamics with line-scan FCS, Biophysical Journal, 96(5), 1999-2008

[107] A. Pernuš, J. Langowski (2015) Imaging Fos-Jun transcription factor mobility and interaction in live cells by single plane illuminatopn-fluorescence cross correlation spectroscopy, PloS One, 10(4), e0123070

[108] W. Lee, Y.I. Lee, J. Lee, L.M. Davis, P. Deininger, S.A. Soper (2010): Cross-talk-free dual-color fluorescence cross-correlation spectroscopy for the study of enzyme activity, Analytical Chemistry, 82(4), 1401-1410

[109] H. Glauner, I.R. Ruttekolk, K. Hansen, B. Steemers, Y.D. Chung, F. Becker, S. Hannus, R. Brock (2010): Simultaneous detection of intracellular target and off-target binding of small molecule cancer drugs at nanomolar concentrations, British Journal of Pharmacology, 160(4), 958-970

Bibliography

JOURNAL PUBLICATIONS

Pernuš Agata, Jörg Langowski: Imaging Fos-Jun transcription factor mobility and interaction in live cells by single plane illumination-fluorescence cross correlation spectroscopy, PLOS ONE, 2015, 10(4): e0123070.

CONFERENCE PUBLICATIONS

Pernus Agata, Krieger Jan, Buchholz Jan, et al.: Protein-Protein Interactions in vivo Studied by Single Plane Illumination Fluorescence Correlation Spectroscopy (SPIM-FCS), 57th Annual Meeting of the Biophysical Society, Philadelphia; Biophysical Journal, Volume: 104/ 2, 575A-575A, January 2013.

Singh P. Anand, Krieger Jan, **Pernus Agata**, et al.: SPIM-FCCS: A Novel Technique to Quantitate Protein-Protein Interaction in Live Cells, 57th Annual Meeting of the Biophysical Society, Philadelphia; Biophysical Journal, Volume: 104/2, 61A-61A, January 2013.

Buchholz Jan, Krieger Jan, **Pernus Agata**, et al.: Dual-Color Single Plane Illumination Fluorescence Correlation Spectroscopy (SPIM-FCS) Using a Single Photon Detector and Hardware based Image Processing, 56th Annual Meeting of the Biophysical Society, San Diego; Biopysical Journal, Volume: 102/3, 207A-207A, January 2012.

Buchholz Jan, Krieger Jan, **Pernus Agata**, et al.: High Speed FPGA Based Multi-Tau Correlation for Single-Photon Avalanche Diode Arrays, 8th EBSA European Biophysics Congress, Budapest; European Biophysics Journal with Biophysics Letters, Volume 40, 123-123, August 2011.

Krieger Jan, Buchholz Jan, **Pernus Agata**, et al.: Single Plane Illumination Fluorescence Correlation Spectroscopy Using High Speed Image Sensors, 8th EBSA European Biophysics Congress, Budapest; European Biophysics Journal with Biophysics Letters, Volume: 40, 127-128, August 2011.

Krieger Jan, Buchholz Jan, **Pernus Agata**, et al.: Single Plane Illumination Fluorescence Correlation Spectroscopy (SPIM-FCS) Using a Position-Sensitive Detector, 55th Annual Meeting of the Biophysical Society, Baltimore; Biophysical Journal, Volume: 100/3, 469-469, February 2011.

Ng Xue Wen, Singh P. Anand, Krieger Jan, **Pernus Agata**, et al.: A Quantitative Approach of Detecting Biomolecular Processes in vivo: SPIM-FCCS, 13th Conference on Methods and Applications of Fluorescence, Genoa, Italy, September 2013.

Singh P. Anand, Krieger Jan, **Pernus Agata**, et al.: SPIM-FCS/FCCS: A Demonstration of Live Cell Protein Dynamics with Single/Dual Color Single Plane Illumination Microscope, LSFM meeting, New York, September 2013.

Krieger Jan, **Pernus Agata**, Singh P. Anand, et al.: Two-Color Fluorescence (Cross-) Correlation Spectroscopy on a SPIM, Focus on Microscopy, Maastricht, The Netherlands, March 2013.

Buchholz Jan, Krieger Jan, **Pernus Agata**, et al.: Single Photon Avalanche Diode Arrays for SPIM-FCS, Focus on microscopy, Maastricht, The Netherlands, March 2013.

Pernus Agata, Krieger Jan, Buchholz Jan, et al.: SPIM-FCS, A New Technique to Image Protein Mobility and Interactions in Live Cells and in Real Time: Application to the Fos/Jun Transcription Factor System, DKFZ Graduate school poster presentation, Heidelberg, Germany, November 2012.

Krieger Jan, Buchholz Jan, **Pernus Agata**, et al.: SPIM-FCS: Measurements in Cells and First Results on Dual-Color Cross-Correlation, LSFM meeting, Frankfurt, Germany, September 2012.

Liepe Juliane, Felizzi Federico, **Pernus Agata**, Hanulova Maria: Microtubule Tracking from Stochastic Optical Reconstruction Microscopy Images, Proceedings of the 8th WCSB, Zuerich, Switzerland, June 2011.

Acknowledgements

I would like to thank the following people without whom this Thesis would not have been possible:

- Most of all I would like to thank my Thesis supervisor Prof. Dr. Jörg Langowski for giving me the opportunity to work on this interesting project and supporting me over the past five years.

- I would also like to thank my committee members Prof. Dr. Victor Sourjik, Prof. Dr. Stephan Frings and Dr. Johann Bollmann for their time and interest.

- I would like to thank Prof. Dr. Thorsten Wohland and Anand Prataph Singh from NUS for a great collaboration and for hosting me in Singapore. I really enjoyed meeting and talking to you.

- I would like to thank Gabriele Müller for all help with the cell culture and transfection procedures. You have always been there willing to help and for that I am very grateful.

- I thank Jan W. Krieger for building the SPIM setup, implementing the data evaluation in the *QuickFit 3.0* software and helping with the analysis and measurements.

- To all the present and former B040 lab-members: thank you for the fun and support.

- I would also like to thank my dear friends for their love, support, discussions, advice, coffee breaks, dinners, chats and so much more. In no particular order: Klara, Marta, Ida, Katja, Ana L., Manca, Anja, Vesna, Kata, Rok, Damjana, Petra, Ana S., Andreja, Uroš, Jana and Marija. You are the best!

- I cannot imagine being the same person I am today without my dear sister Sara. You are the best person in the whole world and I am so happy to have you in my life. Thank you for supporting me during the past five years, for understanding me and for always being there for me. Najraj!

- To my grandparents who would have been so proud of me. I miss you.

- A special thanks to my wonderful parents Marjeta and Franjo. I cannot express how grateful I am for your love, all the support and encouragement not only during the past few years, but also before in my life. You have always been there for me. Without you all this would not have been possible. Rada vaju imam! I would additionally like to thank my father for spending so much time proofreading, correcting and helping me with this Thesis.

- At the end I would like to express my appreciation to my dear Jaakob, who has been with me all these years. Thank you for your support, for believing in me, for listening to me and making me laugh. I would not have been able to do this without you. I love you.